

PHONON SCATTERING BY IMPURITIES IN SEMICONDUCTORS

by

Abderrahim Ramdane, Diplômé d'Études Supérieures, Algiers

Thesis submitted to the University of Nottingham
for the degree of Doctor of Philosophy

December 1980

To my parents

	Page No.
ABSTRACT	iv
ACKNOWLEDGEMENTS	vi
INTRODUCTION	1
<u>CHAPTER 1 DESCRIPTION OF EXPERIMENTAL TECHNIQUES</u>	
1.1 Thermal Conductivity Techniques	4
1.1.1 Introduction	4
1.1.2 Cryostats and magnets	4
1.1.2.1 Cryostats	4
1.1.2.2 Magnets	5
1.1.3 Thermometry and measuring technique	6
1.1.3.1 Mounting the thermometers	6
1.1.3.2 Measuring technique and calculation of thermal conductivity K(T)	7
1.1.3.3 Magnetothermal conductivity measurements	9
1.1.4 Measurements under uniaxial stress	11
1.1.4.1 Introduction	11
1.1.4.2 Mounting of sample and application of stress	12
1.1.4.3 Measurement of thermal conductivity under stress	14
1.2 Thermally Detected EPR	15
1.2.1 Introduction	15
1.2.2 Sample holder and microwave circuits	16
1.2.3 Bolometer arrangement	17
1.2.4 Thermometer bridge	18
1.2.5 Cryostat and magnets	19
1.2.6 Temperature control	19
<u>CHAPTER 2 SHALLOW ACCEPTORS IN Ge and Si</u>	
2.1 Introduction	21
2.2 High-field magnetothermal conductivity of p-Ge	22
2.2.1 Introduction	22
2.2.2 Magnetic field effect on the low temperature phonon scattering	23
2.2.2.1 Qualitative analysis	24
2.2.2.2 The Zeeman splitting of a Γ_8 quartet	24
2.3 Application of Thermally Detected EPR to p-Ge and p-Si	26
2.3.1 Introduction	26
2.3.2 TDEPR - Sensitivity and applicability	27
2.3.2.1 Sensitivity of Thermal Detection	27
2.3.2.2 Applicability of Thermal Detection	29
2.3.3 The results	30
2.4 Conclusion	33

CHAPTER 3 LOW-TEMPERATURE THERMAL CONDUCTIVITY OF
Cr-DOPED GaAs

3.1	Introduction	37
3.2	Thermal conductivity of GaAs. Review of past work	38
3.3	Experimental results	40
3.4	Theoretical background. The Callaway model	42
3.5	Scattering processes	43
3.5.1	'Intrinsic' processes	43
3.5.1.1	Boundary scattering	43
3.5.1.2	Phonon-phonon scattering	44
3.5.1.3	Point defect scattering	45
3.5.2	'Extrinsic' processes	46
3.5.2.1	'Direct process'	46
3.5.2.2	'Coherent scattering process'	47
3.6	Curve-fitting procedure and results	48
3.6.1	The intrinsic terms	48
3.6.2	The resonance terms	51
3.7	Preliminary interpretation of the results	55

CHAPTER 4 THE MAGNETOTHERMAL CONDUCTIVITY OF GaAs:Cr

4.1	Introduction	58
4.2	Low lying energy levels of GaAs:Cr	58
4.3	Experimental results	62
4.3.1	Field alignment	62
4.3.2	The magnetothermal conductivity of the pure and n-type samples	62
4.3.3	The magneto thermal conductivity of the SI samples	63
4.3.4	Frequency crossing spectra in TI#4, TI#5 and SI GaP:Cr	64
4.4	Discussion	65
4.4.1	A simple model	65
4.4.2	Application to GA735(e)	66
4.4.3	Application to TI#4	68
4.4.4	Crossing effects	70
4.4.5	The anisotropy of the magnetoresistance	71
4.5	Conclusion	72

CHAPTER 5 PIEZOTHERMAL CONDUCTIVITY

5.1	Introduction	74
5.2	The experimental data	74
5.3	Stress and strain: definitions	77
5.4	Jahn-Teller effect	79
5.4.1	The Jahn-Teller theorem	79
5.4.2	Jahn-Teller effects in an orbital triplet	80
5.4.3	The effect of uniaxial strain on the Jahn-Teller centres	82
5.5	Interpretation of experimental results	83
5.5.1	Qualitative analysis	83
5.5.1.1	Effect of stress along $\langle 001 \rangle$	83
5.5.1.2	Effect of stress along $\langle 110 \rangle$	85
5.5.2	Effect of strain on the ground state of Cr^{2+} . The Jahn-Teller energy	87
5.5.2.1	Estimate of the Jahn-Teller energy	87
5.5.2.2	Effect of misalignment of stress	91
5.6	Conclusion	93

CHAPTER 6 PHOTO-INDUCED EFFECTS IN GaAs:Cr

6.1	Introduction	94
6.2	Optically induced charge state conversion by EPR measurements	95
6.3	Persistent phonon scattering centres in n-GaAs:Cr, Si	98
6.3.1	Experimental procedure	98
6.3.2	Results and discussion	99
6.3.3	Persistent effects	102
6.4	Conclusion	103

CHAPTER 7 DISCUSSION

7.1	Introduction	105
7.2	Ground state splitting of $\text{Cr}^{2+}/\text{Cr}^{3+}$ ions in GaAs	106
7.2.1	Ground state splitting of Cr^{3+} ions	106
7.2.2	Ground state splitting of Cr^{2+} ions	107
7.2.3	Optical spectroscopy data	109
7.3	Does substitutional Cr^{1+} exist in GaAs:Cr?	111

APPENDIX 1		117
------------	--	-----

REFERENCES		119
------------	--	-----

ABSTRACT

Thermal conductivity measurements have been used to study the low lying energy levels of Cr ions in GaAs. Strong resonant phonon scattering was observed in semi-insulating (SI) and p-type samples, which is attributed to Cr^{2+} or Cr^{3+} ions, while the scattering in the n-type samples additional to that in undoped material was very small. From the computer fits of the thermal conductivity, zero-field ground state splittings have been deduced. A splitting at $\sim 23 \text{ cm}^{-1}$ is attributed to Cr^{3+} ions, others at $\sim 0.7 \text{ cm}^{-1}$ and 4.9 cm^{-1} are thought to be due to Cr^{2+} .

The phonon scattering in the n-type samples did not show any magnetic field dependence while big effects were observed in SI and p-type ones. This seems consistent with the results of the zero-field work.

The effect of uniaxial stress on the phonon scattering has been measured in the temperature range $\sim 2 - 15 \text{ K}$. Again no effects were seen in n-type material. The results for SI and p-type material are interpreted in terms of a static Jahn-Teller effect of Cr^{2+} ions.

A preliminary investigation was made of the effect on the phonon scattering of sub-band-gap illumination. In a n-type sample, the decay in the increase in the thermal resistivity produced by photoexcitation showed two parts. The first part with a characteristic time of $\sim 1 \text{ hour}$ is attributed to electron-capture at Cr^{2+} ions. The second decay was very slow (persistent)

with a characteristic time $\tau \gg 10^5$ s. This effect has tentatively been attributed to the occurrence of large lattice relaxation.

The phonon scattering by the Cr ions is found to be consistent with the 'double acceptor' model for Cr in GaAs. Another model where Cr can act as a hole trap is discussed.

Finally the effect of high magnetic fields on the thermal conductivity of acceptors in Ge was measured. From this and previous results, the g -values describing the Γ_8 ground state were found to be much lower than the predicted ones.

A Thermally Detected EPR apparatus was designed and constructed in an attempt to check on the ground state structure of p -Ge and also p -Si but no results were obtained. This is believed to be due to the very large line widths resulting from strain splitting of the Γ_8 ground state.

ACKNOWLEDGEMENTS

I am grateful to Professor L.J. Challis and Professor K.W.H. Stevens for extending to me the facilities of the Physics Department, and to the Algerian MESRS for a maintenance grant held during the course of the work.

I would particularly like to thank Professor L.J. Challis for his continuing encouragement, friendly and helpful supervision of this work.

I much appreciate the kind hospitality of SBT, CEN Grenoble during my period of stay there. In particular I am very grateful to Bernard Salce for his friendly cooperation and many helpful discussions.

My thanks also go to:

My immediate colleagues (past and present), in particular Dr. S. Balibar, Dr. A.A. Ghazi, Dr. J.M. Grimshaw, Mr. D.J. Hancock, Dr. D.J. Jefferies, Dr. Y. Korczynskij, Mr. R.S. Wardlaw, Dr. M.N. Wybourne for their help in many ways.

Dr. M.R. Brozel and Dr. L. Eaves for advice and useful discussions.

Mr. M. Carter for his encouragement and skillful construction of apparatus; Mrs M.A. Carter for her help with the computing and for typing this thesis so efficiently; Mr. J.L. Dennis and Mr. J.R. Middleton for a continuous supply of helium; Mr. G. Hayes for introducing me to the workshop machinery; Mr. W.B. Roys for his assistance in the preparation of samples.

Finally my very warm thanks to Yarra (KBK) and Luda Korczynskij (Jo and Dylan) for providing me with a second home.

INTRODUCTION

The thermal conductivity of semiconductors at low temperatures can be dramatically reduced by the presence of very small dopant impurity concentrations. In this work, the phonon scattering within low lying energy levels of acceptors in Ge and GaAs has been investigated at low temperatures.

Phonons of energy $h\nu_0$ making up part of the heat current, are resonantly scattered when the energy separation of two electronic energy levels equals $h\nu_0$, which results in a change of the thermal conductivity K . The greatest change takes place when $h\nu_0$ equals the energy of the dominant phonons in the heat current, i.e. $h\nu_0 \approx 3.8 k_B T$. This is seen as a dip in the K -versus- T curves. In the analysis of experimental results, the parameters describing the phonon scattering processes are varied until a fit is obtained. This in return provides information on the structure of the low lying impurity energy levels.

The GaAs:Cr system has been the subject of many studies in the last few years, due to its great technological importance. Cr impurities render GaAs semi-insulating (SI) at room temperature (Haisty and Cronin 1964) and this property is used in many electronic device applications. However there does not exist any model which explains all known experimental results related to the Cr ions. It is now generally accepted that Cr can exist in several charge states in GaAs. We have used thermal conductivity measurements to investigate the low temperature phonon scattering

in various GaAs:Cr samples (n-type, p-type and SI) (Chapter 3). We show evidence of resonant scattering of phonons due to Cr. (Previous thermal conductivity measurements by Vuillermoz et al (1975) were explained in terms of scattering by structural defects).

However in these measurements broad band sources are utilized, resulting in a rather poor resolution. The application of an external perturbation such as magnetic field or uniaxial stress can yield much higher resolution. This can be particularly valuable when it leads to the observation of 'frequency crossings'. This term is used to describe the situation where two resonant frequencies are brought to coincide by the application of e.g. a magnetic field. For a system with two such frequencies, ν_1 and ν_2 , that are well separated, the reduction in the heat current is the sum of the contributions from each scattering process. When the two frequencies are made equal, the phonon scattering is reduced giving rise to a sharp minimum in the magneto-thermal resistance. The position of field of these temperature independent minima can yield very useful spectroscopic information on the system under investigation. Most of previous studies using this technique were done on transition metal impurities in dielectric host lattices (see e.g. Anderson and Challis 1975).

The effect of magnetic field on the phonon scattering by Cr ions in GaAs is presented in Chapter 4. Isotropic frequency crossing lines were observed.

Chapter 5 describes the thermal conductivity of the GaAs samples when subjected to an applied uniaxial stress. This was a collaborative project with Dr. B. Salce of Centre d'Études

Nucléaires de Grenoble. The study brought evidence of the occurrence of Jahn-Teller distortions in GaAs:Cr.

The phonon scattering data were found to be consistent with a previous model describing the possible Cr charge states in GaAs (Brozel et al 1978). In Chapter 6, the effect of sub-band-gap illumination on the populations of the different charge states was studied at low temperatures. Photo-induced persistent phonon scattering effects were observed in one n-type sample.

In Chapter 7 the ground state splittings of the GaAs:Cr system obtained with different techniques are summarized. A discussion is also made of a new interpretation of the Cr charge states.

Finally in Chapter 2 the effect of high magnetic fields (up to 13T) on the thermal conductivity of p-Ge has been studied in the temperature range 1 - 4 K. This was part of a project using thermal phonons as a probe to investigate the nature of the ground state of acceptors in Ge (Challis et al 1977). The spectroscopic g -values were found to be much smaller than the theoretically predicted ones. To check on this, an attempt was made to try to determine the g -values using Thermally Detected EPR which is a technique more suitable for strongly coupled ions and broad lines.

CHAPTER 1

DESCRIPTION OF EXPERIMENTAL TECHNIQUES

1.1 THERMAL CONDUCTIVITY TECHNIQUES

1.1.1 Introduction

The 'Searles bar' steady-state method was used for our measurements at low temperature. A heat flux \dot{Q} flows along the sample of cross-section A . Thermometers are attached at two places along the crystal, a distance ℓ apart, and the temperature difference ΔT between them is measured. Provided $\Delta T \ll T$, where T is the average temperature, the thermal conductivity K is given by

$$K(T) = \frac{\ell \dot{Q}}{A \Delta T}$$

The distance between the two thermometers is measured using a travelling microscope. Because of the finite width of the thermometer contacts, the precision on this measurement is typically 5% (for $\ell \sim 1$ cm). A is determined by means of a micrometer but to only $\sim 1\%$ due to non-uniformity of the sample. The heat flux \dot{Q} and the difference in temperature ΔT are known much more accurately and the overall precision on an absolute measurement of $K(T)$ is $\sim 6\%$. This systematic error can be worse for small samples.

1.1.2 Cryostats and Magnets

1.1.2.1 Cryostats

The measurements were made using cryostats already described in previous work (e.g. Brown 1971, Ghazi 1978). Figure 1.1 shows schematically the experimental chamber used for the thermal

conductivity dependence on temperature and magnetic field, in the temperature range 1 - 4 K. The sample is clamped to a hollow copper rod in which liquid helium has access, thus providing a good heat sink. The 'pot' is filled with liquid helium through a needle valve and its temperature can be lowered down to 1 K by pumping on it. Heating of the sample may be done with one heater coil which consists of ~ 5 feet of non-inductively wound 44 SWG Evanohm wire. The sample holder, thermometers and 'pot' are enclosed in a brass vacuum jacket with a narrow tail which fits in the bore of a superconducting magnet. Details on the magnets used in this work will be given later. The space available for work is rather restricted and great care has to be taken to avoid thermal shorts of the wires. The vacuum jacket is supported by the pipework and immersed in liquid helium contained in a British Oxygen stainless-steel dewar.

Conductivity measurements above 4 K were performed in a 'dipstick' apparatus designed by Brown. This dipstick could be immersed in a helium vessel and was very practical for determination of $K(T)$ in the temperature range 4 - 20 K. The experimental cell is shown in Fig. 1.2. The sample holder is in thermal contact with the helium bath via a spectroscopically pure copper post. We could heat up the system above 4 K with the auxiliary heater and the absolute temperature is given by a germanium thermometer. The whole assembly is enclosed in a brass jacket. Mounting of samples was easier in this dipstick than in the 1 - 4 K apparatus.

1.1.2.2 Magnets

Two superconducting magnets were used during the course of the present work:

(i) A 55 kG Helmholtz coil, manufactured by Oxford Instruments Co. The coils were wound with niobium-titanium (NbTi) multifilament wire. It has a built-in magnetoresistance probe calibrated by the manufacturers - ($H/I = 1.29 \text{ kG/A}$, $I_{\text{max}} = 42.49 \text{ A}$). The current from a 12 V lead-acid battery is passed through the probe in series with a 500Ω standard resistor and the field is calculated from the voltage and current values using a computer program written by D.L. Williams. This program extrapolates between calibration points. At high fields a precision of 0.05 kG could be obtained.

(ii) A 130 kG split pair, made by the Intermagnetics General Corporation and supplied by the Oxford Instruments Co. The superconductor is niobium-tin (NbSn) and the maximum current 162 A. A constant current of 50 mA is passed through a built-in probe and the field is calibrated against the magnetoresistance ratio $R(H)/R(0)$.

In each case the magnet current is swept linearly with time from zero to a preset maximum value and the voltage across the standard resistor is used to drive the X-axis of an X-Y chart recorder.

1.1.3 Thermometry and Measuring Technique

1.1.3.1 Mounting of thermometers

The temperature difference ΔT across the sample was measured with Allen-Bradley carbon thermometers. These were calibrated each run against either helium vapour-pressure (1958 scale) in the 1 - 4 K range or a pre-calibrated germanium thermometer in the 4 - 20 K range.

In previous work on magnetothermal conductivity of p-Ge (Haseler 1976) the thermometers were bound to the sample using a single turn of 28 SWG copper wire wound tightly around the specimen and maintained

in place with an epoxy resin (Stycast 2850 FT, catalyst 24 LV). However, it was suggested by Tokumoto and Ishiguro (1976) that this way of mounting the thermometers (Fig. 1.3(a)) could induce serious stress effects, making the data unreliable. To check on this we designed new spring loaded clamps schematically shown in Fig. 1.3(b). A bronze-beryllium leaf spring is used to exert a controlled force on one face of the sample. The leaf is bent at its two ends with 14 BA nuts. The two faces of the clamp are tinned with indium ensuring a good thermal contact between the sample and the thermometer which is soldered at one end of a 20 SWG copper wire, the other end being soldered to one face of the clamp. Most of this work was carried out using these clamps but we did not find any difference from the results using copper wire-stycast collars. The GaAs, GaP samples were more brittle than the Ge, Si ones and we found that one sample, GA735(e), had cleaved after applying uniaxial stress. The cleavage occurred at the thermometer bond and we changed the way the copper wire was twisted, making sure it was not in close contact with the four edges of the sample (Fig. 1.3(c)). M. Locatelli and B. Daudin (Note SBT No. 510/79) designed clamps to be used with very small or brittle samples. One such clamp shown in Fig. 1.3(d) was used by Locatelli in the measurement of GA735(e) in the temperature range 50 mK - 2 K.

1.1.3.2 Measuring technique and calculation of thermal conductivity K(T)

An automatic low noise ratio arm bridge supplied by Automatic Systems Laboratories Ltd (ASL) was used to measure the resistances of the Allen-Bradley carbon thermometers. The two fixed arms were inductors so that a better sensitivity than in a conventional

bridge using resistors could in principle be obtained since the sensitivity should then be limited by the noise generated in the resistances being measured and these were at liquid helium temperatures. In practice the noise was larger than this; this is discussed in section 1.1.3.3.

The temperature differences across a sample are determined by measuring the resistance of one thermometer and the difference in resistance between the two. This procedure reduces the error due to drifts in the mean temperature of the two thermometers (Challis 1961).

The bridge measures and displays in a digital form the ratio:
$$f = \frac{R_a}{R_a + R_b}$$
 where R_a and R_b are the resistances being measured. The wiring of the thermometers to the bridge via a switch box was such that two ratios could be displayed:

$$f_1 = \frac{R_F}{R_1 + R_F}$$
$$f_{12} = \frac{R_1}{R_1 + R_2}$$

where R_1 is the thermometer near to the heat sink

R_2 is the thermometer near to the heat source

R_F is a fixed resistor, thermally anchored to the heat sink.

A calibration of f_1 and f_{12} against temperature at ~ 20 points in the range 1 → 4 K or 4 → 20 K was made each run. For each conductivity point we would note the values of f_1 , f_{12} together with the current I through the heater coil and the voltage V across it, for the heater power. The data were analysed using a computer program based on one first developed by Challis (1961). A least squares procedure was used to fit the calibration data to the interpolation formulae:

$$T = \frac{A}{R - \Delta} + B, \quad 1 \leq T \leq 4.2 \text{ K}$$

$$R_{12} = R_1 - R_2 = C_0 + C_1 R_1 + C_2 R_1^2$$

where A, B, C_0, C_1, C_2 are constants chosen to give the best fit. The fit was satisfactory only over a restricted temperature range and it was found necessary to split the data into four ranges.

The temperature difference used in the calculation of the thermal conductivity is given by:

$$\Delta T = \left(\frac{R_{12} - R_{12}^0}{\frac{dR_1}{dT} - \frac{1}{2} \frac{dR_{12}^0}{dT}} \right)_{T_0}$$

where R_{12}^0 is the value of R_{12} at the mean temperature $T_0 = T_1 + \frac{1}{2}\Delta T$. For the thermometers used in the present work, a "matched pair", $\frac{1}{2} \frac{dR_{12}^0}{dT} \ll \frac{dR_1}{dT}$ and the error in ΔT is mainly due to the error in dR_1/dT . An iterative procedure is used to determine ΔT and T_0 .

A similar procedure was used for the data above 4.2 K except that the interpolation formula used for the temperature dependence of the resistance of the carbon thermometers was:

$$\frac{1}{T} = A + B \ln R + C (\ln R)^2$$

where A, B and C are constants.

1.1.3.3 Magnetothermal conductivity measurements

The change in thermal conductivity when applying a magnetic field B was monitored at fixed temperature, between 1 and 4 K. To avoid magnetic field effects on the thermometers themselves, these were mounted away from the centre of field (~ 24 cm) and shielded with niobium foil.

From the expression for the temperature difference we can write:

$$\Delta T \propto R_{12Q} - R_{12}^0$$

where R_{12Q} is the difference in resistance of the two thermometers, at a mean temperature T_0 , with heater power on and R_{12}^0 is the difference in resistance of the two thermometers without any heat flux through the sample, evaluated at the same mean temperature. It can be shown that for small ΔT :

$$W \propto f_{12Q} - f_{120}$$

where W is the thermal resistance and f_{120} is the value of f_{12} without heat flow.

$$\text{Then } \frac{W_B}{W_0} = \frac{f_{12QB} - f_{12OB}}{f_{12QO} - f_{12OO}}$$

where $f_{12OB} = f_{12OO}$.

In the experimental procedure the out-of-balance signal ΔV from the bridge is monitored as the magnetic field is swept. Now for small changes

$$\Delta V \propto f_{12QB} - f_{12QO}$$

so that

$$\Delta V \propto \frac{(f_{12QB} - f_{12OB}) - (f_{12QO} - f_{12OB})}{f_{12QO} - f_{12OO}}$$

i.e.

$$\Delta V \propto \frac{W_B}{W_0} - 1$$

The out-of-balance signal ΔV which is fed to the Y-axis of an X-Y recorder is then directly proportional to the fractional change in thermal resistivity $(W_B - W_0)/W_0 \equiv \Delta W/W_0$ due to the magnetic field. When the effect is small $\Delta V \propto -\frac{K_B - K_0}{K_0}$ ($K = 1/W$, $K_0 \approx K_H$).

The level of noise associated with the measurements was found to vary from run to run and is believed to be noise caused by the vibrations of the thermometers, probably due to the pumping system. Changes in conductivity down to $\sim 8 \times 10^{-5}$ could be detected, although on some occasions this would increase to $\sim 7 \times 10^{-4}$. With an improved mounting system this has very recently been reduced to $\sim 5 \times 10^{-6}$. A detailed discussion of the noise present, is given in Wybourne et al (1979).

Most of this work was carried out using the 55 kG split coil magnet. Large 'spikes' in the $\Delta W/W_0$ plots used to occur when sweeping the field to its highest value. These 'bursts' are believed to be due to flux jumps in the filaments or mechanical movement of the wires or coils. These would probably produce small sharp field steps which could affect the system in two ways. Rapid magnetization of the paramagnetic sample would cause it to heat up, thus destroying the thermal equilibrium. The other effect could be the occurrence of Eddy currents in the thermometer leads which would heat up the thermometers directly.

1.1.4 Measurements Under Uniaxial Stress

1.1.4.1 Introduction

The stress work was carried out at Centre d'Études Nucléaires, Grenoble, in collaboration with Dr. B. Salce. Previous thermal conductivity measurements under stress at CENG were performed by B. Salce on $\text{Al}_2\text{O}_3:\text{Ni}$ (Salce and de Goër 1979). S. Haseler measured the piezothermal conductivity of p-Ge using Salce's apparatus (Challis and Haseler 1978).

Salce was faced with the same problems of the mounting of the samples when he tried to look at systems other than Al_2O_3 (Salce 1978). He then designed a new compressional apparatus where the system for applying uniaxial stress was not at room temperature but at liquid helium temperature. The design requirements and details concerning the construction of the apparatus will soon be published by B. Salce and we shall here only very briefly describe the experimental set-up.

1.1.4.2 Mounting of sample and application of stress

The experimental cell consists of a cage (Fig. 1.4) made of two parallel planes connected by three stainless-steel rods, ensuring the rigidity of the whole assembly.

The sample is maintained between two copper blocks with a generous amount of silicon grease. In previous calibration measurements on cylindrical Al_2O_3 samples, Salce fitted these in holes drilled in the copper pieces and of diameter slightly bigger than the samples diameter. He used silicon grease for thermal contacts and this way of bonding the samples proved to be very satisfactory. When cooled down to helium temperatures the grease solidifies and acts as a mould for the sample, giving good mechanical support when the stress is applied. The upper copper block is movable and we can orientate it relatively to the lower one to make the two faces parallel. We did not experience any problem of parallelism of the two planes. Care has also to be taken to make sure the sample ends are flat and parallel.

The force is given by a piston enclosed in stainless-steel bellows and operated with pressurized pure helium-4 gas which is

brought in through a capillary. The cross-section of the piston is such that a maximum force of ~ 250 kgf can be reached. When helium gas is admitted into the bellows the flat end of the piston comes into contact with the copper block and the force is transmitted to the sample through this copper block.

During a stress sweep we monitor the change in helium gas pressure in the capillary and at the same time the variation of the force exerted on the sample, the two variations following each other. The force is measured using a 'capacitor-stress-gauge' which is introduced at the base of the cage. It has a ring shape and the lower copper block which is in contact with the sample is machined to fit inside the ring and at the same time press the top face of it (Fig. 1.4). The contact copper-stress-gauge is again made with silicon grease. The change in capacitance is measured by a bridge, the output of which drives the X-axis of an X-t chart recorder. The setting of the chart-recorder is such that a force of 10 kgf displaces the pen by 1 cm, thus allowing us to read directly the magnitude of the force on the sample. Knowing the cross-section of the sample, the value of the stress is then determined in a straightforward manner. At the beginning of a sweep the bellows are pumped down and we know exactly when there is no force on the sample: the pressure in the capillary keeps decreasing while the response from the 'capacitor-stress-gauge' remains unchanged after the piston has moved away from the upper copper piece. The bridge is then set to zero.

1.1.4.3 Measurement of thermal conductivity under stress

The upper copper block is used as a secondary heat sink with copper wire thermal shunts connected to the primary heat sink in contact with the helium bath. This enables us to raise the sample temperature to ~ 20 K with a reasonably low dissipation of heat. The helium bath can be pumped down to ~ 2 K using a rotary-diffusion pumping system. The working lower temperature is then ~ 2.3 K although we could work at an even lower temperature by switching a 'booster' pump on.

All the stress measurements were taken at constant temperature. The cold thermometer, which is an Allen-Bradley carbon resistor, is kept at a constant temperature using an SEIN temperature controller (see section 2.6). It forms one arm of the bridge, the other arm being a decade resistor at room temperature with which we set the temperature we want to work at. The hot thermometer is a calibrated germanium resistor, the resistance of which is read on a DVM. The measurement of the conductivity $K(\sigma)$ at a particular value of stress σ involves the reading of the value of the germanium resistance with (R_Q) and without (R_0) heat flux through the sample, the value of the force on the sample and the value of the main heater power (I and V). It may be shown that since the temperature of the cold thermometer does not vary, the thermal conductivity of the sample is inversely proportional to $T(R_Q) - T(R_0)$. $T(R_Q)$ and $T(R_0)$ are determined from the germanium resistances R_Q and R_0 . R_0 should remain constant during the stress sweep but any slight drift is accounted for in the computer program which calculates $(K(\sigma) - K(0))/K(0)$ where $K(0)$ is the conductivity without stress.

For each temperature the slope of the $K(T)$ curve is also fed into the computer program.

We first measure $K(0)$ and then progressively apply the stress in steps, each time awaiting the return of thermal equilibrium. In the first run, the sample was not in good enough thermal contact with the heat sink, at low values of stress, giving rise to long time constants for equilibrium. In the subsequent runs the thermal contacts were via the silicon grease but also thermal shunts made of copper sleeves. These shunts were attached to the sample ends with stycast and connected to the secondary heat sink and to the base of the cage (Fig. 1.4). The auxiliary and main heaters were also removed from the copper blocks and soldered to the sleeves. We also found it was better to put the stress to its highest value and then decrease it. The thermal time constants are then shorter than when the stress is gradually increased from zero. The sweep-up results and sweep-down ones were not found to change significantly. For all the samples measured the heat leak through the base of the cage and the stainless-steel rods is negligible but steps are taken by Salce to completely null this heat leak which can be important for samples having a very low thermal conductivity.

1.2 THERMALLY DETECTED ELECTRON PARAMAGNETIC RESONANCE

1.2.1 Introduction

In this section the thermal detection spectrometer used in the study of p-Ge and p-Si is described. A simple experimental arrangement was designed and constructed. Microwaves from a

klystron source are directed onto a sample mounted in an evacuated section of the waveguide. The sample is maintained at liquid helium temperatures by a small heat leak to the bath via thermometer leads. The sample holder is in the intense region of the field produced by a superconducting magnet. The change in resistance of the thermometer due to the heat arising in the sample after resonant absorption of microwaves is monitored using phase-sensitive detection. The spectrometer can be operated at X-band frequencies, using magnetic field up to 13 T.

1.2.2 Sample Holder and Microwave Circuits

The spectrometer is based on those previously used by Clark (1975) and Knowles (1976) in this department.

The sample holder employed in this work is essentially a short circuit termination of the waveguide (Fig. 1.5). It satisfies both requirements of thermally isolating the sample from the helium bath and preventing microwave power reaching the thermometer.

The sample is stuck with a small amount of GE varnish onto a single crystal quartz rod which conducts heat from the sample to the thermometer. The piston which holds the quartz rod is choked (Knowles (1976)) to avoid leakage of the microwaves to the thermometer. Single crystal quartz rods are used for their good thermal conductivity and small specific heat at helium temperatures (see section 2.3.2). The 'melinex' plastic supports the cylindrical rod. A triangular hole is cut into the sheet so that we have point contacts and thus a small heat leak to the helium bath. The length, diameter of the rod and associated

hole in the piston are chosen so as to cut-off the microwaves. The rod is 50 mm long, with a 3 mm diameter and the corresponding hole in the piston is 4.5 mm. The bottom plate is sealed to the cylinder with indium wire (1 mm diameter).

One of the advantages of thermal detection of EPR is the simplicity of the microwave circuits. The microwave source is a 50 mW klystron operated at a frequency of 9.6 GHz. The essential elements (Fig. 1.6) are a waveguide from microwave source to sample, with frequency and power measuring facilities. In order to increase the power available at the sample a sliding stub tuner is used. This can make the length of waveguide between the tuner and the sample holder into a resonator with a Q of up to about 1000.

1.2.3 Bolometer Arrangement

The change in temperature of the sample assembly is monitored using a carbon resistance thermometer. The sensitivity requirements (see section 2.3.2) for thermal detection are such that the thermometer should have a small specific heat and be in good thermal contact with the quartz rod. The thermometer is made by painting a thin layer of carbon paint (Acheson 580) on the quartz rod, between two foil leads. The room temperature resistance is about 400 Ω . The aluminium foil leads (~ 4 mm x .5 mm x .01 mm) are attached to the quartz rod and to two copper wires with spots of conducting silver paint (Dupont 4666). The copper wires are soldered to glass metal seals. The heat leak to the helium bath is controlled by the dimensions of the Al foil leads. In our experiments at 4.2 K, the thermometer time constant is 1 to 2 s. It has a measured $\left(\frac{1}{R} \frac{dR}{dT} \right)$ of $\sim 0.09 \text{ K}^{-1}$, and a change in temperature of 1 mK could easily be detected (see section 2.3.2).

One problem in using carbon films as bolometers is the effect of the DC magnetic field on their resistances. A magneto-resistance plot is shown in Figure 1.7, and it is desirable to flatten this baseline if we want to detect small changes in temperature. For this purpose another carbon film which has about the same room temperature resistance as the bolometer, is painted on a glass rod situated in front of the quartz rod. The resistances of the carbon films form two arms of an A.C. bridge and the difference in the two signals can be monitored. Figure 1.7 also shows a baseline when this set-up is used.

1.2.4 Thermometer Bridge

An inductive ratio bridge (1 : 1) was constructed to monitor the change in resistance of the carbon thermometer. We use an A.C. bridge as to avoid problems with thermo-electric effects which can be important with a D.C. bridge, at the small levels of input power ($\sim 10^{-7}$ W).

A Hewlett-Packard 204D oscillator supplies the power to the bridge and also the reference signal to a Brookdeal 9503 lock-in amplifier (Fig. 1.8). The bridge is operated at a 2.5 kHz frequency which is the resonance frequency of the inductance. The inductors are made of a centre tapped 1000 turns coil wound with 36 SWG copper wire on a ferrite 'pot' core. R_b , the resistance of the bolometer, is in parallel with a variable capacitor (~ 200 pF). This accounts for the stray capacitance of the variable resistance R and of the leads. As mentioned in the previous section, R can be replaced by the resistance of another carbon film at helium temperature. At balance $R_b = R$ and any out-of-balance signal is

amplified and phase sensitively detected. The D.C. output of the PSD is then used to drive the Y axis of a chart recorder.

1.2.5 Cryostat and Magnets

The spectrometer was designed to try to observe EPR lines with very small g -values (see section 2.3.1). For this we had to use high magnetic fields for the range of frequency available (X-band).

The sample holder was machined to fit in the bore of the available 55 kG split coil magnet or the 130 kG one, already described in section 1.1.2. All the runs were done using the stainless-steel Oxford Instrument cryostat.

To prevent significant heat losses from the sample assembly other than through the aluminium foil leads it is necessary to maintain a portion of the waveguide and the thermometer chamber under vacuum. A vacuum of about 10^{-5} torr is obtained using a mercury diffusion pump backed by a rotary pump.

1.2.6 Temperature Control

In two runs the temperature of the system was lowered to ~ 1.9 K by pumping on the helium bath. The bath temperature could be stabilized using a temperature controller supplied by Société d'Électronique Industrielle et Nucléaire (SEIN).

An Allen-Bradley carbon thermometer was fixed to one of the tubes supporting the magnet, in the helium bath, away from the magnetic field. It formed the fourth arm of a Wheatstone Bridge circuit, two arms of which are fixed 100Ω resistors. The bridge

was balanced using a decade resistance box. The off-balance signal was amplified and used to control the power supplied to a wire wound coil auxiliary heater, also placed in the helium bath.

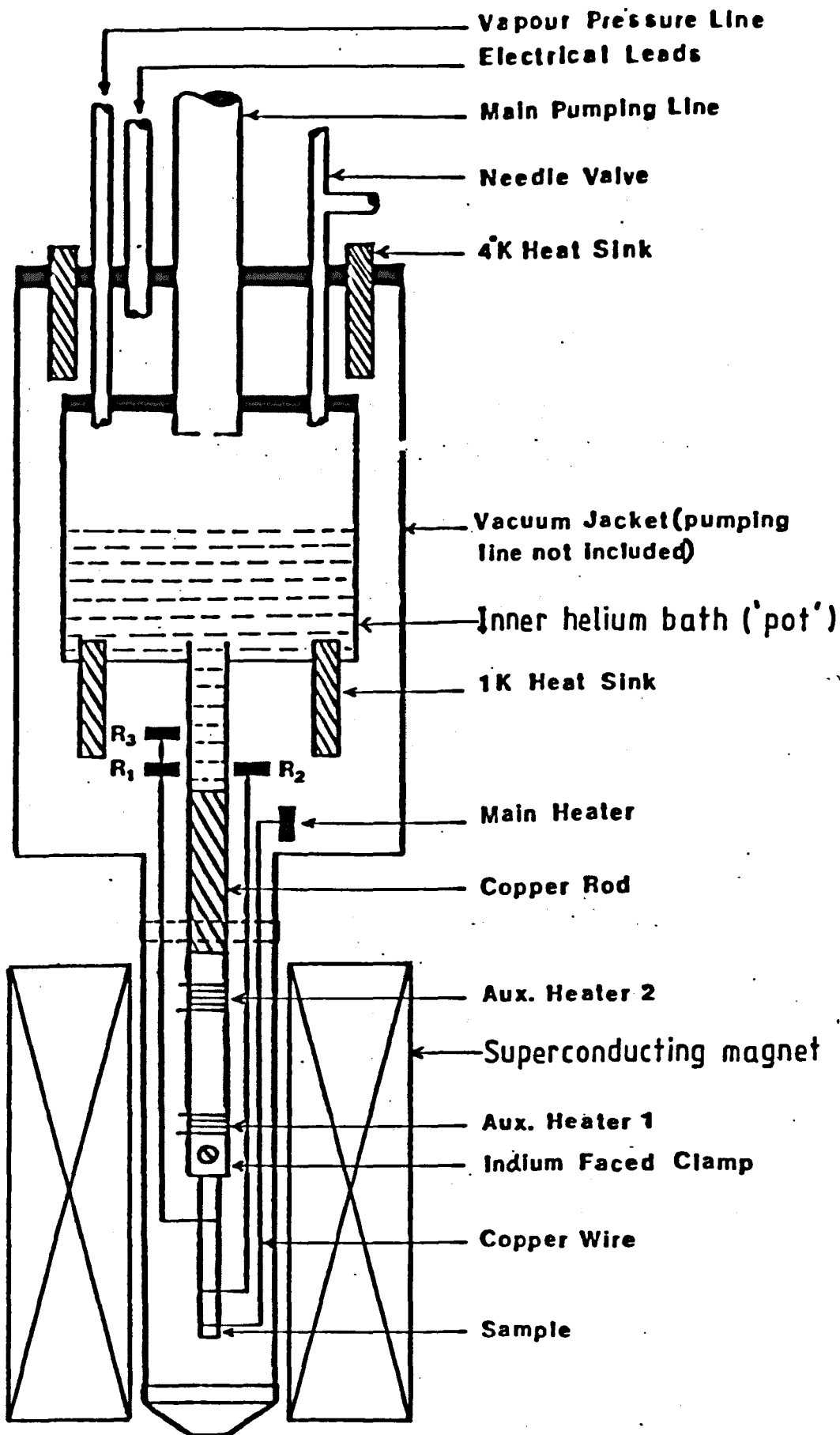


FIGURE 1.1 Cryostat for conductivity measurements between 1 and 4 K, and magnetic field measurements.

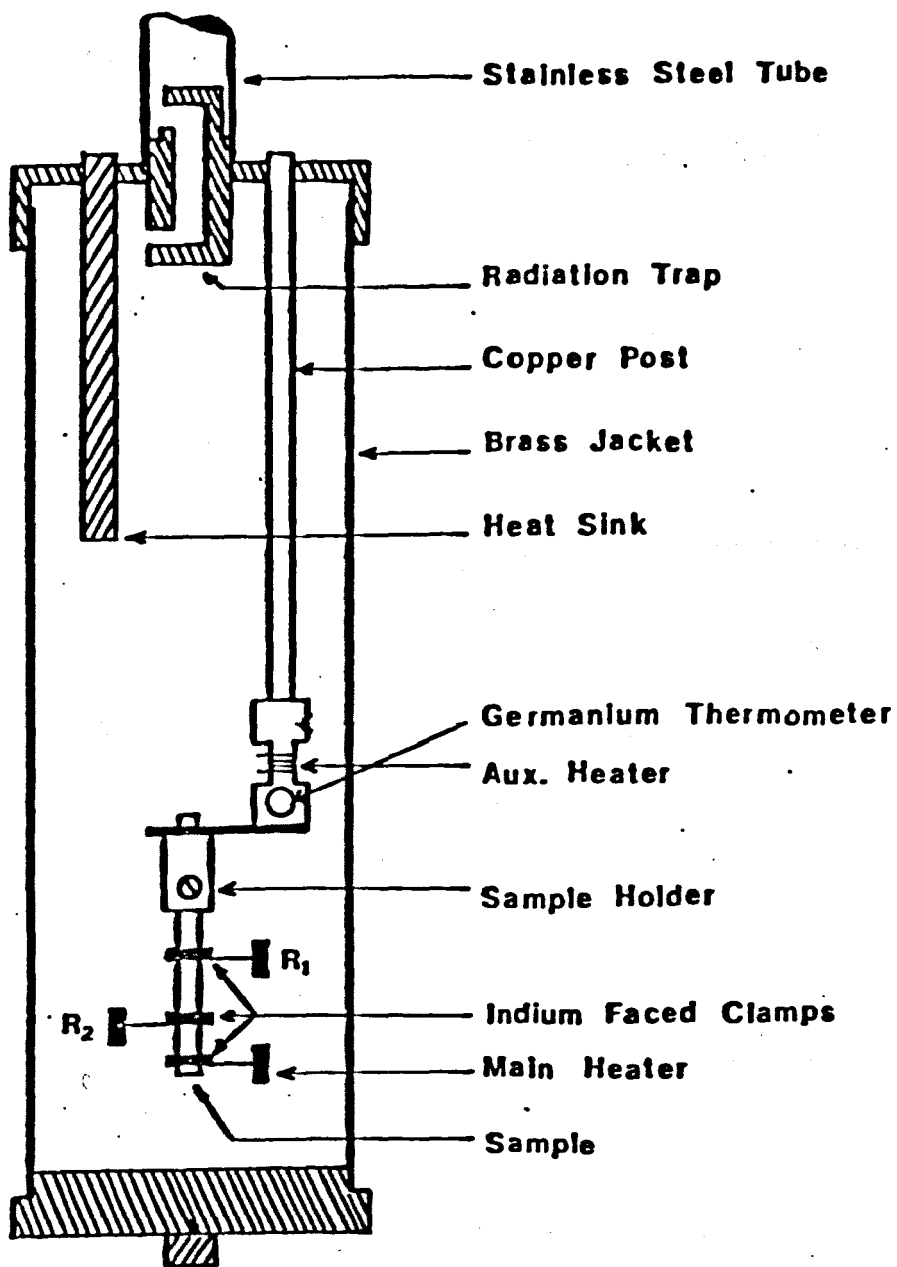


FIGURE 1.2 *Experimental chamber for conductivity measurements above 4 K.*

(From Ghazi 1978).

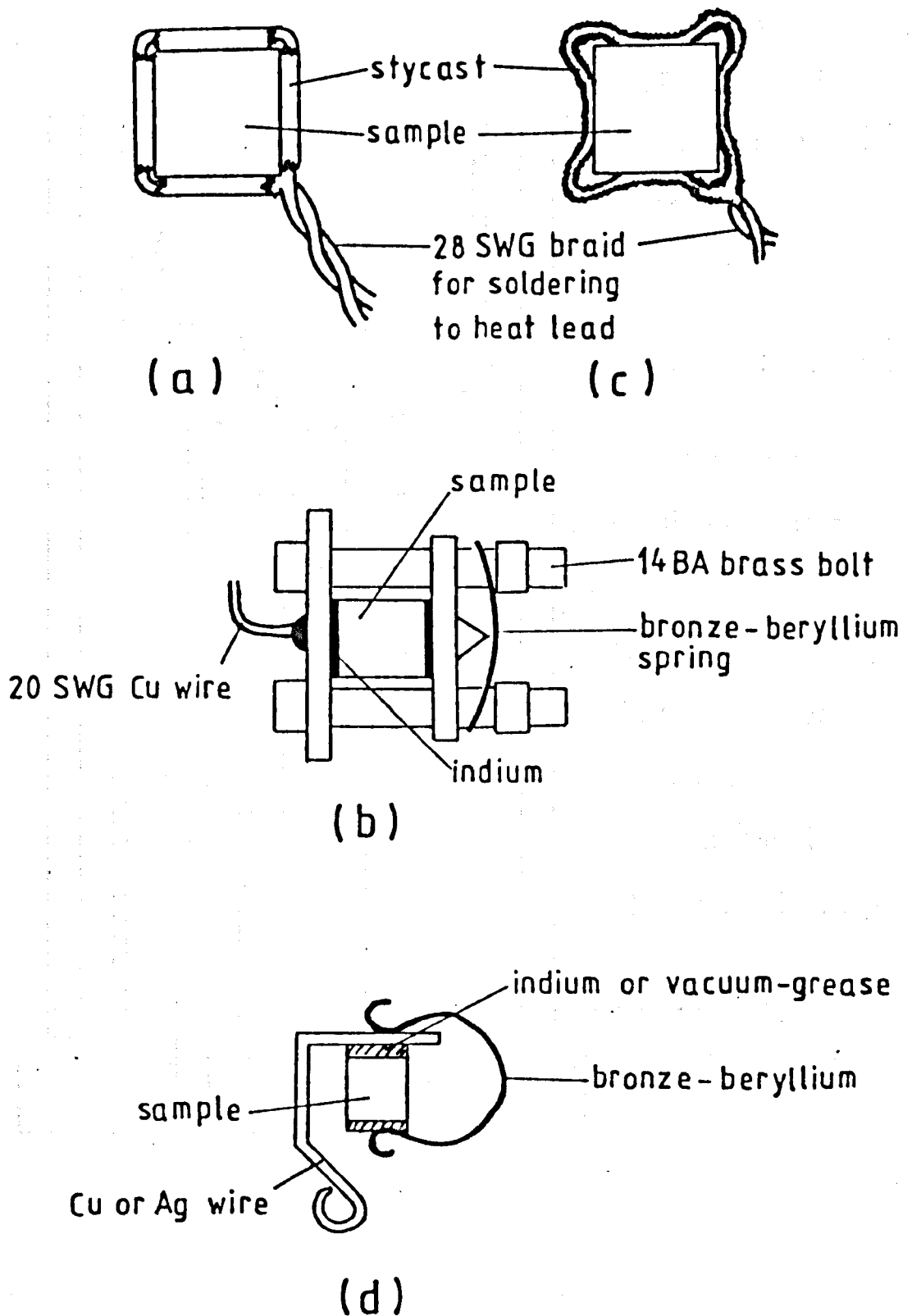


FIGURE 1.3 Thermometer contacts.

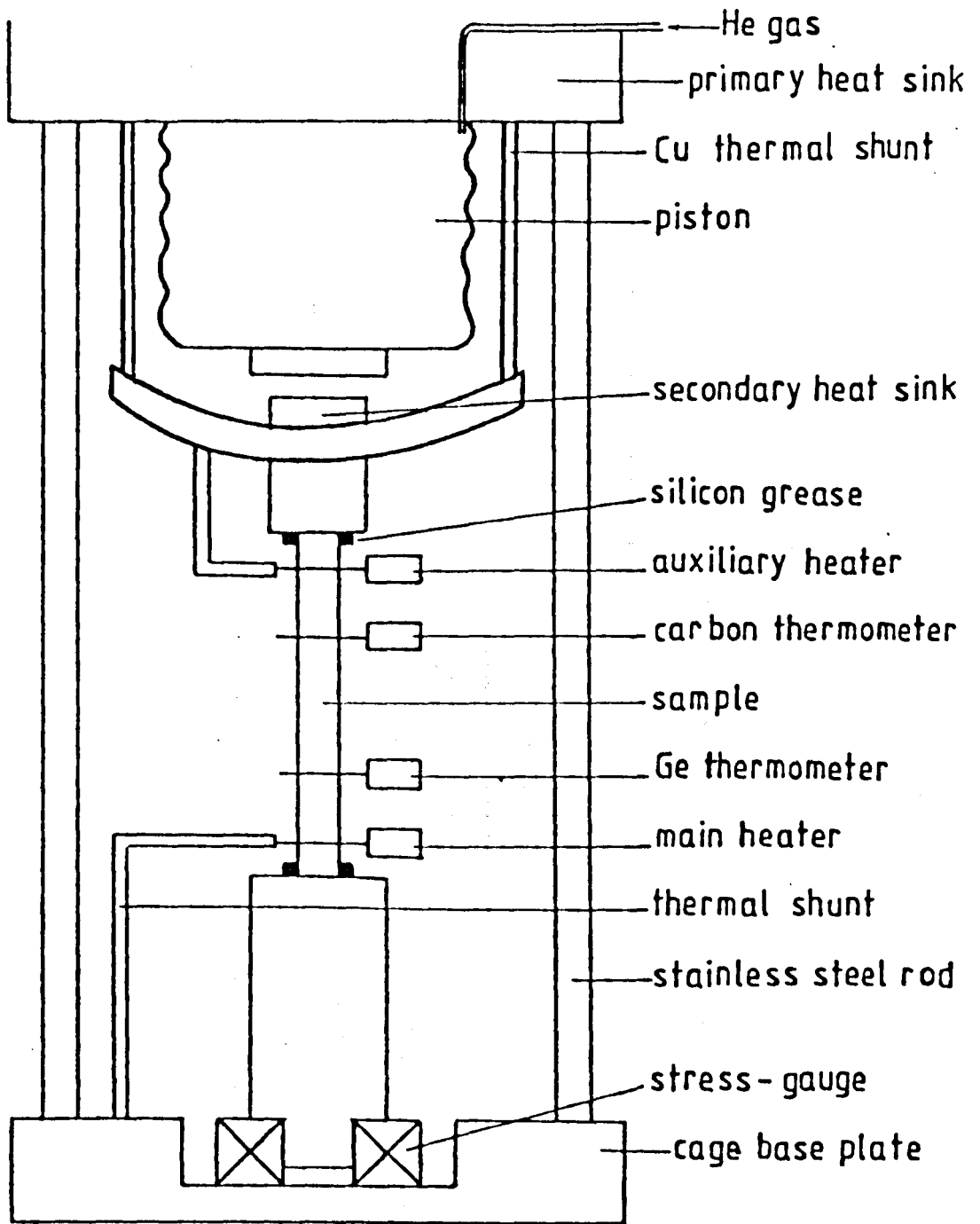


FIGURE 1.4 Stress apparatus.

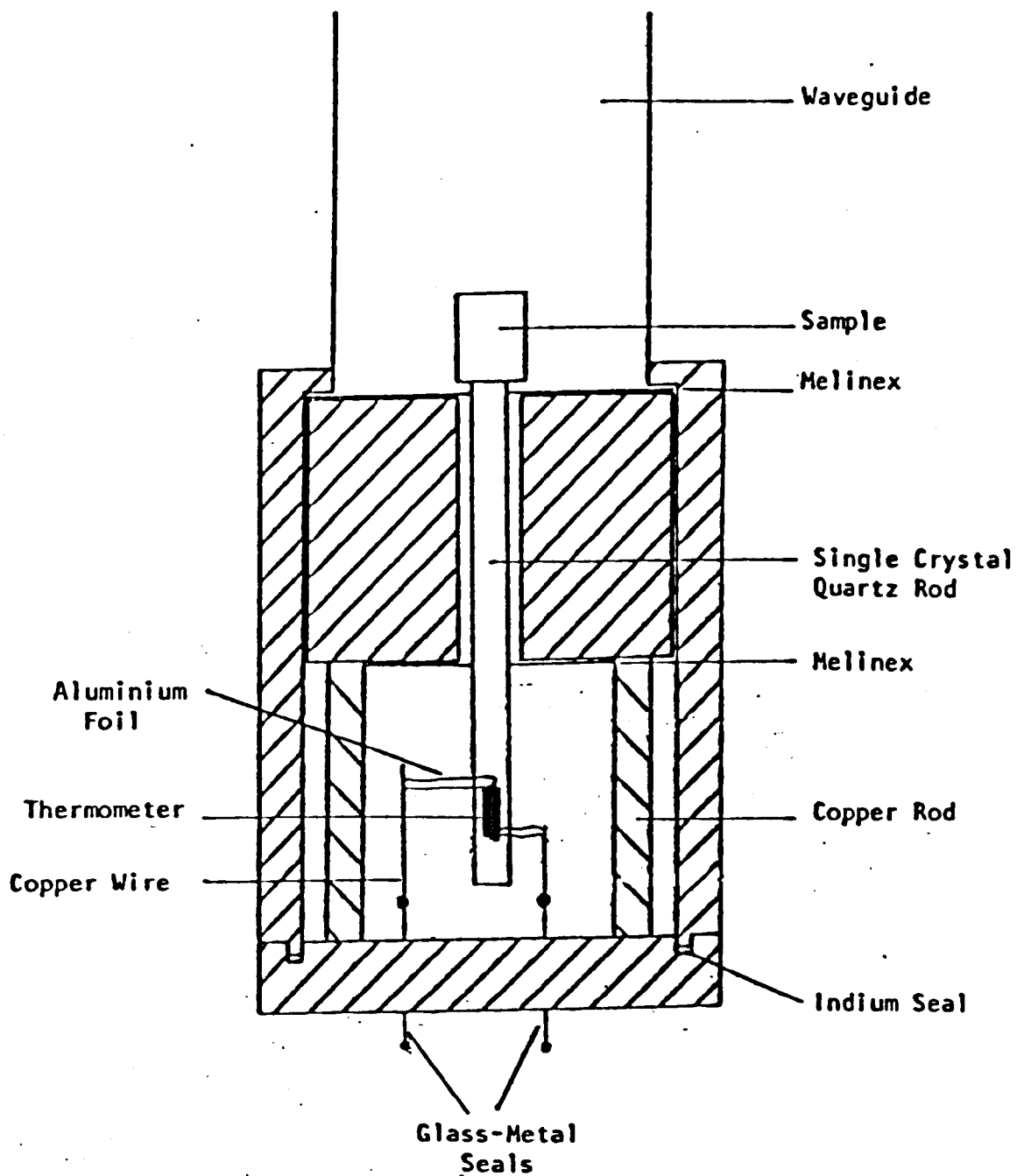


FIGURE 1.5 TDEPR sample holder.

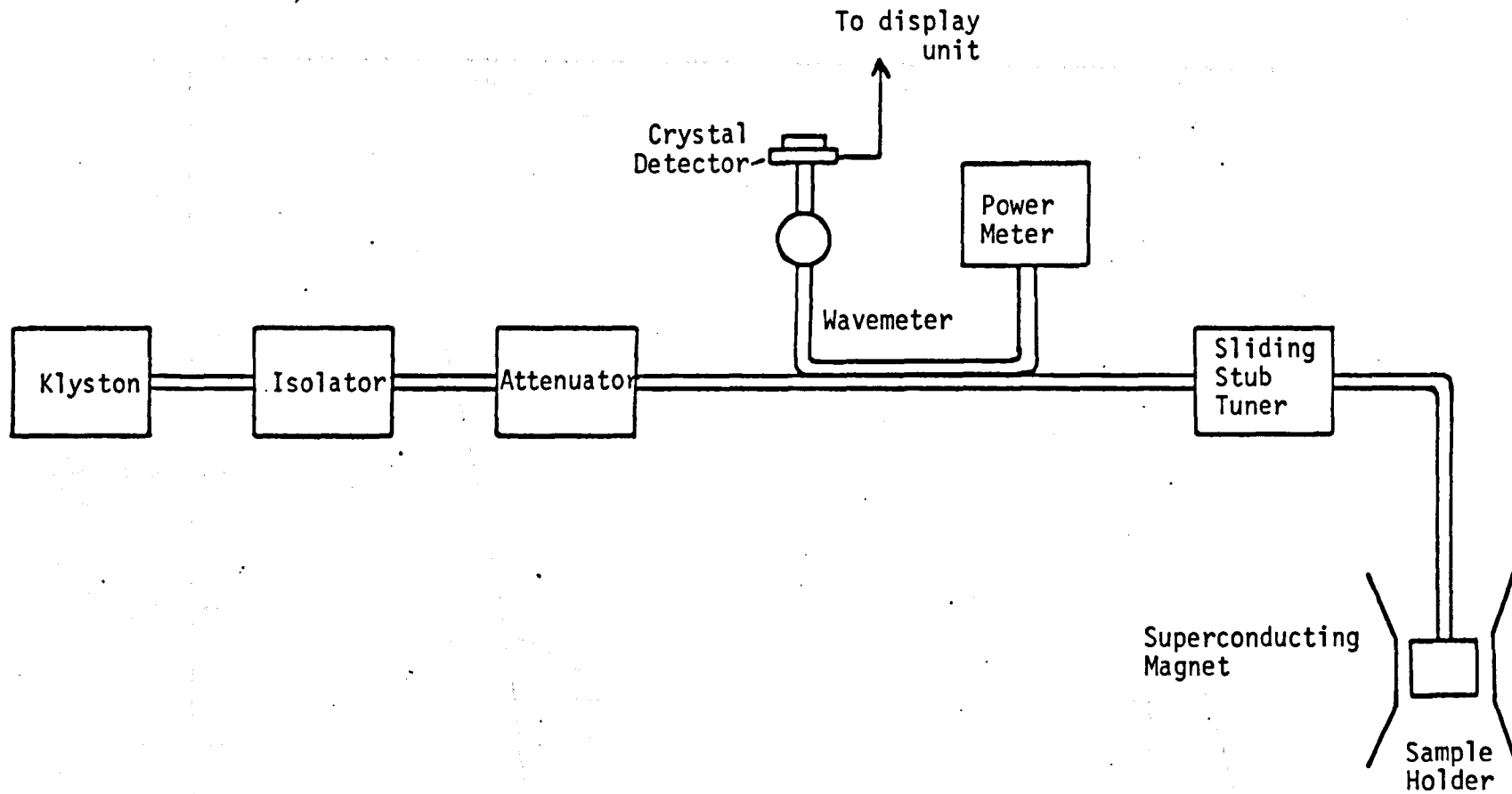


FIGURE 1.6 *Microwave Circuit.*

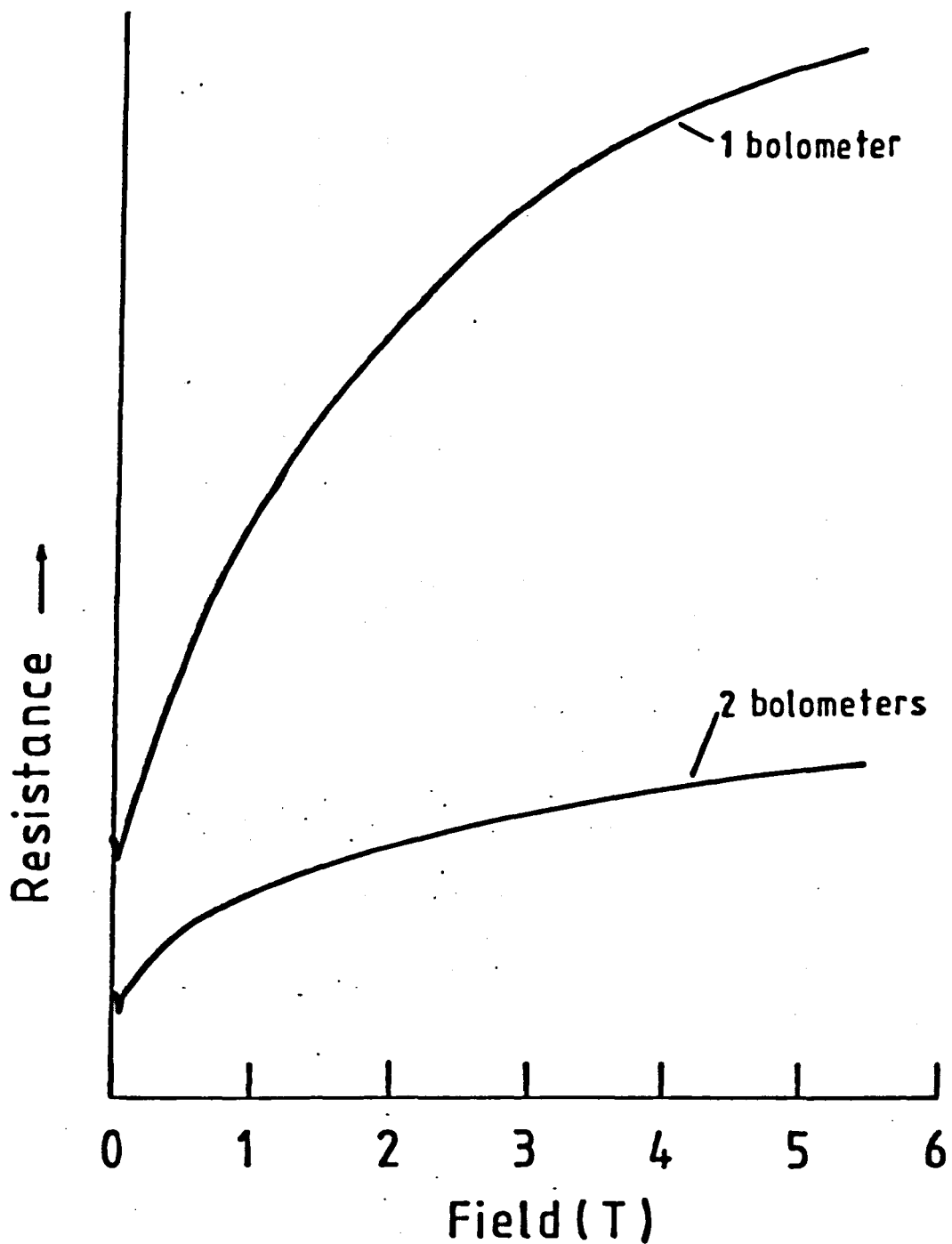


FIGURE 1.7 *Magneto-resistance of carbon film.*

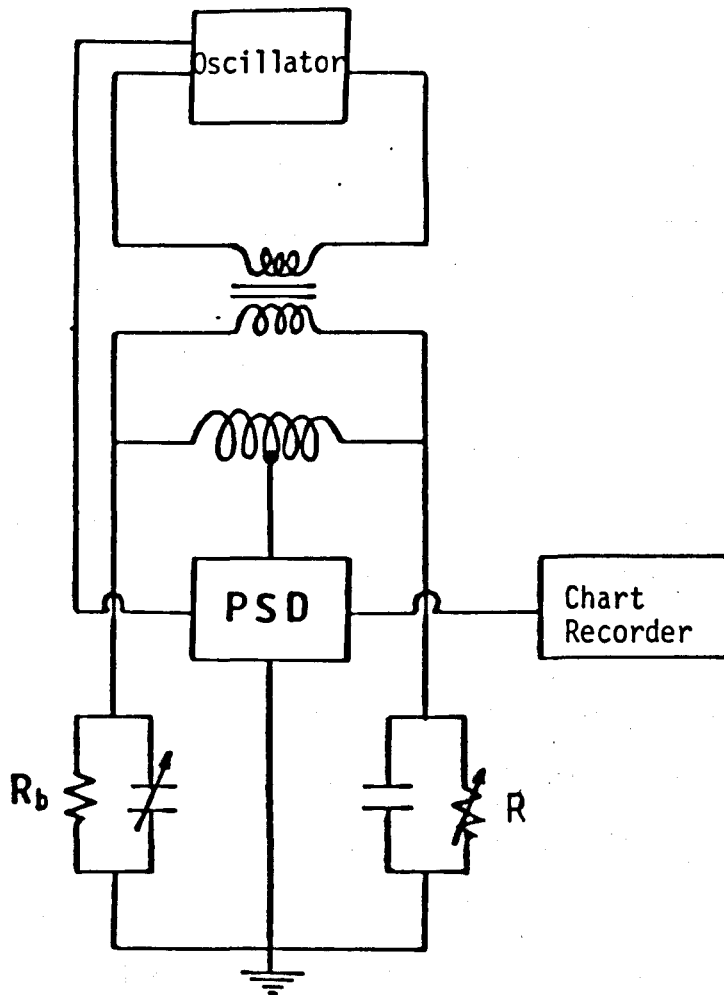


FIGURE 1.8 Thermometer bridge.

CHAPTER 2

SHALLOW ACCEPTORS IN Ge AND Si

2.1 INTRODUCTION

The work described in this chapter is part of an investigation of the acceptor ground state in Ge and Si using thermal conductivity techniques, as well as Thermally Detected Electron Paramagnetic Resonance (TDEPR).

In undistorted sites the acceptor ground states of Ge and Si are both fourfold degenerate (Γ_8). Early magnetothermal conductivity measurements by Challis and Halbo (1972) showed however that the ground state structure in Ge differed considerably from theoretical prediction and from this and other evidence, the authors suggested that could be the result of a dynamic Jahn-Teller distortion. In section 2.2 our contribution to a further study of the ground state of acceptors in Ge by high field magnetothermal conductivity measurements is presented (Challis et al 1978). From that investigation it was concluded that the anomalous phonon scattering between Zeeman split levels of the acceptor ground state was the result of very small spectroscopic g -values. However this is not now thought to be the result of a Jahn-Teller effect.

In an attempt to check on that and also on the ground state of p -Si, a TDEPR spectrometer was designed and constructed

(section 2.3). Early conventional EPR measurements had failed to detect any resonance from acceptors in Ge and resonance could only be detected in p-Si which had been uniaxially strained (Feher et al 1960). It was hoped that Thermal Detection of EPR which is a technique more suited for systems which are strongly coupled to the lattice would allow a direct determination of the ground state g-values (section 2.3).

2.2 HIGH-FIELD MAGNETOTHERMAL CONDUCTIVITY OF p-Ge

2.2.1 Introduction

Most of the experimental data reported in Challis et al (1978) was measured by Haseler (1976). The aim of our measurements was to check on possible strain effects due to the way of mounting the thermometers, and also to study possible differences due to different field orientations. The results are presented in section 2.2.2. At this stage it is worth summarizing the zero-field work (Challis et al 1977).

The low temperature thermal conductivity of three Ge samples doped with either Ga or In in the concentration range 5×10^{14} to $\sim 10^{16} \text{ cm}^{-3}$ was measured down to 50 mK. The phonon scattering above $\sim 1.5 \text{ K}$ could be accounted for quite well by considering an elastic-non-resonant process for the transitions within the fourfold degenerate Γ_8 ground state. Below this temperature however it was found necessary to add a resonant scattering term in the calculation of the thermal conductivity to obtain reasonable agreement with the experimental data. A Gaussian distribution of splittings of width $\sim 30 \text{ GHz}$ for the split quartet states was

introduced in the relaxation rate. The authors then suggested only about half the acceptors appeared to fall within that distribution, the other half having splittings $\lesssim 4$ GHz. This 'two-site' model for p-Ge would then reconcile the thermal conductivity results and the results obtained by optical absorption and magneto-acoustic measurements (Challis et al 1977). A similar model was recently used to account for the effect of internal strains on thermal-phonon scattering in Li-doped Si at low temperatures (Adolf et al 1980). It was assumed ~ 20% of Li donors were in distorted sites represented by a Gaussian distribution of splittings of width ~ 50 GHz.

Recent work on 'ultrapure' germanium (net-acceptor or net-donor concentration $< 10^{11} \text{ cm}^{-3}$) has shown the existence of several new shallow levels in the band gap (Haller et al 1980). Photothermal ionization spectroscopy (PTIS) has been used by the authors for the study of hydrogen-related acceptor-complexes. In less pure samples, complexes of the same sort could also be present in higher concentrations and could influence the low-temperature phonon scattering.

2.2.2 Magnetic Field Effect on the Low Temperature Phonon Scattering

The measurements, in the temperature range 1 - 2 K were taken up to 13 T using the IGC magnet (Chapter 1). The results for $B \parallel [001]$ are shown in figures 2.1 and 2.2 for two Ga-doped samples ($1 \times 10^{14} \text{ cm}^{-3}$ and $8 \times 10^{15} \text{ cm}^{-3}$ respectively). These data together with previous ones (Haseler 1976) were analysed in detail in Challis et al (1978). We shall here only briefly report the main features of the results.

2.2.2.1 Qualitative analysis

The detail of a characteristic low field sweep is shown in figure 2.3. The rise in conductivity at low fields indicates a weakening of the phonon scattering occurring in zero field. It was shown that the rise in conductivity was due to a reduction in the scattering by the distorted ions. The high-field minimum in conductivity would occur when the effective Zeeman splitting of the ground state quartet becomes equal to the energy of the dominant phonons in the heat current. This interpretation is consistent with the shift of the minimum to higher fields as the temperature increases. The positions of the shallow maximum at ~ 5 T and the minimum at high fields are used to determine the parameters of the spin Hamiltonian for a Γ_8 state.

2.2.2.2 The Zeeman splitting of a Γ_8 quartet

From symmetry considerations, Bhattacharjee and Rodriguez (1972) have constructed the most general-form of the Zeeman Hamiltonian for the acceptor ground state in terms of the total angular momentum operator \vec{J} ($J = 3/2$) as:

$$\begin{aligned} \mathcal{H} = & \mu_B g'_1 (\vec{B} \cdot \vec{J}) + \mu_B g'_2 (B_x J_x^3 + B_y J_y^3 + B_z J_z^3) + q_1 B^2 + \\ & q_2 (\vec{B} \cdot \vec{J})^2 + q_3 (B_x^2 J_x^2 + B_y^2 J_y^2 + B_z^2 J_z^2) \end{aligned} \quad (2.1)$$

where the parameters g'_1 , g'_2 , q_1 , q_2 and q_3 depend on the unperturbed wave function of the acceptor ground-state. The components of field and of J refer to the cubic x , y and z axes of the crystal. Although the spin Hamiltonian applies only in the low-field limit $\gamma \ll 1$ where $\gamma = \hbar\omega_c^*/2R^*$, $\omega_c^* = Be/m^*$ and

$R^* = m^*e^4/32\pi^2\hbar^2\epsilon_r^2\epsilon_o^2$ so that at 10 T, $\gamma = 0.3$ and 6.7 for $m^*/m = 0.3$ (heavy holes) and 0.04 (light holes) respectively (Challis et al 1978), it was used as an approximation throughout the analysis. The allowed transition frequencies which contain both linear and quadratic Zeeman terms are obtained from the energies of the Zeeman levels given by Bhattacharjee and Rodriguez (1972) for different field orientations.

The spin Hamiltonian parameters derived from the analysis are compared with the values obtained by other workers in Table 2.1. The g -values obtained in this investigation are much less than those calculated (first four sets in Table 2.1). The next set of values (SF) were obtained from magneto-optical data. There are in fact thirty two sets that will fit the data and the values shown are those which give values closest to the theoretical ones. The present spin Hamiltonian estimates are in good agreement with the values obtained by Tokumoto and Ishiguro (1977a) from an extensive investigation of magneto-acoustic attenuation in high-fields. Tokumoto and Ishiguro have also shown that there exists a set of Zeeman parameters that fit the optical data of Soepangkat and Fisher and which are consistent with their values (Table 2.1). Measurements of the Zeeman-splitting of the Al-acceptor levels in pure Ge have been performed using photothermal ionization spectroscopy (Broeckx et al 1978). The analysis is consistent with very small splittings of the ground state ($\lesssim 0.15 \text{ cm}^{-1}$ for $B \lesssim 2 \text{ T}$, i.e. $g \lesssim 0.2$), i.e. all lines reflect splittings in the excited states. The reason why the g -values are much smaller than the theoretical ones is not clear.

2.3 APPLICATION OF THERMALLY DETECTED EPR (TDEPR) TO p-Ge

AND p-Si

2.3.1 Introduction

The results of the magnetothermal conductivity led us to try to investigate the ground state of p-Ge using TDEPR. This technique is more suited for broad resonance lines (section 2.3.2). It has been successfully used in this laboratory in the detection of EPR of transition metal ions in dielectrics which were not detectable with conventional EPR (e.g. Moore et al 1973). At the start of this investigation no EPR signal from p-Ge had been reported. This is not surprising. The very small g-values would give signals at X-band in field > 30 kG much higher than the usual fields used and also it is quite likely that the resonance lines would be too broad to be detected by conventional methods. EPR absorption from acceptors in Si was reported for the first time by Feher et al (1960). The reasons for the failure to observe the paramagnetic absorption in p-Si earlier, are associated with the degeneracy of the valence band which leads to a Γ_8 quartet ground state. The presence of random internal strains in crystals results in a ground state splitting which varies from one acceptor centre to another. This mixes the $|\pm 1/2\rangle$ and $|\pm 3/2\rangle$ states and so leads to a broad distribution of g-values making the resonance unobservable. Application of uniaxial stress to the samples removes this degeneracy and forces all the ions into the same state, thus allowing the observation of the paramagnetic resonance signal (Feher et al 1960). However the g-values for the ground state measured under

stress by these authors are not in good agreement with optical measurements. The different values are presented in Table 2.2.a. To check on this, it was hoped we would be able to measure the p-Si g-values by TDEPR, without applying uniaxial stress.

2.3.2 TDEPR. Sensitivity and Applicability

2.3.2.1 Sensitivity of thermal detection

The energy absorbed at resonance by the spins is re-emitted as monochromatic phonons. These phonons undergo phonon-phonon scattering and quickly thermalize, thus causing an increase in the temperature of the sample. In a Thermally Detected EPR experiment, the change of temperature of the sample is monitored as the magnetic field is swept. The energy flow diagram for the thermal detection system is shown in figure 2.4. The quartz rod insures a good thermal contact between the thermometer and the sample containing the resonant spins so that we can consider they are at the same temperature at all times. We define a heat conductance $K = K_1 + K_2 + K_3$ (figure 2.4) for the thermal coupling between the assembly sample-quartz rod-thermometer of heat capacity C , and the helium bath at a temperature T_0 . The flow of heat to the helium bath can be through metallic thermometer leads, mechanical supports or conduction through traces of gas in the vacuum space (figure 1.5). For vacuum pressures less than $\sim 10^{-4}$ Torr and for point contact plastic supports, the heat conductance K is mainly determined by the thermometer leads, i.e. $K = K_3$ (Clark 1975).

At thermal equilibrium the thermometer is at the temperature T_0 of the helium bath. If the thermometer absorbs a power $P(t)$,

transmitted by relaxing resonant spins in the sample, the variation ΔT of the temperature of the sample assembly is given by:

$$C \frac{d}{dt} \Delta T + K \Delta T = P(t) \quad (2.2)$$

where the a.c. measuring power has been neglected.

In the steady state the temperature rise at the thermometer is then

$$\Delta T = \frac{P(t)}{K} \quad (2.3)$$

and the time constant for approach to equilibrium, following a change in incident power $P(t)$, is

$$\tau = \frac{C}{K} \quad (2.4)$$

From equation (2.3) it can be seen that to obtain maximum sensitivity it is necessary to minimize the heat leak to the bath. However, equation (2.4) shows this is in conflict with the requirement of a short enough time constant to allow a reasonable rate of field sweep. To satisfy both these requirements the heat capacity must be made as small as possible. At the working temperatures of $\lesssim 4.2$ K, the specific heat of the sample and quartz rod is normally small so the carbon film bolometer mass must be kept very small ($\lesssim 1$ mg) since the carbon has a much greater specific heat capacity than the quartz. Working in the liquid helium temperature range is also advantageous as the sensitivity of the bolometer increases when the temperature is decreased. Typically a change of 1 mK is easily detected by the bolometer at 4.2 K.

2.3.2.2 Applicability of thermal detection

Schmidt and Solomon (1966) report a detailed investigation of the theory of Thermal Detection. As shown by these authors, the electromagnetic power Π at frequency ν absorbed by N paramagnetic spins at temperature T is:

$$\Pi = \left(\frac{P}{P + P_S} \right) \left(f(T) \right) \left(\frac{Nh\nu}{T_1} \right) \left(\frac{S(S+1)}{3} \right) \quad (2.5)$$

The first bracket is the saturation factor, P being the incident microwave power and P_S the power required to reduce the spin magnetization to half its equilibrium value. The second bracket is the Boltzmann factor for the pair of levels involved in the transition. The third bracket is the power expected if all spins are saturated ($P \gg P_S$) - T_1 is the spin-lattice relaxation time - and the fourth arises from the usual quantum mechanical treatment of the magnetization.

From equation (2.5) it appears that the absorbed power Π is larger for a line with a short T_1 , i.e. systems which are strongly coupled to the lattice. Several studies have shown that acceptors in Si and Ge are very strongly coupled to the lattice (for references see Challis and Halbo 1972). Broad resonance lines would then be expected not only because of lifetime effects but also because of coupling to lattice strains (Feher et al 1960). T_1 was measured in the case of p-Si, also by EPR under stress, and was found to be very short at low temperatures (Ludwig and Woodbury 1961).

For these systems, TDEPR is then more sensitive than conventional EPR since we can use high microwave powers, before

saturation occurs. In conventional detection the noise associated with the microwave power fluctuations increases as the power increases (e.g. Moore et al 1973). For thermal detection these fluctuations are averaged out by the thermal time constant of the sample assembly and usually the noise is independent of the incident microwave power level (Clark 1975). The TD signal is also directly proportional to microwave power whereas a conventionally detected signal is proportional to the square root of the power.

Moreover the sensitivity of TDEPR is independent of linewidth because no modulation is used when the magnetic field is swept. In conventional spectrometers the sensitivity tends to decrease as linewidth increases because of the difficulty of producing large modulation amplitudes at high frequency (e.g. Wertz and Bolton 1972 - Appendix D).

Thermal Detection is also more attractive if we consider the simplicity of the spectrometer (section 1.2).

2.3.3 The Results

To check on the experimental rig a few runs were first conducted using samples already studied by TDEPR or conventional EPR. Figure 2.5 shows a characteristic spectrum of ruby at 4.2 K. This system has been extensively investigated by Knowles (1976) using TDEPR. Figure 2.6 shows the hyperfine structure of V^{3+} in Al_2O_3 . The octet arises from the interaction with the ^{51}V nucleus.

Two samples of Ge (Ga) and Si:B with concentrations $8 \times 10^{15} \text{ cm}^{-3}$ and $5.2 \times 10^{16} \text{ cm}^{-3}$ respectively were used in the investigation. No EPR signal was detected in fields up to 5.5 T and in microwave powers up to ~ 50 mW. Several attempts were made to try to increase the sensitivity of the spectrometer.

Using only one thermometer resulted in a baseline with a steep slope due to the carbon magnetoresistance. A second carbon film was then painted on a glass rod next to the thermometer, with about the same room temperature resistance. These two thermometers formed then a 'matched' pair and the difference in resistance of the two was monitored as the field was swept. This resulted in a flattened baseline making the observation of any change in slope easier. It also made the system less sensitive to temperature drifts.

The effect of residual strains in the crystals is to broaden the EPR line (Feher et al 1960). The semiconductor samples are stuck with G.E. varnish on the quartz rod and this could lead to more strain effects because of the different low temperature expansion coefficients of the two materials. In one run a pure Si sample was first stuck to the quartz and the p-Si sample was then mounted on top of it. This was not a success either.

On two occasions the temperature of the helium bath was lowered below the λ -point, to 1.85 K. It was hoped that this would increase the sensitivity for three reasons. First there would be an increase in the Boltzmann factor (see equation 2.5). The second effect would be to lengthen the spin-lattice relaxation time T_1 (Ludwig and Woodbury 1961), and this actually reduces the

power absorbed (equation 2.5) but could have made the signal easier to detect if the resonance line was intrinsically broadened, and third the bolometer sensitivity would be increased and the specific heats lowered. Still no signals were seen however.

It became clear that the main problem in the study of p-Ge and p-Si by Thermally Detected EPR was the occurrence of a rather large non-resonant heating of the samples by the microwaves. Any resonance signal would then be superimposed on a large background and the performance of the spectrometer might quickly deteriorate because of fluctuations in the microwave power.

An investigation was made of the magnitude of this heating which was very small when only the quartz rod and a small amount of GE varnish were irradiated by the microwaves. The sensitivity $\left[\frac{1}{R} \frac{dR}{dT} \right]$ of the carbon film at 4.2 K was calibrated using an Allen-Bradley thermometer for comparison so that absolute values of increases in temperature due to non-resonant absorption of microwaves could be determined. These changes in temperature were readily converted to equivalent power levels using the relation $P = K\Delta T$ (equation 2.3), where $K = C/\tau$. τ is measured each run and the specific heat C for the sample-quartz rod-carbon film assembly is estimated at 4.2 K. It was then possible to compare the power absorption measured with that calculated for various processes.

One possible reason for the heating is Joule heating due to the microwave electric field and the extrinsic conductivity. This effect was investigated for three Ge samples with concentrations

ranging from $\sim 10^{13} \text{ cm}^{-3}$ to $\sim 10^{17} \text{ cm}^{-3}$. The measured heating power was found to increase with concentration. However the estimated values for the power dissipated in the samples by Joule effect at microwave frequencies would be very negligible as compared to the measured power levels. (Tanaka and Fan (1963) have shown that the microwave resistivity of p-Si at 4.2 K was orders of magnitude smaller than the DC resistivity and we assumed the same behaviour in Ge samples).

Tanaka et al (1964) have measured the microwave absorption in p-type and n-type silicon, in the concentration range 6.7×10^{15} to $2.2 \times 10^{16} \text{ cm}^{-3}$, at low temperatures. The microwave conductivity showed strong non-ohmic characteristics in all the samples and this was attributed to direct absorption of electromagnetic radiation in ionized impurity pairs.

However, electric field induced transitions between strain-split levels of the Γ_8 acceptor ground state are allowed (Bir et al 1963) and the absorption observed in our samples, in the absence of a magnetic field, could possibly be due to that process occurring in individual acceptor centres. This would then be in agreement with the observed concentration dependence.

2.4 CONCLUSION

We failed to detect any EPR spectrum of p-Ge or p-Si using Thermal Detection, probably due to undesirable non-resonant microwave absorption, resulting in a reduction of the sensitivity of the bolometer.

The g-values evaluated from the observation of resonance lines in Si:B in zero-applied stress (Table 2.2.b) are then in

fair agreement with the values of Merlet et al (Table 2.2.a). Neubrand (1978a) also reports values determined by Shimizu and Tanaka (1973) and these and other worker's (Table 2.2.a) are in less satisfactory agreement. As suggested by Neubrand the differences in the g -factors could be accounted for by the different experimental conditions. The same spin-Hamiltonian, linear in field, was used by all the authors and additional non-linear correction terms should presumably be added to account for these differences (Neubrand 1978a).

The observation of EPR lines at zero-stress has become possible by the high degree of crystal perfection now attainable in Si-crystal growth. The samples used by Neubrand are grown by Wacker Chemitronic F.R.G. (WASO and WASO S quality). These samples are dislocation-free and any line broadening is due to point defect strains. EPR investigations could then be useful in determining the residual impurity content of single crystals by studying the effect of point defects on the EPR linewidth and lineshape (Neubrand 1978b).

The same quality material (WASO from Wacker Chemitronic) was used in an investigation of the splitting of acceptor ground state in Si:B using ultrasonic relaxation (Lassman and Zeile 1980). In these high quality silicon crystals these splittings are thought to be largely determined by the random electric fields from residual donors.

	g'_1	g'_2	g_2 (GHz T ⁻²)	g_3 (GHz T ⁻²)	$ g_m[001] $	$ g_m[110] $
BBP	5.66	-0.26	-	-	10.4	10.2
SOH (a)	-1.44	0.56	-	-	0.92	0.88
SOH (b)	-0.91	0.56	-	-	0.91	0.92
LW	-1.13	0.63	-	-	0.92	0.92
SF	-1.73 ± 0.11	0.78 ± 0.07	-	-	0.81	1.02
TI	-0.16 ± 0.08	0.08 ± 0.04	0.10 ± 0.04	0.012 ± 0.004	0.22	0.10
SF (TI)	-0.26 ± 0.11	0.12 ± 0.07	-	-	0.14	0.16
Present	~±0.2 ± 0.2	~±0.1 ± 0.1	±0.12 ± 0.12	<< 0.12	0.2 ± 0.2	0.2 ± 0.2

Table 2.1 Spin-Hamiltonian parameters of the acceptor ground state in germanium.

BBP = Bir et al (1963), SOH (a) and (b) = Suzuki et al (1964), LW = Lin-Chung et al (1969), SF = Soepangkat et al (1973), TI = Tokumoto et al (1977a), (the value used for $|g_m[001]|$ is $2g_{1/2}$ which differs somewhat from $g'_1 + 13g'_{2/4}$), SF (TI) = the data of SF reinterpreted by TI.

	g'_1	g'_2	
BBP (T)	0.76	-0.02	
SOH (T)	0.93	0.13	
FHG (EPR)	1.21 ± 0.01	0.00 ± 0.01	(a)
CA (O)	0.84 ± 0.09	0.13 ± 0.08	
MPAJ-L (O)	1.03 ± 0.07	0.04 ± 0.04	
<hr/>			
N (EPR)	-1.071 ± 0.002	-0.031 ± 0.001	
ST (N) (EPR)	-1.048 ± 0.005	-0.061 ± 0.002	(b)

Table 2.2 Comparison of the g-factors for the ground state of boron in silicon.

BBP = Bir et al (1963), SOH = Suzuki et al (1964), FHG = Feher et al (1960), CA = Cherlow et al (1973), MPAJ-L = Merlet et al (1975), N = Neubrand (1978a), ST (N) = the values derived by Neubrand from the data of Shimizu et al (1973).

T = Theoretical

EPR = Electron Paramagnetic Resonance

O = Optical work

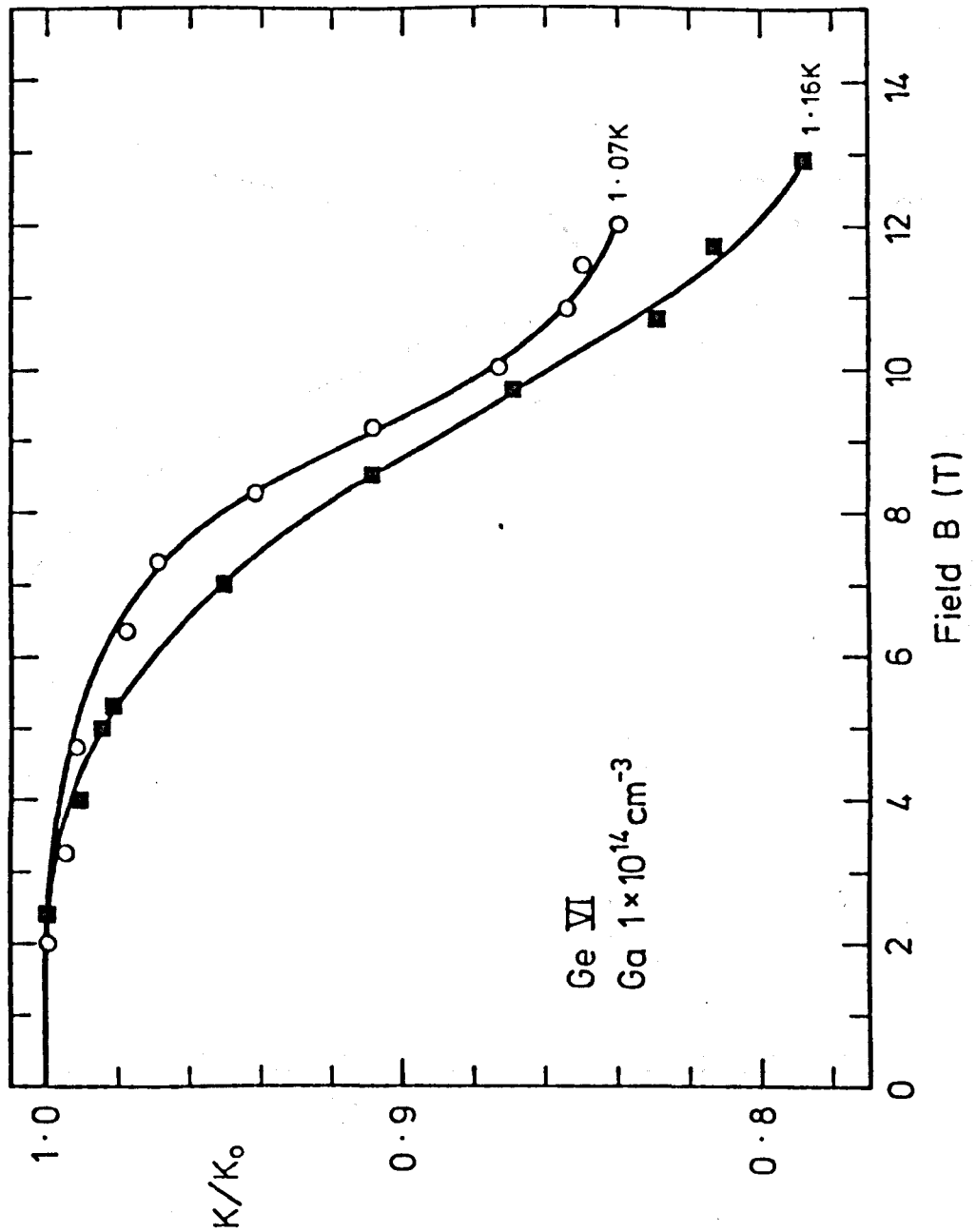


FIGURE 2.1 K/K_0 against transverse field for sample VI
(Ga: $1 \times 10^{14} \text{ cm}^{-3}$), $B_{||} [001]$.

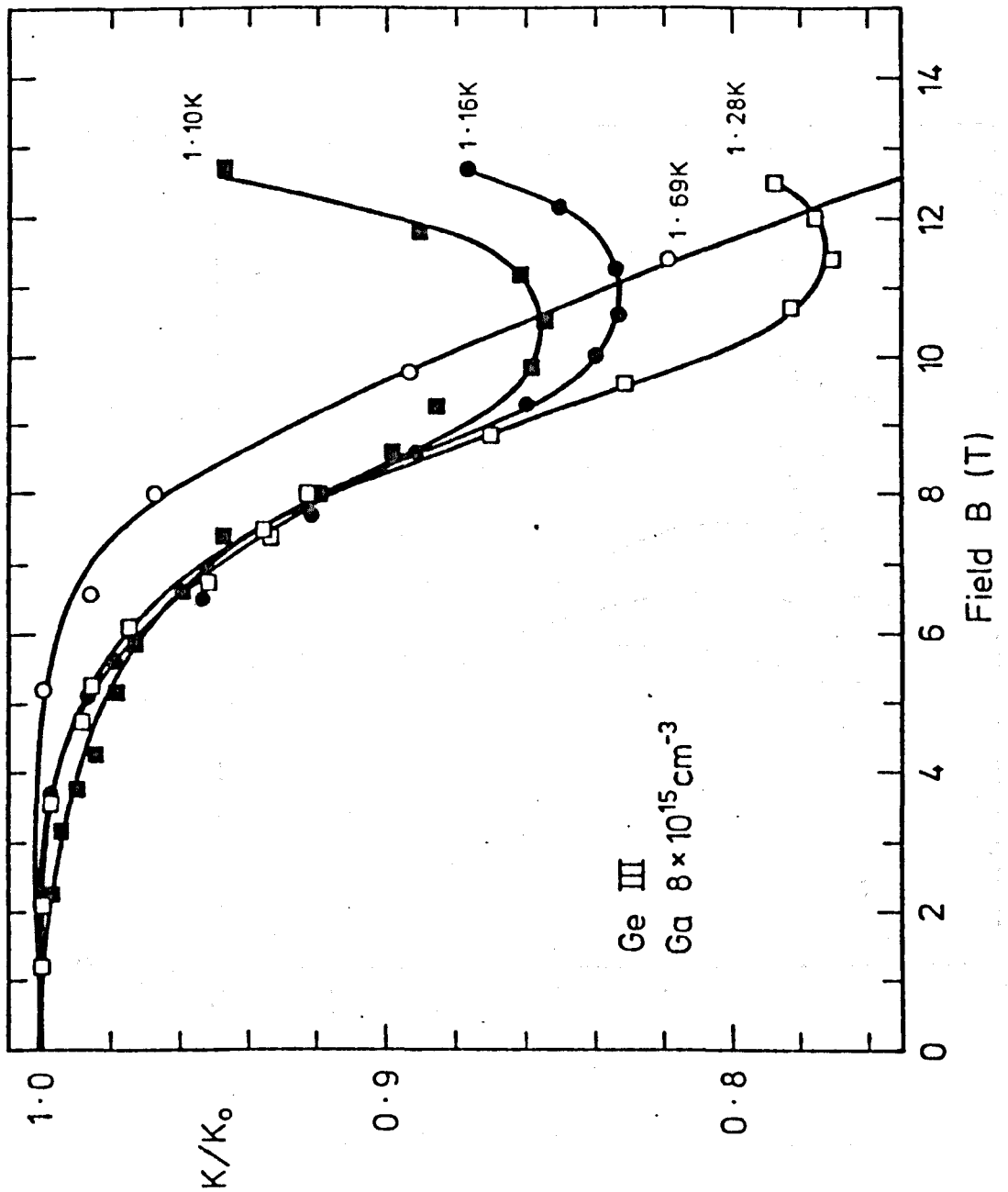


FIGURE 2.2 K/K_0 against transverse field for sample III
(Ga: $8 \times 10^{15} \text{ cm}^{-3}$), $B_{\parallel} [001]$.

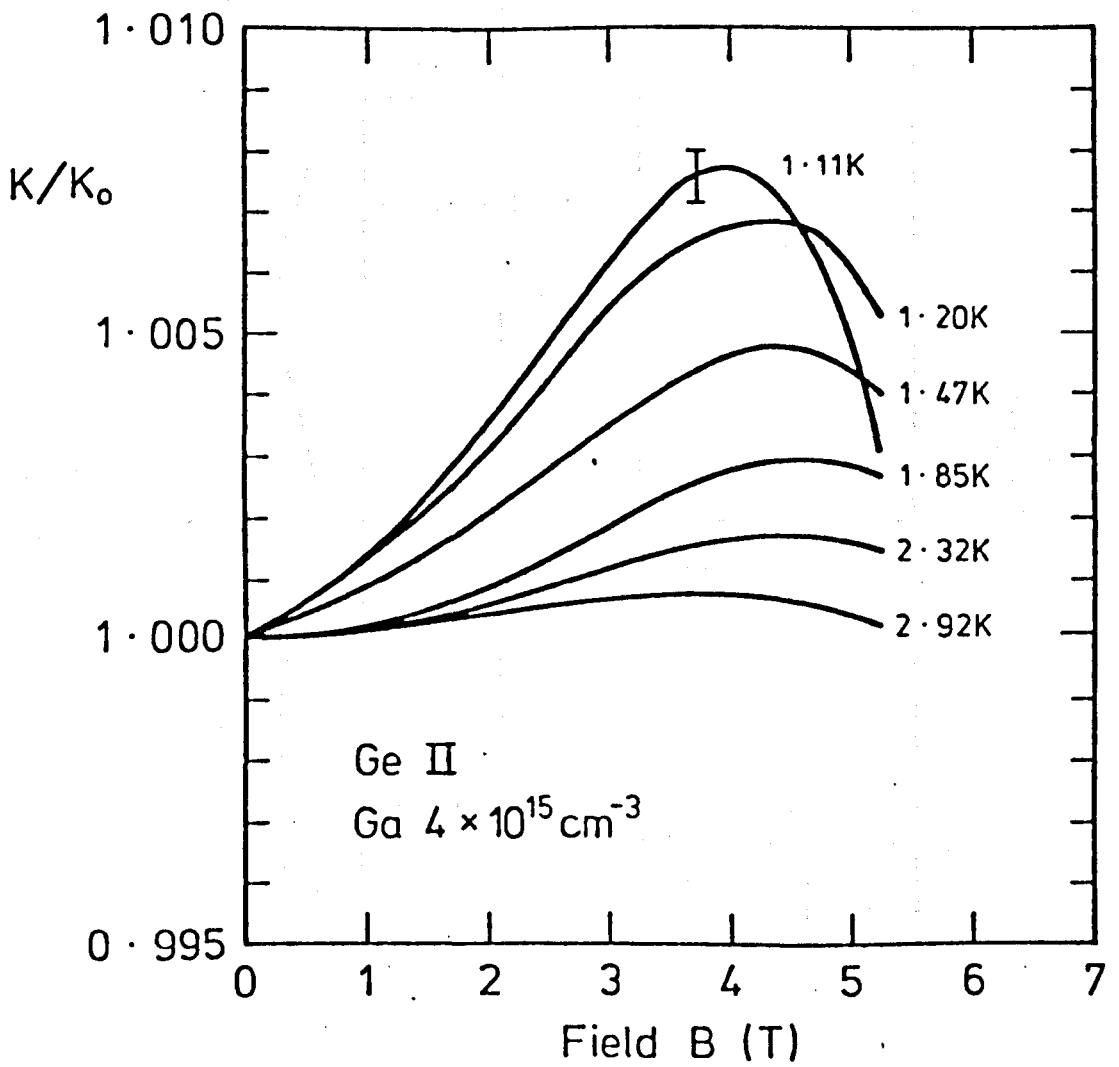


FIGURE 2.3 K/K_0 against longitudinal field for sample II (Ga: $4 \times 10^{15} \text{ cm}^{-3}$), $B_{||}$ [001].
(After Haseler 1976).

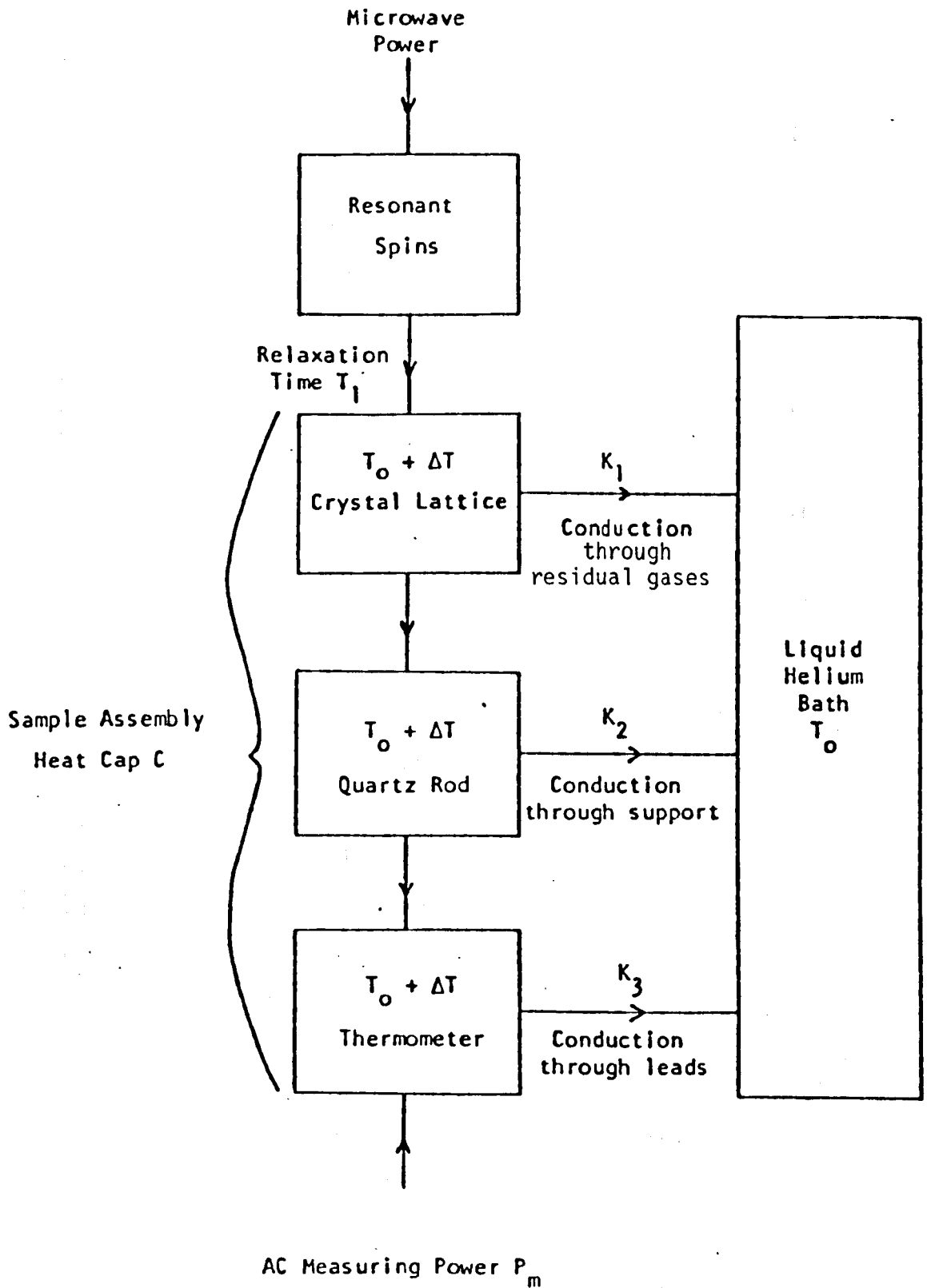


FIGURE 2.4 Energy flow diagram for Thermal Detection of EPR.

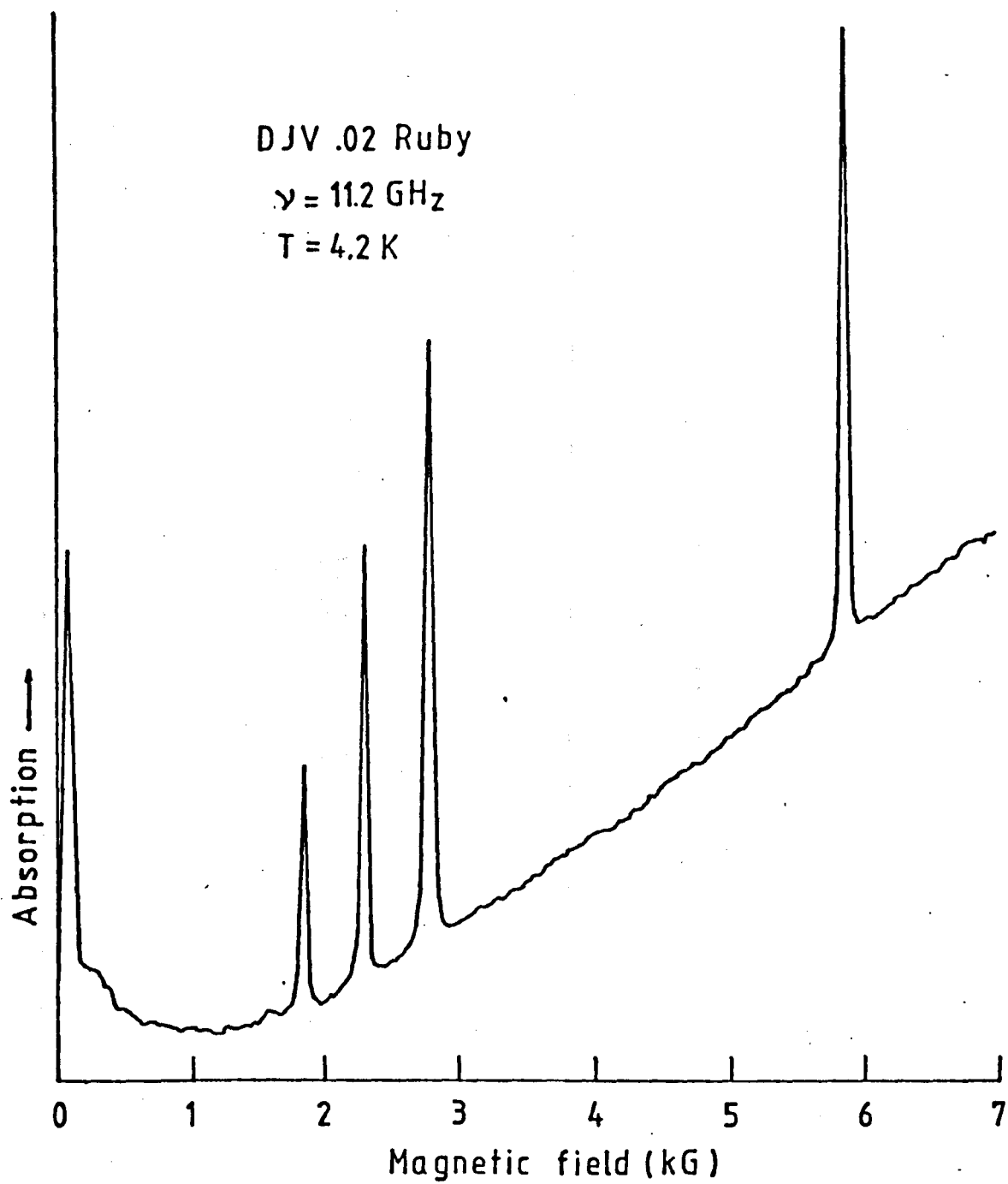


FIGURE 2.5 TDEPR spectrum of ruby.

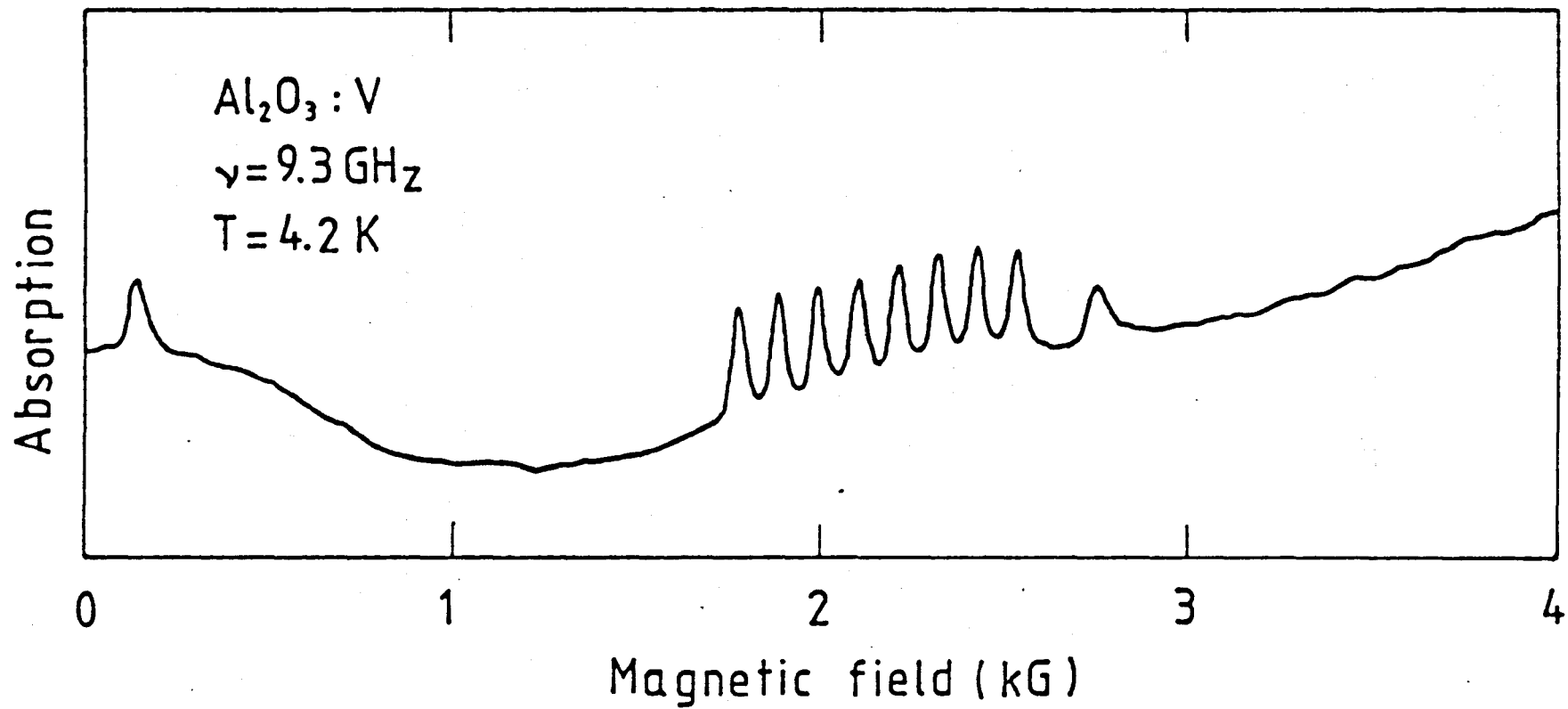


FIGURE 2.6 TDEPR spectrum of V^{3+} in Al_2O_3 (1100 ppm).

CHAPTER 3

LOW TEMPERATURE THERMAL CONDUCTIVITY OF Cr-DOPED GaAs

3.1 INTRODUCTION

The thermal conductivity of 7 GaAs samples doped with Cr/Si or Cr/Zn has been measured in the temperature range 1 - 20 K. We are most grateful to Drs. Locatelli and Salce of Centre d'Études Nucléaires Grenoble for extending the measurements down to 50 mK on three of the samples. The characteristics of the samples are given in Appendix 1.

Some of the results have already been published (Challis and Ramdane 1980; Bury et al 1980a). Previous thermal conductivity measurements on the same system are presented in the next section. The aim of the study was to investigate the phonon scattering by the Cr ions which present several charge states in GaAs (e.g. Brozel et al 1978). Most of the samples show strong scattering of phonons with 'dips' in the thermal conductivity curves. This may be interpreted as due to resonant phonon scattering by the low lying energy levels of the different charge state chromium ions.

3.2 THERMAL CONDUCTIVITY OF GaAs - REVIEW OF PAST WORK

Holland (1964a) measured the thermal conductivity of a number of III-V and II-VI semiconductors between 2 and 300 K. His results, together with previous work on Ge and Si were used to check on the validity of the relaxation time expressions usually utilized in the computation of the thermal conductivity integral. Two samples of undoped GaAs, one 'less pure' than the other, were measured. His analysis was based on the Callaway model (Section 3.4). Increased boundary scattering and impurity scattering (mass-difference) thought to be related to impurities present in the crystal were found.

Measurements on doped GaAs (Te, Cd, Zn, Mn) were also performed by the same author (Holland 1964b). In every case the phonon scattering at low temperatures was found to be much stronger than that predicted from boundary scattering alone.

Similar results on Zn- and Te- doped GaAs were obtained by Carlson et al (1965). The p-type samples (Zn-doped) showed much lower values of the thermal conductivity than the n-type ones (Te-doped) for about the same amount of doping impurities.

The thermal conductivity of Cr-doped GaAs at low temperatures (2 - 90 K) was first investigated by Chaudhuri et al (1973). They looked at one semi-insulating sample, grown by the horizontal Bridgman method in their laboratory. The conductivity was found to be markedly reduced over the whole temperature range and there was also evidence of a 'dip' occurring at about 7^o K. (This behaviour had already been reported by Holland (1964b) in GaAs

doped with another transition metal ion, manganese). There was a sharp change in the slope of the thermal conductivity-versus-temperature ($K(T)$) curves, near 10 K. From their analysis Chaudhuri et al concluded there was a possibility of resonant scattering of phonons but did not explain the origin of this possible resonant scattering. They suggested it might arise either because of the presence of low-lying energy levels of the magnetic chromium ions or due to electron-phonon interaction.

Finally we report on the work of Vuillermoz and collaborators (1975). These authors studied four Cr-doped samples. Three were grown by the Czochralski method and one by the Bridgman's. The concentration of the Cr atoms was thought to be about 10^{18} cm^{-3} . The electrical resistivity was high, greater than $10^7 \Omega\text{cm}$ at room temperature. The conductivity was also much lower than the predicted one for a pure sample. The extra phonon scattering at low temperatures was believed to be by structural defects. From their analysis also based on the Callaway model, stacking faults appeared to be the principal large structural defect. However, scattering by microprecipitates had to be considered, to actually obtain a good 'fit' to the experimental data. A 'dip' in the $K(T)$ curves could also be deduced in the temperature range 4 - 10 K, but the temperature at which it occurred varied from sample to sample and the effects were said to be small, within the experimental error. The authors did not find it justifiable to analyse their results in terms of resonant scattering of phonons by the magnetic chromium ions.

3.3 EXPERIMENTAL RESULTS

In figure 3.1, the data are compared for all the samples, in the temperature range 1 - 60 K.

The sample with the highest conductivity is GA803, for which the maximum is reached at about 14 K and $K(14K) \approx 15 \text{ W/cmK}$. This specimen is not doped with chromium.

The addition of Cr has different effects on the thermal conductivity of the samples. We can split the experimental data into two sets.

First, the conductivity of GA785 and GA735 (O64), both n-type samples, is reduced over the whole temperature range but there is no evidence of resonant scattering of phonons. Although the two samples contain approximately the same amount of Cr impurities ($\sim 1.5 \text{ ppm}$), the scattering is larger in GA785. This sample has a bigger-cross-section but contains much more silicon than any other sample from the Plessey Co. or Sumitomo Co. The extra scattering in these two samples could well be due to the presence of Cr and Si impurities, acting as point defect scatterers (see section 3.5.1.3).

The second set of data curves show the conductivity of respectively, TI#4, GA735(e), GA781 and TI#5. These samples are all semi-insulating apart from GA781 which is p-type (Zn-doped, in addition to Cr).

The slope of the different curves differs markedly from a T^3 dependence which should be expected at these low temperatures (see section 5.1.1). A 'dip' can be seen in GA735(e), GA781 and

TI#5 at about 9 K. These dips in thermal conductivity curves are indicative of resonant scattering of phonons (see e.g. Pohl 1962). TI#4 also shows a dip at a lower temperature (~ 2 K). The maximum for this sample is shifted to higher temperatures and occurs at about 28 K. An abrupt change in GA735(e) slope appears for $T \leq 2$ K.

The measurements performed in Grenoble, for temperatures down to ~ 50 mK are shown in figure 3.2.a where the results are plotted in the form K/T^3 to show any departure from the T^3 dependence of the thermal conductivity for a pure sample.

There is evidence of resonant scattering in the three measured samples, the maximum of the effect occurring at ~ 0.4 K. Even at the lowest temperatures the boundary scattering regime is not reached and there seems to be additional scattering for GA735(e) and TI#5 at $T \sim 0.1$ K.

The additional resistivity due to resonant scattering is better seen if we compare the resistivities W of the different samples with that of GA735 (O64) (W_1) which does not show resonant phonon scattering. The ratios W/W_1 are plotted in figure 3.2.b for the whole temperature range (GA735 (O64) has not been measured down to 50 mK but we extrapolate its resistivity down to this temperature, assuming a T^3 dependence of K).

In conclusion, the introduction of rather small concentrations of Cr impurities in the GaAs host lattice (~ 1.5 ppm) leads to considerable phonon scattering. In the n-type samples the extra resistivity is thought to be due to point-defect scattering while in the rest of the samples (SI and p-type), phonons are scattered

resonantly at two frequencies. Furthermore there could be another scattering process taking place around 2 K for TI#4 and GA735(e). All these effects are discussed in section 3.7 in terms of the possible charge states of the Cr ions.

3.4 THEORETICAL BACKGROUND. THE CALLAWAY MODEL

For the samples studied in this work, thermal energy may be considered to be transported, at low temperatures, by the atomic vibrations of the crystal. The energy contained in a mode of vibration is called a phonon. The heat current is carried by phonons. The model discussed by Callaway (1959) for the lattice thermal conductivity has been used throughout the analysis of the results. The relaxation time approximation is used for solving the Boltzmann heat transport equation. A Debye model is assumed for the solid. Phonons may undergo different scattering processes characterized by relaxation times $\tau_i(\omega, T)$ which are functions of temperature and frequency. The scattering processes are considered to be independent of each other. If there are several processes acting simultaneously, the combined relaxation time, $\tau(\omega, T)$ is written $\tau^{-1} = \sum_i \tau_i^{-1}$.

Only the first integral in the Callaway expression for the thermal conductivity is considered. That integral represents then the model first proposed by Debye (1912) for the variation of K with temperature. $K(T)$ is then proportional to a weighted average of the total phonon relaxation time $\tau(\omega, T)$ and is given by:

$$K(T) = \frac{k_B}{2\pi^2 v} \left(\frac{k_B T}{\hbar} \right)^3 \int_0^{\theta_{D/T}} f(x) \tau(x, T) dx$$

where $x = \hbar\omega/kT$

$$f(x) = \frac{x^4 e^{-x}}{(e^x - 1)^2}$$

θ_D is the Debye temperature

v is the average phonon velocity.

The usual procedure in analysing thermal conductivity experiments is to adjust the coefficients in the expressions for τ until a 'fit' to the experimental data is obtained. This, in return, gives information on the different scattering processes. Expressions for the relaxation times appropriate to phonon scattering processes which might be present in our samples are presented in the next section.

3.5 SCATTERING PROCESSES

$\tau^{-1}(\omega, T)$ can be divided into two parts:

$$\tau^{-1}(\omega, T) = \tau_I^{-1}(\omega, T) + \tau_E^{-1}(\omega, T).$$

3.5.1 'Intrinsic' Processes

$\tau_I^{-1}(\omega, T)$ describes the 'intrinsic' process, always present in a real crystal.

3.5.1.1 Boundary scattering

At low enough temperatures the phonon mean free path is limited by the crystal boundaries. The form of the relaxation time for this scattering process, for a rough surface, is given

by (Casimir 1938)

$$\tau_{b_0}^{-1} = \frac{v}{L_c}$$

v is the average phonon velocity

$L_c = \frac{2}{\sqrt{\pi}} (\ell_1 \times \ell_2)^{1/2}$, is the 'Casimir length',

$\ell_1 \times \ell_2$ is the crystal cross-section.

To account for the finite length of the samples a correction factor obtained, from Berman et al (1955) is used in the previous expression, so that

$$\tau_b^{-1} = \frac{v}{L_c \cdot F}$$

F is a function of the width-to-length ratio of the sample and is taken directly from Berman et al curves. If the only scattering of the phonons is from the boundaries, the conductivity is proportional to the third power of the temperature ($K \propto T^3$).

3.5.1.2 Phonon-phonon scattering

Phonon-phonon interactions occur in a crystal because of the anharmonic coupling forces between the atoms. At low temperatures, only the three-phonon processes are thought to be important. Holland (1964a) used, to fit his measurements on GaAs, an expression of the form $\tau_{p-p}^{-1} = B\omega^2 T^3$ for the phonon-phonon interaction. This expression was derived by Herring (1954). It is appropriate for 'normal-processes' (total wavevector in any direction is conserved) in a cubic material, and is valid for longitudinal waves at low temperatures. The same form was utilized in analysing our data.

The phonon-phonon interaction is not important in the temperature range considered (50 mK - 20 K).

3.5.1.3 Point defect scattering

The scattering of lattice waves by point imperfections was treated by Klemens (1955). This scattering arises from the mass difference of the impurity ion, changes in the binding force constants between the atoms and from the crystal strain field around the defect. Klemens wrote the total scattering rate as

$$\tau_{\text{impurity}}^{-1} = A_{\text{imp}} \omega^4$$

where A comprises the three contributions due to the introduction of the defect.

The reciprocal relaxation time for mass-difference scattering only given by Klemens must be modified for compounds (see e.g. Holland 1964a).

$$\tau_{\text{mass-difference}}^{-1} = B\omega^4 = v\omega^4 \Gamma / 4\pi v^3$$

$$\text{with } \Gamma = \frac{x}{(x+y+z+\dots)} \left(\frac{M_A}{\bar{M}}\right)^2 \Gamma(A) + \frac{y}{(x+y+z+\dots)} \left(\frac{M_B}{\bar{M}}\right)^2 \Gamma(B) + \dots$$

$$\text{where } \Gamma(A) = \sum_i f_i \frac{(M_{iA} - \bar{M}_A)^2}{\bar{M}_A^2}$$

f_i = fraction of isotopes of mass M_{iA} present,

$$\bar{M}_A = \sum_i f_i M_{iA},$$

The compound is $A_x B_y C_z \dots$, V is the molecular volume and

$$\bar{M} = \frac{xM_A + yM_B + zM_C + \dots}{(x + y + z + \dots)} .$$

It is difficult to evaluate the scattering from point defects other than isotopes and often the numerical coefficient A_{imp} is treated as an adjustable parameter in any data fit (e.g. Challis et al 1972).

3.5.2 'Extrinsic' Processes

$\tau_E^{-1}(\omega, T)$ describes the 'extrinsic' processes due to scattering of phonons by the low lying energy levels of the magnetic Cr ions. The mechanism generally accepted for phonon-spin interactions is as follows (see e.g. Dreyfus 1972). The phonon waves passing a magnetic ion in the lattice will change the positions of its neighbours, thus causing distortions in the crystalline field at the ion site. These 'orbit-lattice' interactions have been discussed by several authors (Orbach 1960, Zadworny 1965)). The perturbative treatment where the electrostatic field is expanded in Taylor's series yields satisfactory fits to experimental data. The different terms (usually first and second order terms) in the series treated in first or second order perturbation theory give rise to different processes for which expressions of relaxation times are calculated. A review of the most common processes and their relaxation times is given in Brown's thesis (Brown 1971) and we shall mention here only those processes which may account for resonant scattering of phonons.

3.5.2.1 'Direct process'

If the phonon energy is equal to the energy separation $\hbar\omega_0$ between two energy levels of the magnetic ions, then the phonon can be absorbed. The de-excitation takes place by emission of a virtual photon.

The process can also take place by emission of a phonon first (figure 3.3.a). The relaxation time obtained is of the form (Zadworny 1965):

$$\tau_D^{-1} = D_D \omega g(\omega - \omega_0)$$

D_D is a numerical constant which depends amongst others on the difference in the populations of the spin levels. $g(\omega - \omega_0)$ is the lineshape function which describes the broadening due to intrinsic processes or strains.

3.5.2.2 'Coherent scattering process'

This is a so-called 'Raman process' in which two phonons are involved in the transition. If the spin-system returns to the same state, we have a case of coherent elastic scattering. The emitted phonon has the same energy as the absorbed one (figure 3.3.b). The derived relaxation time for this process is (Griffin and Carruthers 1963):

$$\tau_C^{-1} = \frac{D_C \omega^4}{(\omega^2 - \omega_0^2)^2}$$

D_C is proportional to the total population of the levels concerned.

The main difference between these two resonant scattering terms, at temperatures where the resonance has its greatest effect, will be in their frequency dependence. The coherent elastic scattering will be more effective if the lifetime of the excited electronic state is determined by the spin-lattice coupling, i.e. $T_2 \gg T_1$ where T_2 is the spin-spin relaxation time and T_1 is the spin-lattice relaxation time. The direct process will be predominant when $T_2 \ll T_1$. For dilute paramagnetic

crystals τ_2^{-1} is approximately independent of the resonance frequency ν_0 while $\tau_1^{-1} \propto \nu_0^3$ (de Goër and Challis 1973), so that for resonances at high temperature we would expect $\tau_1^{-1} > \tau_2^{-1}$ (i.e. the coherent process is more important) while as T falls, eventually the coherent process is replaced by the direct process.

3.6 CURVE-FITTING PROCEDURE AND RESULTS

First the curves for the highest conductivity samples were fitted using standard expressions for the intrinsic relaxation times. The fits for GA735 (O64) which is Cr-doped and does not show any resonant scattering provide the magnitude of the phonon scattering produced by the localized lattice distortions and mass-fluctuations introduced by the Cr ions. The parameters for these fits were subsequently used in the analysis of the extra magnetic scattering. In order to see more clearly the resonance effects, the data for TI#5 and GA735(e) were examined in the form K/T^3 . We also considered the ratio $R = \frac{W_{exp}}{W_{calc}}$, plotted as a function of temperature. W_{exp} is the measured value of the thermal resistivity and W_{calc} is the value calculated using the parameters obtained for GA735 (O64) and including the magnetic scattering terms. A fit was achieved if $R \approx 1$ at all temperatures.

3.6.1 The Intrinsic Terms

In figure 3.4 are shown the calculated curves for different values of $\tau_{boundary}^{-1}$ and $\tau_{impurity}^{-1}$. The upper curve is for a pure sample where $\tau_{impurity}^{-1}$ is due to the mass-difference of isotopes

only. The parameters for the best fits are indicated in Table 3.1 together with the theoretical ones. In the computation of the conductivity integral, the values of the Debye temperature θ_D and average phonon velocity v are those used by Holland (1964a)

$$\theta_D = 345 \text{ K}, \quad v = 3.5 \times 10^3 \text{ ms}^{-1}.$$

The phonon-phonon interaction term $B\omega^2 T^3$ was kept constant in the fits for all samples. The same value of B as Holland's (1964a) was used ($B = 3.6 \times 10^{-23} \text{ sec/K}^3$).

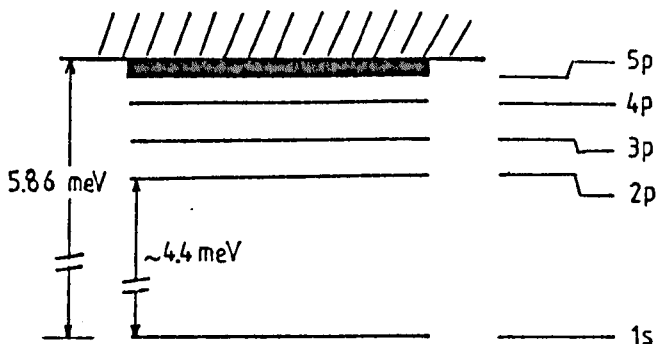
The theoretical value of the boundary scattering relaxation rate, calculated from the Casimir formula, had to be increased by a factor of ~ 2 to fit the temperature range 1 - 6 K for sample GA735 (O64). As mentioned in section 3.2, increased boundary scattering was found in the less pure GaAs sample by Holland (1964a). In order to fit the data at low temperatures the value of $\tau_{\text{boundary}}^{-1}$ had to be increased by a factor of ~ 3.5 over the theoretical value. Holland suggested that effect might be related to impurities. In the case of GA735 (O64) this extra-resistivity is non-magnetic (see Chapter 4) in origin. A possible source of frequency independent scattering are precipitates larger than the dominant phonon wavelength (Schwartz and Walker 1967). Vuillermoz et al (1975) found it necessary to include scattering by precipitates to fit their data. Small precipitates ($\sim 500 \text{ \AA}$ diameter) have been observed in Cr-doped GaAs (Stirland 1977). Clusters of particles whose diameters range from $\sim 100 \text{ \AA}$ to $\sim 1200 \text{ \AA}$ were also seen in Cr-doped GaAs grown by other companies (Augustus and Stirland 1980). It was shown later on that these precipitates consisted of As atoms (Cullis et al 1980). Since the aim of this

work was to study magnetic phonon scattering, no further investigation was attempted on the origin of this increased boundary scattering.

A_{impurity} (section 3.5.1.3) was calculated for a pure GaAs sample assuming only mass-difference for isotopes ($A_{\text{isotopes}} \approx 0.456 \times 10^{-44} \text{ sec}^3$). For the doped samples (Cr/Si, Cr/Zn) the calculated contribution to the scattering from the chemical impurities assuming only mass-difference effects was found to be negligible for the concentration of impurities present ($\sim 1 - 5$ ppm Cr or ~ 120 ppm Si). However it was found necessary to increase the value of A_{isotopes} by a factor of ~ 4 to obtain a reasonable fit for GA735 (O64) and GA785. This shows the differences between host and impurity ions other than mass-effects. We have found that quite large changes in A have little effect on the general shape of the reduced resistivity R . For example for sample GA735(e), which has the highest concentration of Cr and second highest concentration of Si, an increase in A of a factor of 2 results in a decrease in R at 10 K of only 10% of its value. Even at higher temperatures, $T \leq 20$ K, the change is always less than 20% and the overall shape of the curve remains practically unchanged. The point-defect scattering term used in fitting the samples showing resonant scattering was the one previously found for GA735 (O64).

We note that a possible mechanism for scattering of phonons in the n-type samples is electron-phonon interaction. Keyes (1961) has considered the scattering of phonons in n-Ge, at low temperatures. The scattering arises from the large effect of

strain on the energy of an electron in a hydrogen-like donor state. Phonons are elastically scattered due to virtual electronic transitions between the singlet and the triplet of the donor ground state. Griffin and Carruthers (1963) have also considered the resonance scattering of phonons between the singlet and the triplet. The energy levels of donors in GaAs are however different from those in Ge and are shown below (after Stillman et al 1977).



The excited states are about ~ 5 meV above the ground state and shallow donors should have little influence on the thermal conductivity, at low temperatures. This has already been observed by Holland (1964b) in one GaAs sample doped with Te.

3.6.2 The Resonance Terms

Very satisfactory fits have previously been obtained in fitting resonant phonon scattering by a variety of magnetic ions in dielectric host lattices using the relaxation time for coherent scattering discussed in section 3.5.2.2 (e.g. de Goër 1969, Challis et al 1972, Salce and de Goër 1979).

In a first attempt, the GA735(e) data was examined using the same scattering rate, $\tau^{-1} = D\omega^4 / (\omega^2 - \omega_0^2)^2$, for both resonances. The resonant frequency ω_0 is related to the temperature by the approximate relation

$\hbar\omega_0/k_B T = x = 3.8$, for the dominant phonons, so that $\omega_0 \approx 2.5 T \text{ cm}^{-1}$. The dips in the data are centred around 0.4 K and 8 K corresponding respectively to $\sim 1 \text{ cm}^{-1}$ and 20 cm^{-1} . Different values of ω_0 were tried for the two resonances but no satisfactory fit could be achieved.

We then kept the same form for τ^{-1} for the high temperature resonance but used the relaxation rate derived for a direct process, for the low temperature resonance (see section 3.5.2.2)

$$\tau_D^{-1} = D_D \omega g(\omega - \omega_0)$$

The question then was which form to use for the lineshape function $g(\omega - \omega_0)$. Since $\tau_D^{-1}(\omega) \propto \omega g(\omega - \omega_0) \propto \left(\frac{K}{T^3}\right)^{-1}$ for the dominant phonons of frequency $\omega \sim 3.8 k_B T/\hbar$,

$$g(\omega - \omega_0) \propto T^2/K \quad (\text{Challis et al 1977}).$$

The data for GA735(e) plotted in this form (figure 3.5) suggest $g(\omega - \omega_0)$ might be approximately Gaussian,

$$g(\omega - \omega_0) \propto e^{-(\omega - \omega_0)^2/\Delta^2}$$

Using this form in τ_D^{-1} , improved the fit but the result was not very satisfactory.

The next step was to use a Lorentzian lineshape for $g(\omega - \omega_0)$ so that $\tau_D^{-1} = D_D \omega \Gamma / (\Gamma^2 + (\omega - \omega_0)^2)$ where Γ is the width of the distribution. The fit was considerably improved and found satisfactory for the whole temperature range. The reduced resistivity R is displayed in figure 3.6 for both Gaussian and Lorentzian lineshapes. The effects of the two resonances (high temperature -

coherent scattering, and low temperature with a Lorentzian lineshape) acting separately are also shown on the same figure. Figure 3.7 shows the data plotted with the calculated curves using the two lineshapes for comparison. Also plotted on the same figure are the K/T^3 data points with the best fits.

The same resonant terms (coherent scattering process and direct process) gave a good fit for TI#5, using a very slightly lower frequency for the high temperature dip. The ratio W_{exp}/W_{calc} is plotted in figure 3.8, showing the effect of the two resonant terms. The calculated conductivity curve is compared with the experimental one in figure 3.9, which also shows the fit for K/T^3 , $T \leq 10$ K. All the fitting parameters are summarized in Table 3.1.

From figures 3.7 and 3.9, the calculated conductivity curves are somewhat higher than the experimental ones, at the lowest temperatures ($T \leq 0.1$ K). The computed value of K/T^3 for these temperatures tends towards $(K/T^3)_{intrinsic}$, which should be expected in the absence of any other low frequency scattering mechanism but the experimental K/T^3 curve is rather flat and might suggest an additional scattering process. This behaviour was not observed in GA781 (figure 3.2.a) and we did not try to account for this possible, very low frequency ($\sim 0.2 \text{ cm}^{-1}$) process.

The next sample considered was TI#4 for which data was available between 1 and 60 K. The effect of the high temperature resonance is less pronounced in this sample than in GA735(e), GA781 or TI#5. An attempt was made to fit the data using the same resonant terms as previously, and keeping the same resonant

frequencies. This was not successful and it was found necessary to increase the low temperature resonant frequency to obtain a good fit (Table 3.1). The results of the fit are shown in figure 3.10, in which the behaviour of (K/T^3) calculated, at the lowest temperature, is noteworthy. It would be very useful to extend the measurements for this sample down to 50 mK. Figure 3.11 is a plot of the reduced resistivity R . Using the relaxation rate for a coherent scattering process to account for the low temperature dip was found less satisfactory.

In summary, the resonant phonon scattering by small amounts of Cr impurities in GaAs is well described assuming two different scattering processes: a coherent elastic scattering at the higher frequency ($23 \pm 5 \text{ cm}^{-1}$) and a direct process scattering at the lower frequency ($0.7 \pm 0.1 \text{ cm}^{-1}$). The calculated conductivity of sample TI#4 is in good agreement with the experimental one only if the low resonant frequency is increased to $4.9 \pm 1 \text{ cm}^{-1}$, possibly indicating that the low temperature scattering in this sample arises from a different set of energy levels. Any scattering at this frequency in GA735(e) or TI#5 is relatively weak and we do not need to include a third resonant term to account for the experimental data for these samples. In the next section, an attempt is made to try to identify the centres responsible for the scattering.

3.7 PRELIMINARY INTERPRETATION OF THE RESULTS

In this section we discuss the results in terms of the different charge states of the Cr ions which are deduced using a model proposed by Brozel et al (1978). (See Appendix 1 - The notation for the different charge states is also defined). Table 1 of Appendix 1 shows the dominant charge state believed to be in every sample.

Now Cr is believed to substitute for Ga in the GaAs host lattice (see e.g. Krebs and Stauss 1977a). From the data for GA735 (O64) and GA785 it seems clear that the phonon scattering by Cr^{1+} is very small. This is expected since Cr^{1+} ($3d^5$) in a tetrahedral crystal field is an orbital singlet 6S and will be very weakly coupled to the phonons (see e.g. Blume and Orbach 1962).

If we consider the high temperature dip, for a coherent elastic scattering process, the strength of the scattering is proportional to the population of the centre. GA735(e) should have a dominant population of Cr^{2+} centres according to Brozel et al (1978). Also the Cr^{2+} Thermally Detected EPR spectrum similar to that of Krebs and Stauss (1977a) was, very recently observed in this sample (McCann - Private Communication). The p-type sample GA781 and the SI sample TI#5 should contain mainly Cr^{3+} ions. From this and from the strength of the scattering for these three samples (see Table 3.1 and also the data of figure 3.1), it seems very likely that the resonant scattering at $\approx 23 \text{ cm}^{-1}$ is due to Cr^{3+} . This conclusion is also discussed in Chapter 7 in the light of measurements on the same samples, using other techniques in our laboratory.

At this stage it is not clear whether the low temperature resonances ($\sim 0.7 \text{ cm}^{-1}$ and 4.9 cm^{-1}) are due to Cr^{2+} and/or Cr^{3+} or another centre. A tentative interpretation is given in Chapter 7.

	$\tau_{b\ th}^{-1}$ $\times 10^6\ sec^{-1}$	$\frac{\tau_{B\ th}^{-1}}{\tau_{b\ exp}^{-1}}$	$\frac{A_{imp}}{A_{isotopes}}$	D_D	ω_{o_D} (cm^{-1})	Γ (GHz)	D_C	ω_{o_C} (cm^{-1})
GA735 (O64)	1.15	~ 2	~ 4					
GA735(e)	1.08	~ 2	~ 4	8×10^7	0.7 ± 0.1	21	5×10^7	24 ± 5
TI#5	0.58	~ 2	~ 4	1.6×10^8	0.7 ± 0.1	29	2×10^8	23 ± 5
TI#4	0.74	~ 2	~ 4	1.0×10^7	4.9 ± 1	21	8×10^6	23 ± 5

Table 3.1 The resonance terms are

$$\tau_D^{-1} = D_D \omega \Gamma / (\Gamma^2 + (\omega - \omega_{o_D})^2) \quad \text{for the direct process}$$

$$\tau_C^{-1} = D_C \omega^4 / (\omega^2 - \omega_{o_C}^2)^2 \quad \text{for the coherent scattering process.}$$

$A_{isotopes}$ is the calculated value, $A_{isotopes} = 0.548 \times 10^{-44} \text{ sec}^3$.

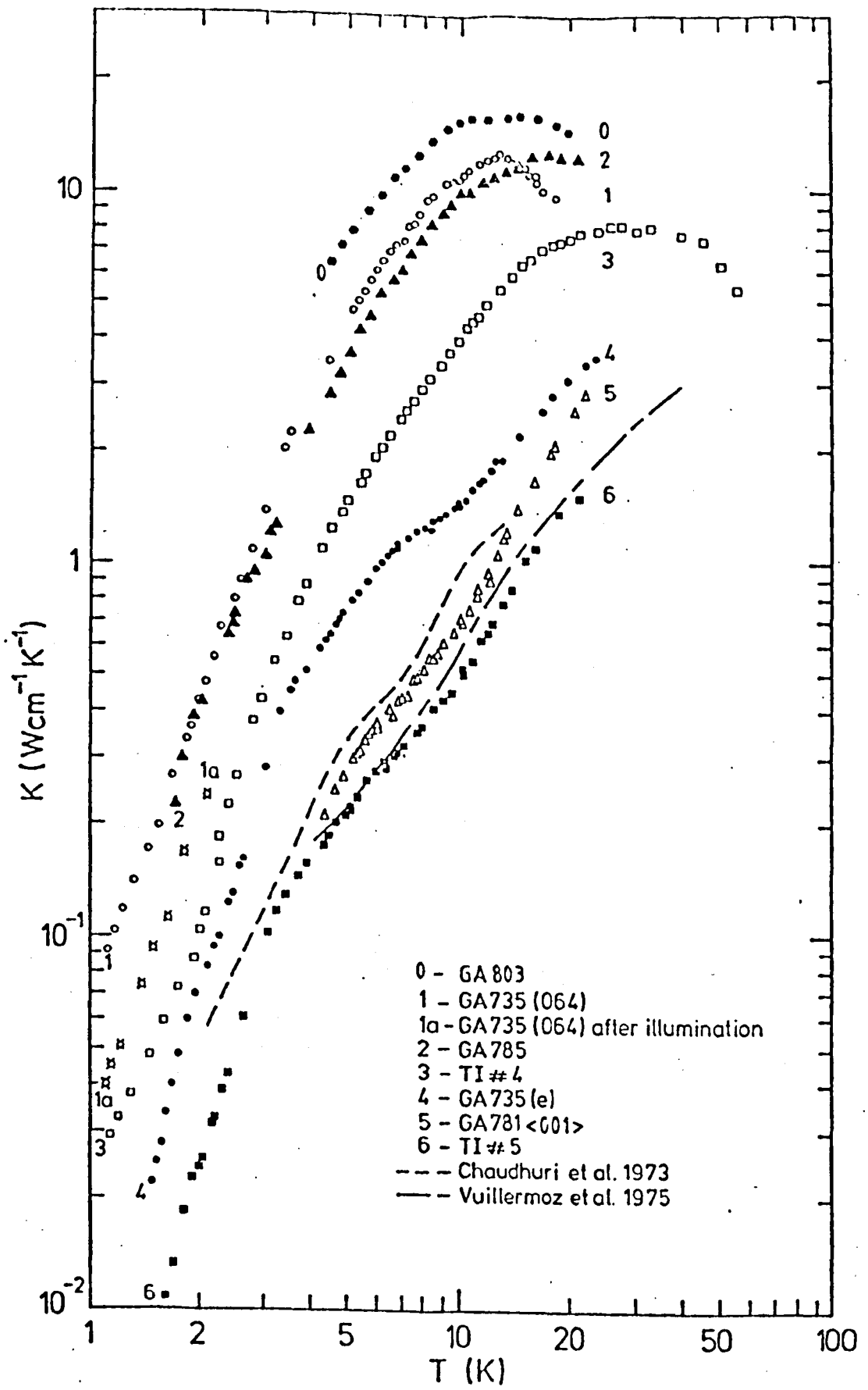


FIGURE 3.1 $K(T)$ for all the samples. The results of previous workers are also plotted for comparison.

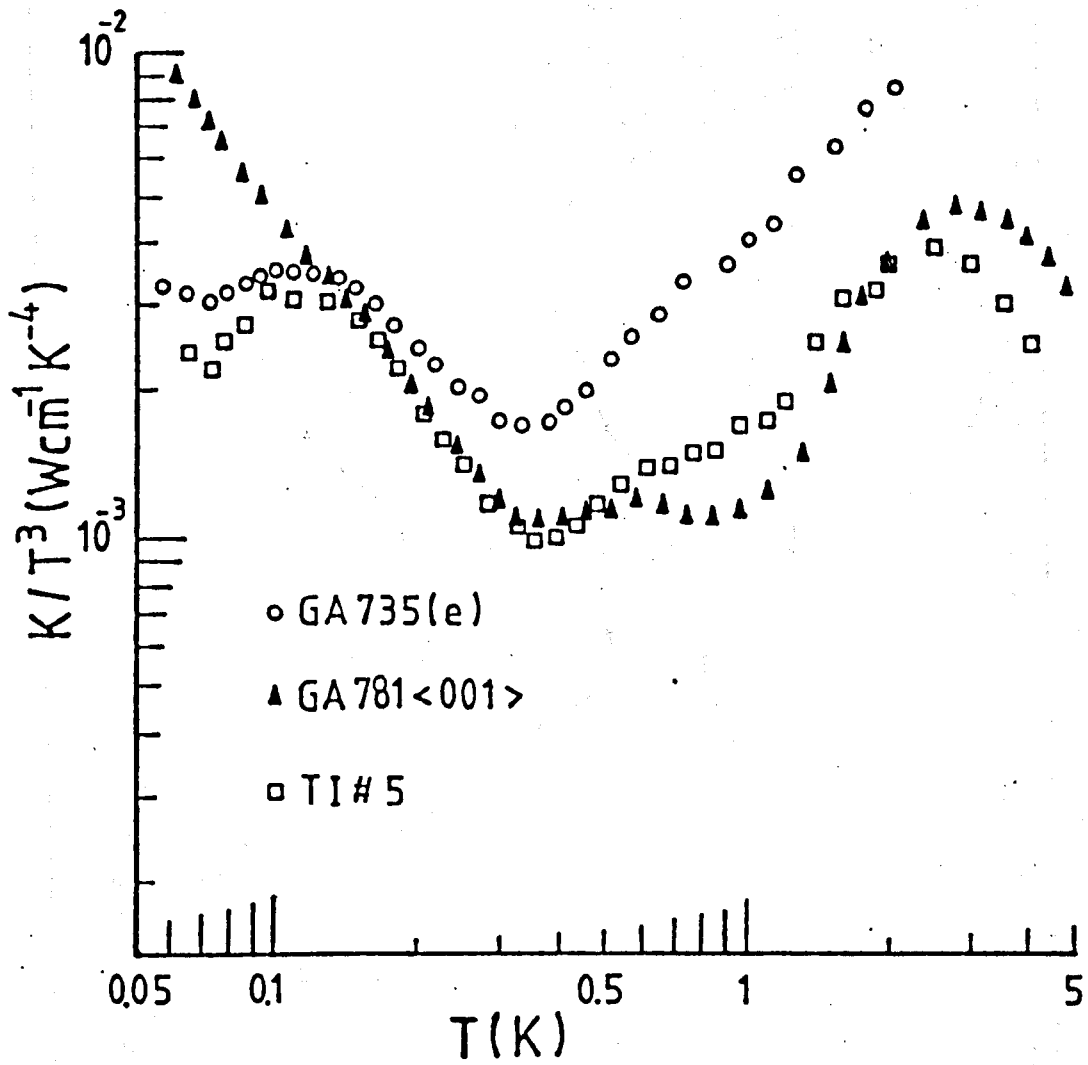


FIGURE 3.2.a

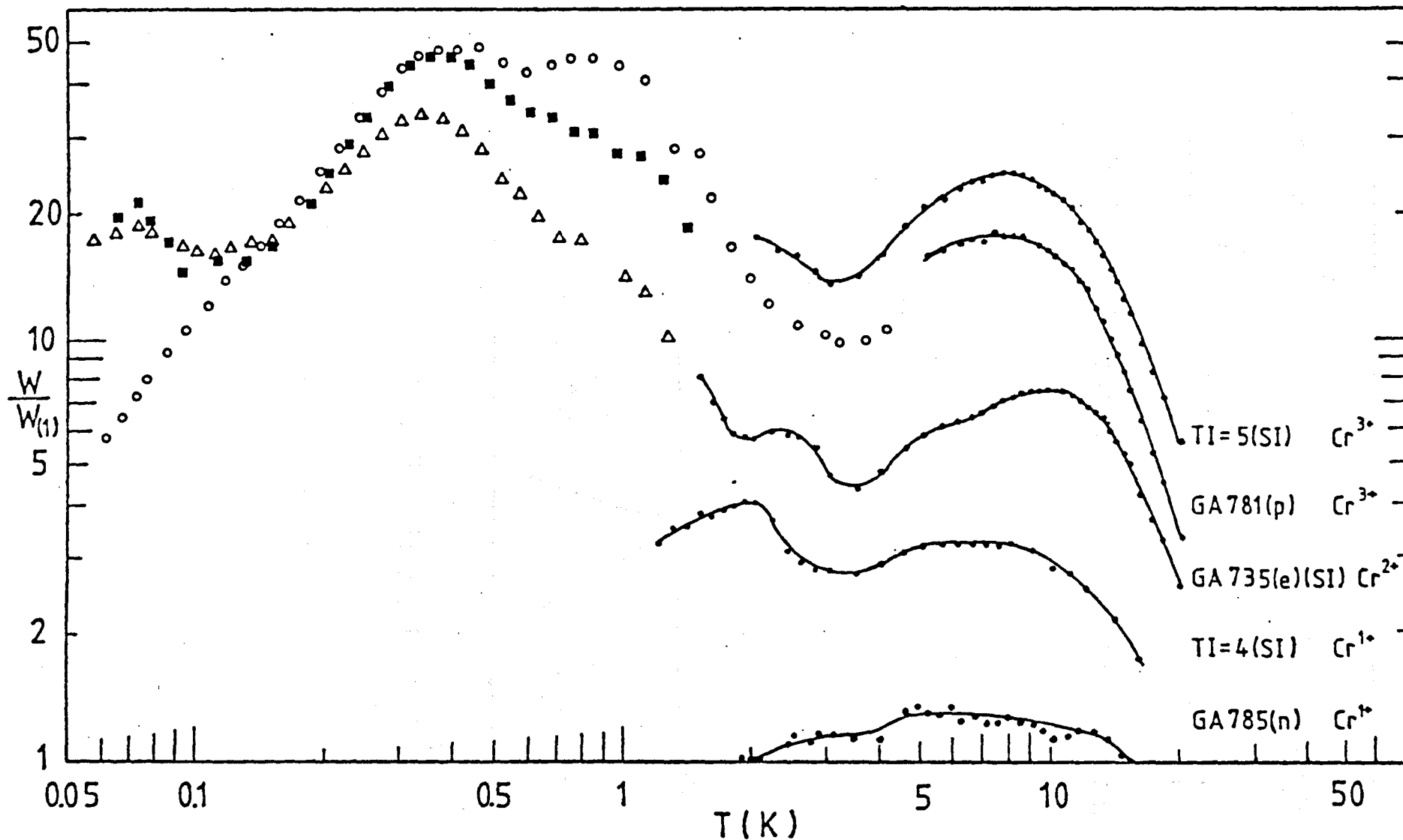
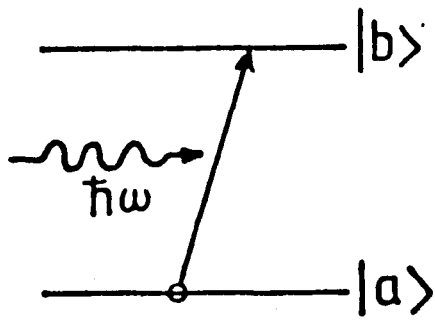
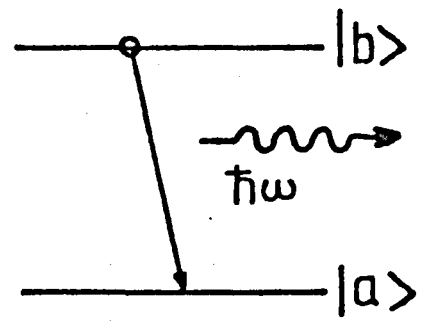


FIGURE 3.2.b $W/W_{(1)}$ -versus- T . $W_{(1)}$ is the resistivity of n-type GA735 (O64).

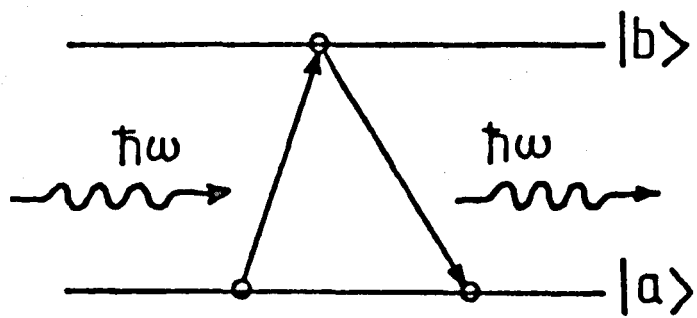


Spin initially in lower level



Spin initially in upper level

FIGURE 3.3.a Diagrammatic representation of direct process.



Spin initially in lower level

FIGURE 3.3.b Diagrammatic representation of coherent elastic process.

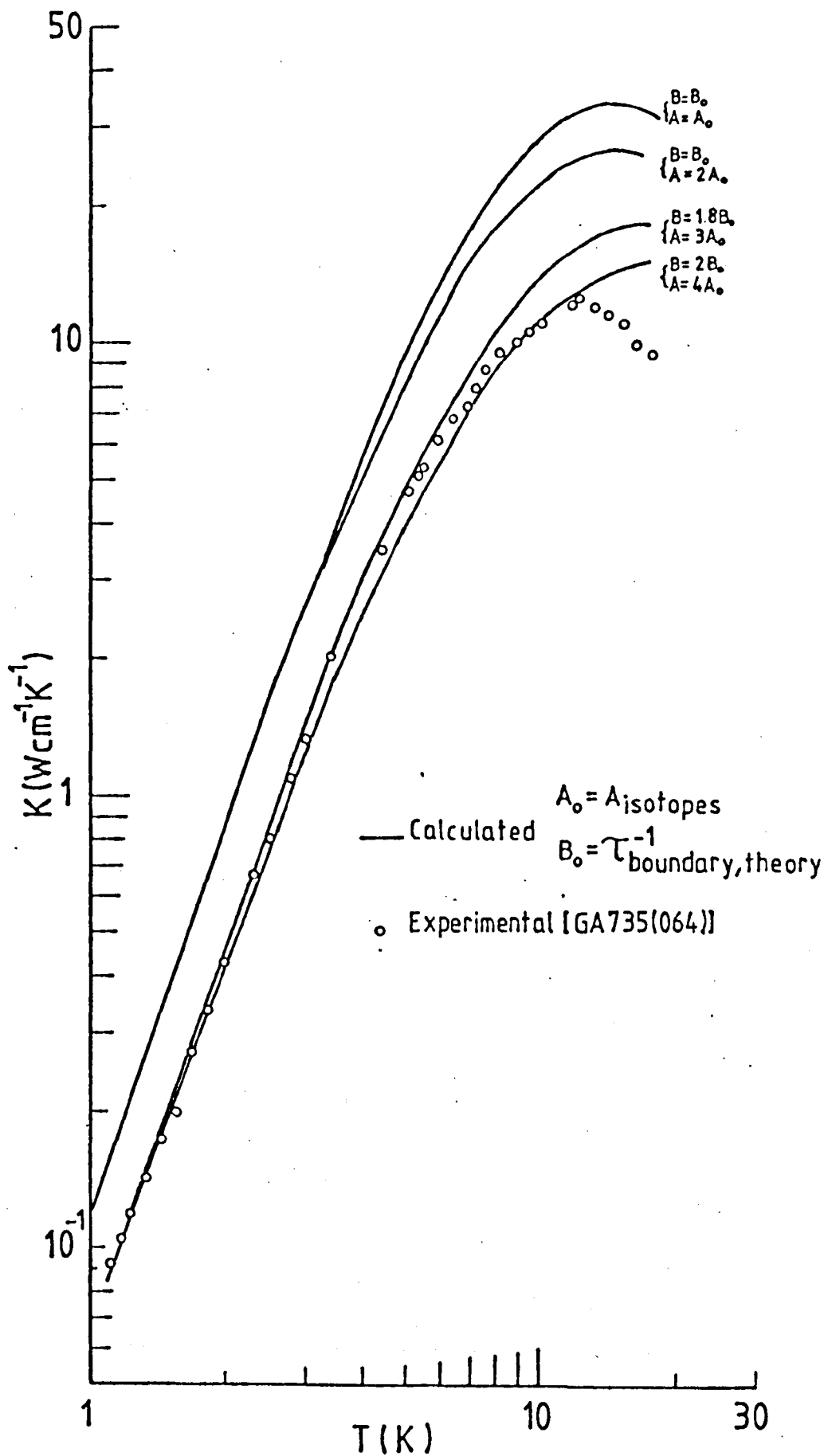


FIGURE 3.4 $K(T)$ calculated for boundary and impurity scattering only ($\tau^{-1} = \tau_{\text{boundary}}^{-1} + A\omega^4$).

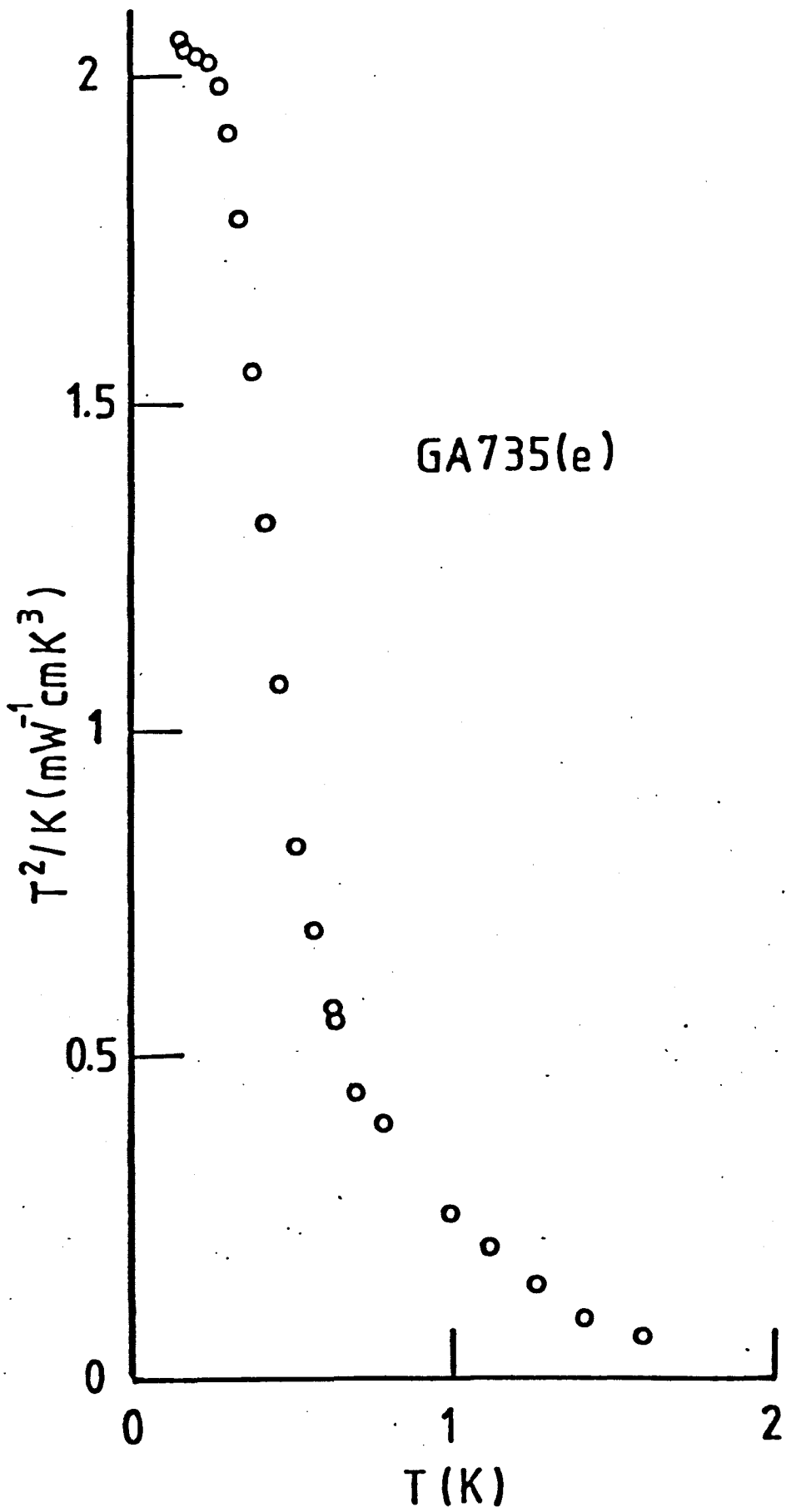


FIGURE 3.5

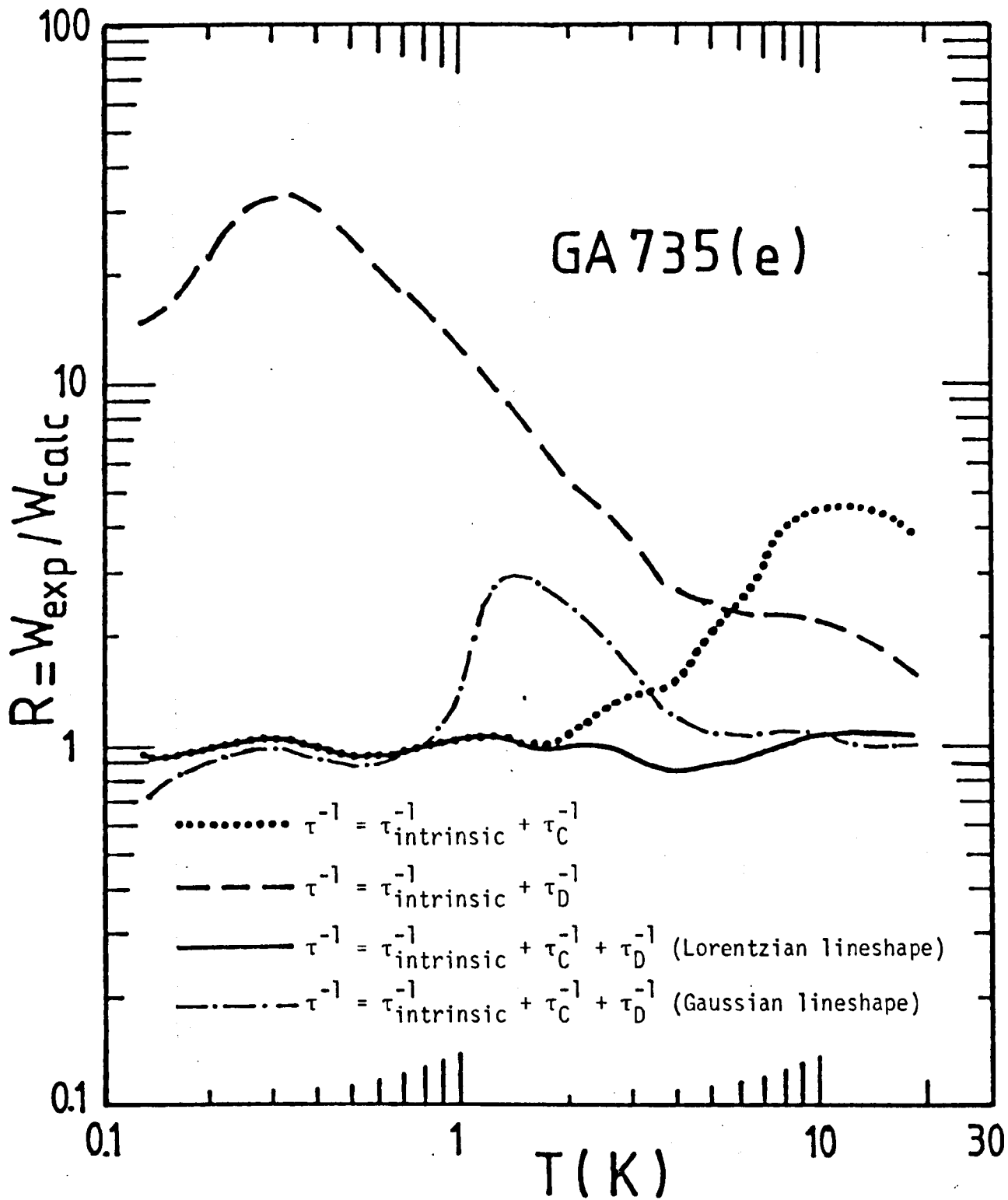


FIGURE 3.6 Reduced resistivity of GA735(e) for different processes and lineshapes.

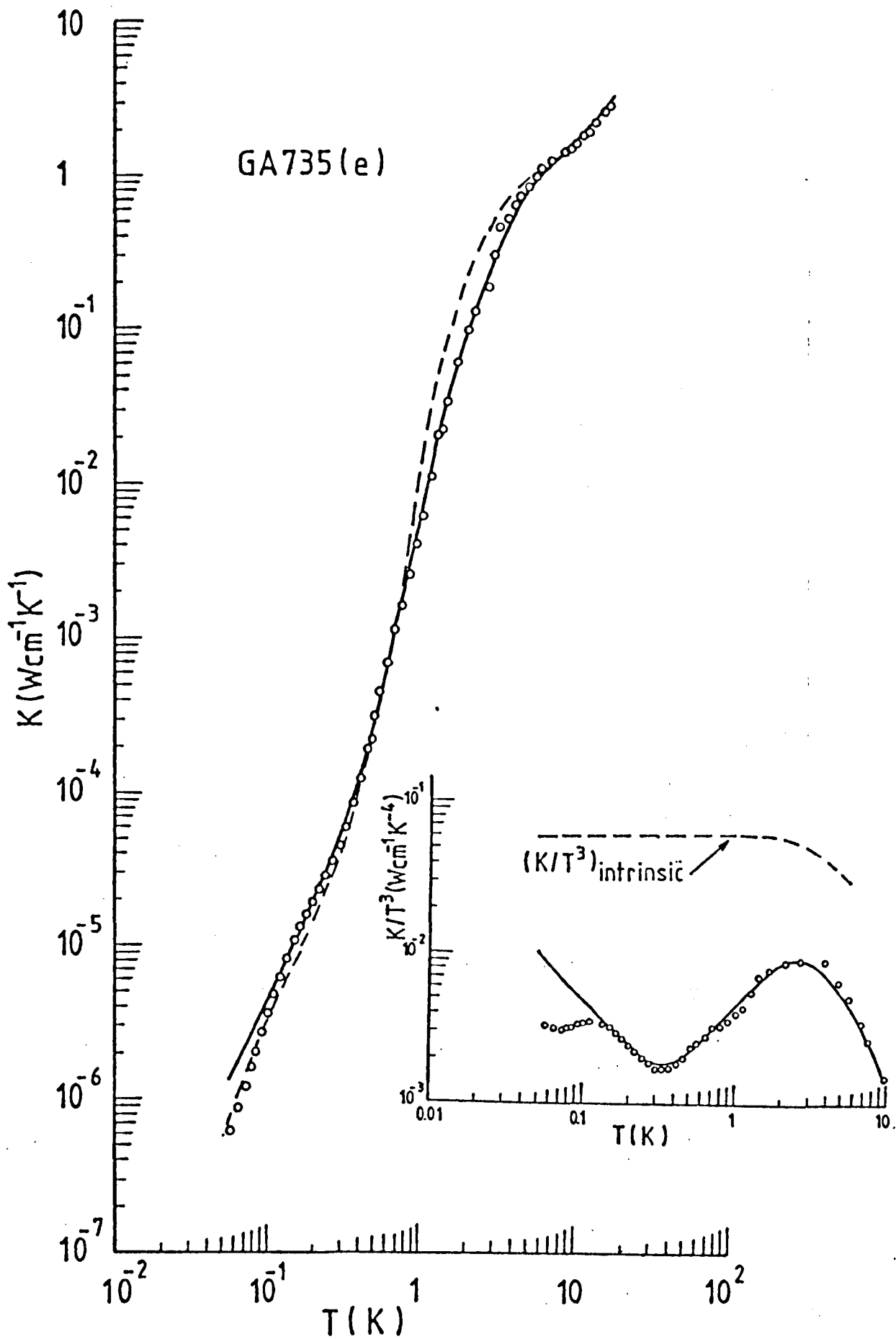


FIGURE 3.7 Thermal conductivity of GA735(e).

(o - experimental, --- - calculated).

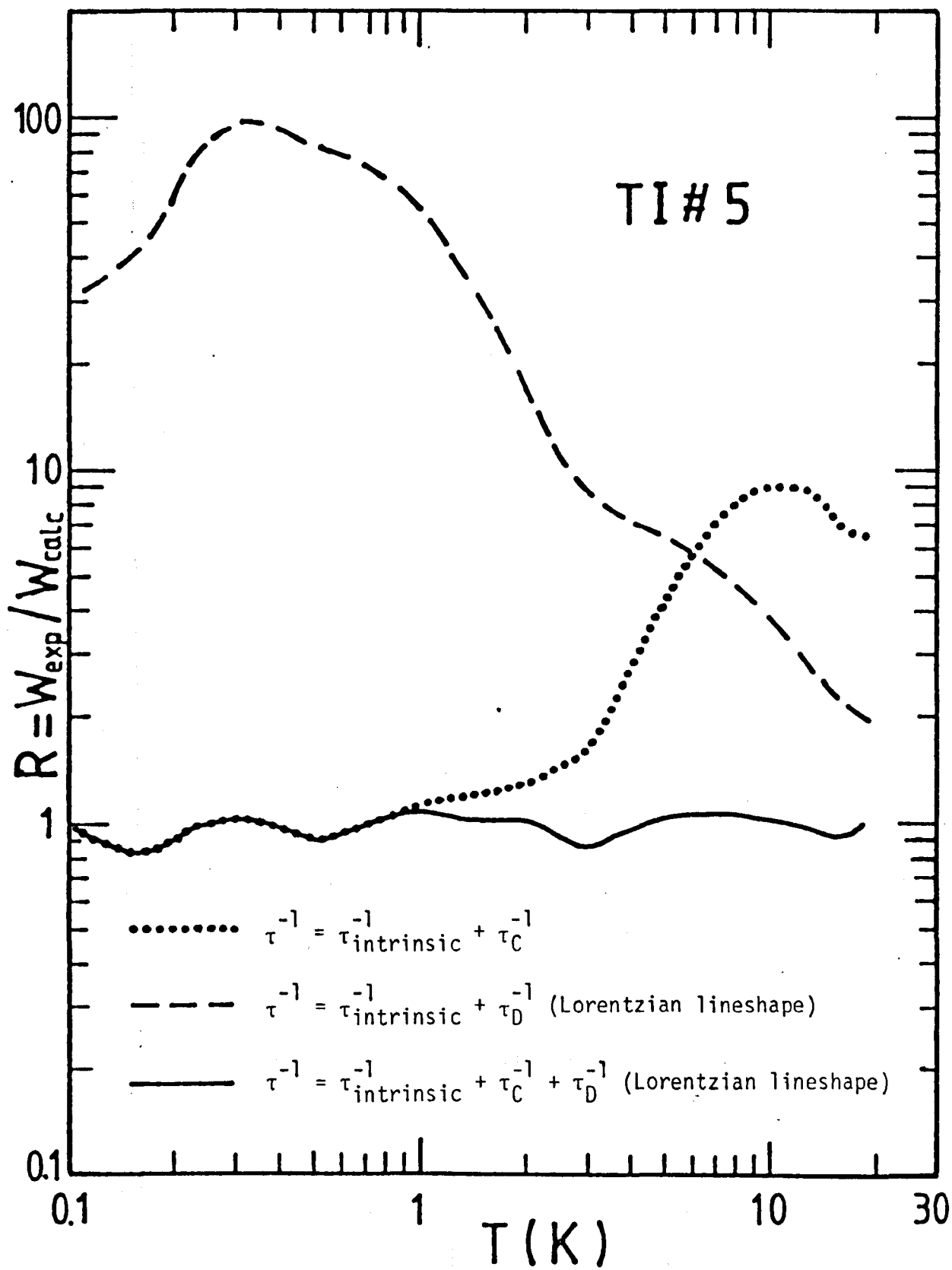


FIGURE 3.8 Reduced resistivity of TI#5.

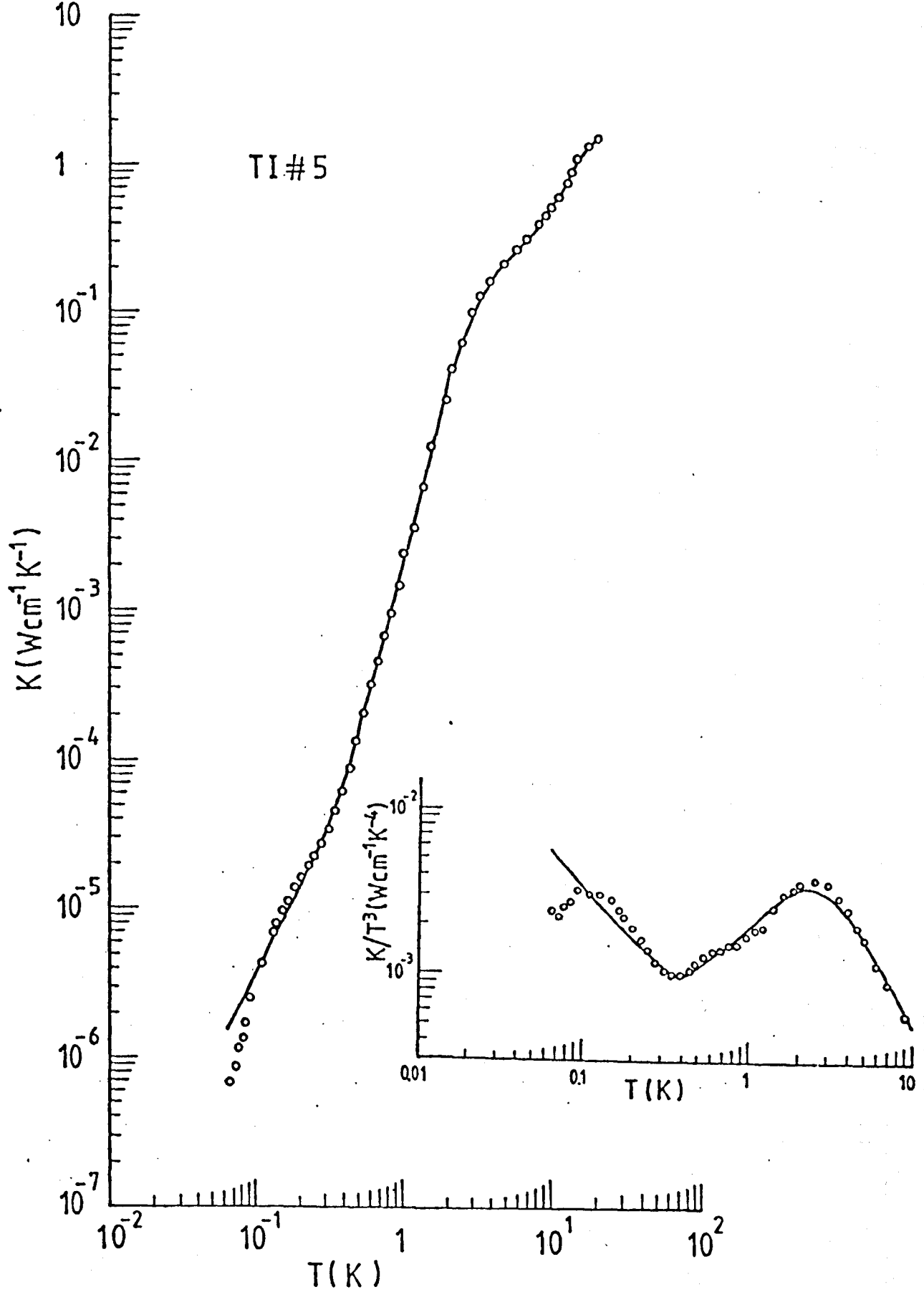


FIGURE 3.9 Thermal conductivity of TI#5.

(o - experimental, — - calculated).

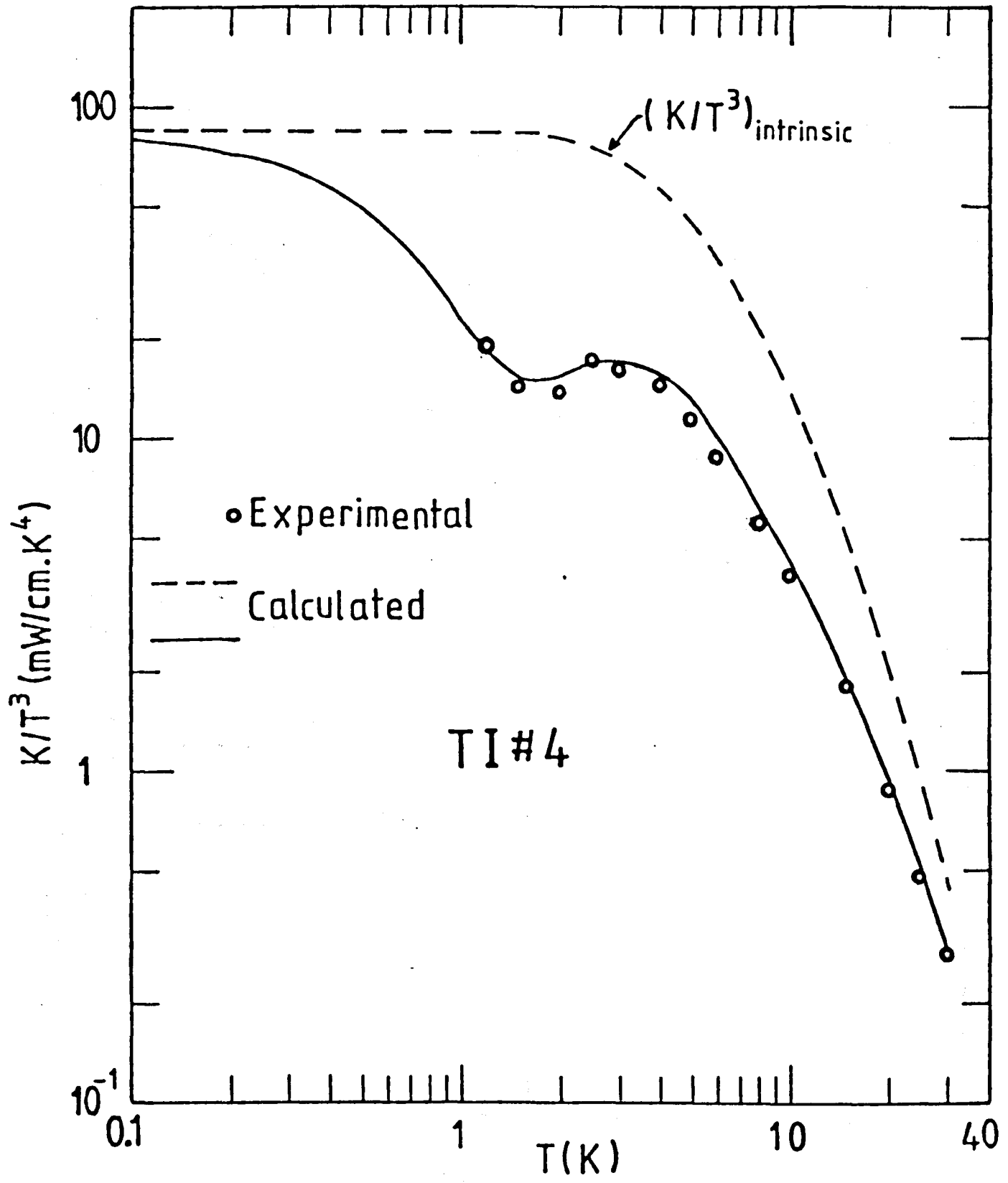


FIGURE 3.10

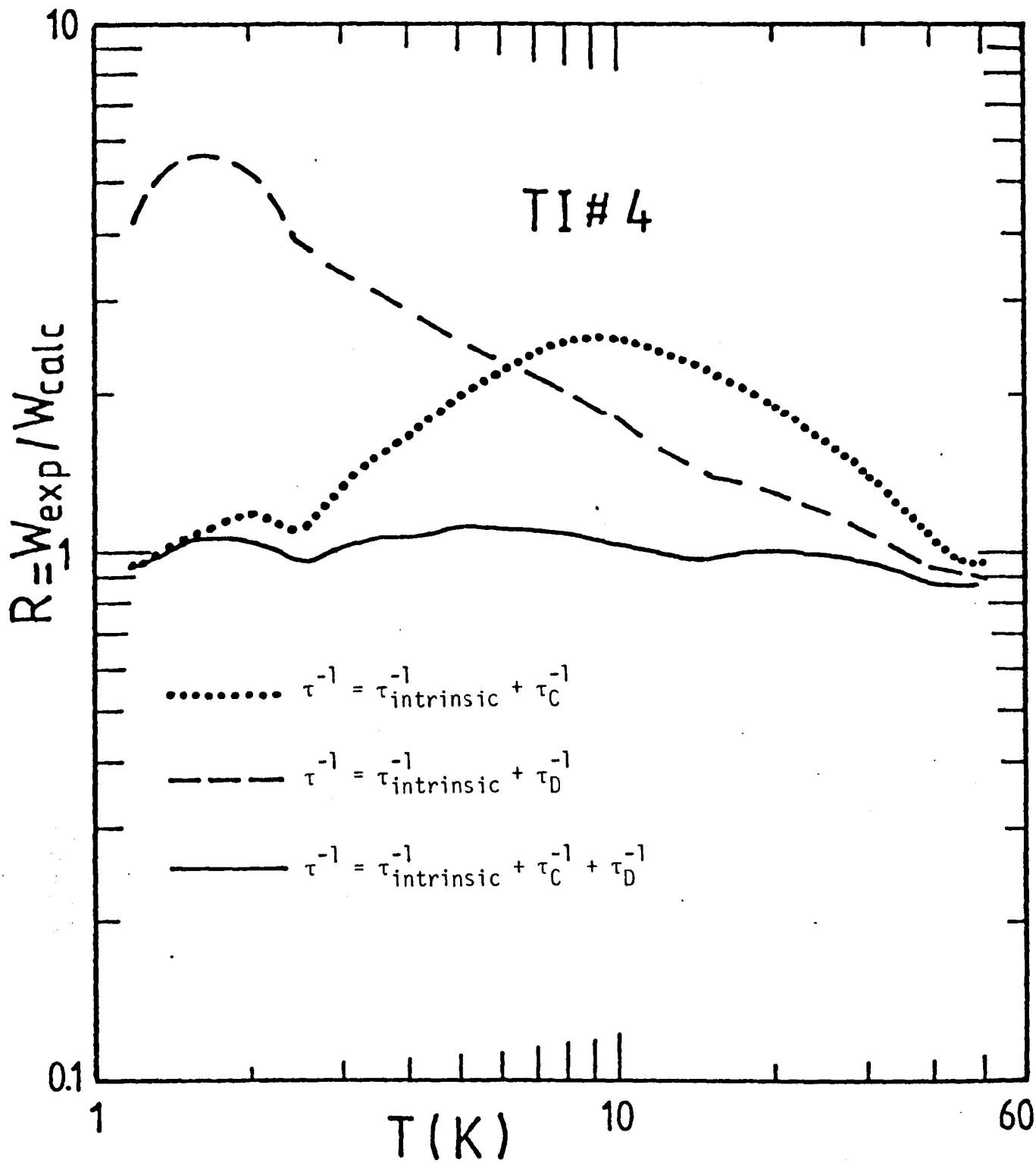


FIGURE 3.11

CHAPTER 4

THE MAGNETOTHERMAL CONDUCTIVITY OF GaAs:Cr

4.1 INTRODUCTION

This chapter describes work undertaken to complement the zero-field data obtained for several GaAs:Cr samples. In view of the apparent discrepancy between optical, APR and EPR results on the structure of the ground state of this system, it was initially hoped that it might be possible to investigate the low lying energy levels using thermal phonons as a probe, with the application of magnetic fields. This technique proved very useful in the study of transition metal ions in dielectrics (see e.g. Anderson and Challis 1975). The observation of a 'frequency crossing' signal can yield valuable spectroscopic information on the system under investigation.

Details of the samples used in this study are given in Appendix 1. In the next section a short summary is given of the different models for the ground state structure of GaAs:Cr. The results are then presented and discussed using a simple model.

4.2 LOW LYING ENERGY LEVELS OF GaAs:Cr

In this section we present a review of different investigations of the behaviour of the Cr atoms in the GaAs host lattice and particularly the structure of the ground state of these impurities.

Most of the studies which could yield a picture of the low lying energy levels of the impurities used the techniques of Acoustic Paramagnetic Resonance (APR) or Electron Paramagnetic Resonance (EPR). The quantum of energy involved in the two techniques is about the same (usually $\approx 0.3 \text{ cm}^{-1}$) but the selection rules are different. In the case of EPR, the transitions are within levels of the same orbital angular momentum number ($\Delta M_L = 0$) but with different spin values ($\Delta M_S = \pm 1$). An acoustic wave induces transitions between levels of different M_L ($\Delta M_L = \pm 1, \pm 2, \dots$) with $\Delta M_S = 0$. APR is particularly suited for ions which are strongly coupled to the lattice and for broad resonance lines but the two techniques are complementary to each other. The different interpretations always used point charge crystal field approximations for determining the energy levels structure.

Ganapol'skii (1975) first reported the interaction of longitudinal sound waves ($9.4 \text{ GHz} \approx 0.3 \text{ cm}^{-1}$) with Cr atoms in GaAs at liquid helium temperatures. A strong resonant absorption of hypersound was observed at $T \sim 1.7 \text{ K}$ and ascribed to the Cr^{2+} charge state on a Ga site (T_d symmetry). A dynamic Jahn-Teller effect was invoked to explain the features of the data (magnitude of the resonant absorption, its temperature dependence, values of the resonance fields for different directions, effects of local strains). The energy levels diagram for the system is shown in figure 4.1. All the effects could be explained by considering transitions within the Zeeman split levels of the Γ_5 triplet state. The nearest excited state Γ_4 is separated by $\sim 5 \text{ cm}^{-1}$.

EPR measurements performed by Krebs and Stauss (1977a, 1977b) have shown the existence of at least three charge states for substitutional Cr in GaAs: Cr^{3+} , Cr^{2+} and Cr^{1+} . Photo-induced charge conversion was observed among the three charge states, each with a different local symmetry.

The X-band EPR spectrum of Cr^{3+} ($3d^3$) in semi-insulating Cr-doped GaAs was explained using an orthorhombic (C_{2v}) symmetry spin Hamiltonian. The Cr^{2+} ($3d^4$) centre presented a tetragonal (D_{2d}) symmetry and in both cases the lowering of the symmetry was attributed to a strong static Jahn-Teller distortion. The Cr^{1+} centre, observed in these SI samples only after sub-band-gap illumination, showed a cubic symmetry (T_d), seemingly implying that the lowering of the local symmetry for Cr^{2+} and Cr^{3+} was not related to the presence of a nearby defect. Kaufmann and Schneider (1976) had previously observed the same Cr^{1+} spectrum after near IR excitation. The energy levels diagrams of Cr^{2+} and Cr^{3+} given by Krebs and Stauss are shown in figures 4.2 and 4.3. In the case of Cr^{2+} , an orbital singlet 5B_2 is lowest with an effective spin $S = 2$. The EPR spectrum arises from transitions between the splittings of 5B_2 by second order spin-orbit coupling and Zeeman effect.

Wagner and White (1979) observed the Far-Infra-Red absorption ($\sim 11.2 \text{ cm}^{-1}$) by Cr^{2+} centres in GaAs at high magnetic fields. They found they could account for their results using the spin-Hamiltonian derived by Krebs and Stauss (1977b).

Thus EPR spectroscopy at two very different frequencies seems to well establish the occurrence of static Jahn-Teller effects in GaAs:Cr at low temperatures ($T \leq 10 \text{ K}$).

The magneto-acoustic resonance absorption in Cr-doped GaAs was also measured by Tokumoto and Ishiguro (1977b) for different impurity concentrations, acoustic frequencies and temperatures. Several sharp resonance peaks were observed and were ascribed to either level-crossing or level anti-crossing but no model which could explain all the experimental data was derived.

More recently, APR measurements at 9.6 GHz were made on SI samples, n- and p-type samples, in our laboratory (Bury et al 1980a). A complex APR spectrum was observed (amongst the stronger lines are the ones observed by Ganapol'skii), indicating that Cr was present in several different sites. Charge state conversion after illumination in the n-type sample and non-observation of any APR absorption in the p-type sample lead the authors to attribute most of the lines to Cr^{2+} . A model assuming the existence of a dynamic Jahn-Teller effect was developed to account for the spectrum (Bates et al 1980).

The structure of the ground state of GaAs:Cr was also deduced from high resolution optical measurements on the 0.82 and 0.839 eV zero-phonon line. This is discussed in Chapter 7.

In summary, this short review shows the complexity of the ground state of the SI GaAs:Cr system. No model which could explain all the different experimental results is available. It is also rather surprising that no zero-field very Far-Infra-Red work has yet been reported, which could be utilized in testing the different proposed models (e.g. Vallin et al 1970).

4.3 EXPERIMENTAL RESULTS

4.3.1 Field Alignment

The specimens were mounted with their axes, the $\langle 110 \rangle$ direction, vertical. The magnetic field was rotated in the (110) plane and so could be applied along all three main crystallographic directions ($\langle 001 \rangle$, $\langle \bar{1}\bar{1}1 \rangle$ and $\langle \bar{1}\bar{1}0 \rangle$). The field was aligned with respect to the $\langle 001 \rangle$ direction, first, by inspection. A more precise alignment was then made by plotting the fractional change in the thermal resistance $\Delta W/W_0$ at fixed temperature and field at every few degrees of rotation of the magnetic field. The rotary diagram produced in this way has cubic symmetry (figures 4.4 to 4.6) and minima with mirror symmetry at angles which coincide with the approximate $\langle 001 \rangle$ directions determined by inspection. (Symmetric minima also occur along $\langle 110 \rangle$ directions). This type of anisotropy is discussed in section 4.4.5.

4.3.5 The Magneto-thermal Conductivity of the Pure and n-type

Samples

The effect of a magnetic field on the thermal conductivity of GaAs:Cr at low temperatures was found to be dependent on the concentrations of the different charge states of the Cr ions in the samples.

No measurable change in the conductivity was observed in the undoped sample (GA803), showing that residual impurities in the samples were not appreciably affected by the magnetic field. Negligible magnetoresistance was also observed in GA785 and GA735 (O64) up to 5.5 T, consistent with the small phonon scattering by Cr ions observed in zero-field (section 3.3).

4.3.3 The Magnetothermal Conductivity of the SI Samples

Large effects were observed in GA735(e), TI#4 and TI#5 and are shown in figures 4.7, 4.8 and 4.9 respectively. The general feature is a broad maximum in the reduced resistivity when the field is increased. At high-field (~ 5.5 T), $\Delta W/W_0$ is less than the zero-field value, showing that the conductivity is increasing. This reduction in phonon scattering is most clearly seen in GA735(e) (figure 4.10) where the measurements were taken up to 13 T. At high enough fields and at low temperatures the scattering appears to saturate and the conductivity reaches a limiting value which is $\sim 20\%$ higher than the zero-field value. However this value is still only $\sim 10\%$ of the value of a pure sample indicating that the Cr ions are still scattering quite strongly. In figure 4.10 is also shown, for comparison, the magnetoresistance of GA785. We also note a change in slope of $\Delta W/W_0$ of GA735(e) at ~ 4 kG and for $T \lesssim 1.5$ K only (figure 4.7).

In TI#4 there is a second main maximum in $\Delta W/W_0$ at a slightly higher field, the size of which is increasing relatively to the first one as the temperature is increased. This second peak is also shifted to higher fields with increasing temperature while the position of the first one remains practically unchanged.

The effects are larger in TI#4 ($\sim 49\%$ change at 1.15 K for the field along $\langle 001 \rangle$) than in TI#5 or GA735(e) ($\sim 26\%$ at 1.26 K and 20% at 1.25 K respectively) at the lowest temperatures. The variation with temperature of the size of the effects is also different in TI#4 where the change at the two maxima, $(\Delta W/W_0)_{\max}$, decreases very rapidly when the temperature is increased.

GA735(e) shows a rather slow and linear change of $(\Delta W/W_0)_{\max}$ with temperature and the results are plotted for both samples in figure 4.11. For $T \gtrsim 1.5$ K the effect becomes larger in GA735(e).

This very different behaviour might suggest the magnetic scattering in the two samples arises from different centres.

4.3.4 Frequency Crossing Spectra in TI#4, TI#5 and SI GaP:Cr

TI#4 proved to be the most interesting sample in the magnetic field study. Several temperature independent minima were observed in the thermal resistivity, superimposed on the broad overall change described in the previous section. These 'frequency crossing' lines can be seen in figure 4.8. Five distinct lines are observed and the position of field at which they occur is, to within experimental error, completely independent of temperature (Table 4.1). A rather striking feature of these 'frequency crossings' is that their positions do not change as the field is rotated in the (110) plane (figure 4.12). This indicates the system responsible for them has complete cubic symmetry.

Similar isotropy was observed in crossings seen in a sample of SI GaP:Cr (figure 4.13). That sample was considered for possible comparison with SI GaAs:Cr but no extensive study of the GaP:Cr system was undertaken.

To conclude, large field effects were seen in the SI samples while the n-type samples did not show any variation with field. In the less heavily (Cr)-doped sample TI#4, which has an intermediate zero-field conductivity, isotropic frequency crossing

signals were observed. Two of these lines could also be detected in TI#5 but they were too weak to study. In the next section, a simple model is used to try to account for these effects.

4.4 DISCUSSION

No detailed calculation has been attempted at this point to explain the experimental data. The basic problem is that we do not know for sure which ion (Cr^{2+} or/and Cr^{3+}) is responsible for the magnetic field effects. Also, even if the centre is unambiguously identified there is no generally accepted model readily available for the structure of the ground state (section 4.2). In what follows we try to explain some features of the data in a qualitative way using a model for the magnetoconductivity proposed by Berman et al (1963).

4.4.1 A Simple Model

In a magnetic doublet, a field B produces a splitting $\hbar\omega_0$ given by $\hbar\omega_0 = g\beta B$, where g is the spectroscopic (Landé) splitting factor and β is the Bohr magneton. In this model, the resonant phonon scattering within the doublet is assumed to be large within a bandwidth $\Delta\omega_0$ centred about ω_0 and small outside this bandwidth. Effectively there is no contribution to the thermal conductivity from the phonons of energy $\hbar\omega_0$. For narrow bandwidths, an expression for the fractional change in the thermal conductivity due to the resonant scattering can be derived, using the expression for $K(T)$ (section 3.4)

$$\frac{\Delta K}{K_0} = - \frac{AT^3 f(x_0, T) \Delta x_0}{K_0} \quad (4.1)$$

where $A = k^4/2\pi^2 v k^3$ and $x_0 = \hbar\omega_0/kT$, v is an average phonon velocity and $f(x,T)$ which describes the spectral distribution of the heat current is given by

$$f(x,T) = \frac{x^4 e^x}{(e^x - 1)^2} \tau(x,T) \quad (4.2)$$

$\tau(x,T)$ describes the scattering processes present in zero field. In the boundary scattering régime, $\tau^{-1} = \frac{v}{L}$ where L is the diameter of the crystal and $f(x,T)$ is shown in figure 4.14. It has a maximum at $x = 3.8$ which corresponds to a wavenumber $\bar{\nu}_m = 2.5 \text{ T cm}^{-1}$. The reduction in the conductivity produced by the resonant scattering is represented by the shaded area (the fractional reduction is the ratio of the shaded area to the total). From the figure and from (4.1) it can be seen that if $\hbar\omega_0 = g\beta B$, the change in $\Delta K/K_0$ produced by sweeping the magnetic field has the same form as $f(x,T)$, provided that $\Delta\omega_0$ does not change with field. In particular the maximum reduction occurs for a field such that the band of phonons is centred under the maximum. Thus, the variation of thermal resistance with field should just trace out the heat current spectrum curve with the splitting of the magnetic ion being used as a 'ruler'. In the next sections the heat current spectra $f(x,T)$ are computed for GA735(e) and TI#4 and used to describe the field effects.

4.4.2 Application to GA735(e)

The heat current spectrum $f(x,T)$, where $\tau(x,T)$ is the total relaxation time in zero field obtained by fitting the zero-field data (Chapter 3), is shown in figure 4.15, for temperatures 1 - 4 K. The shape and variation of the experimental curves (figures

4.7 and 4.10) can qualitatively be interpreted if we consider the $f(x,T)$ curves.

In this sample there is only one broad maximum in $\Delta W/W_0$, when the field is swept and this maximum is shifted to higher fields with increasing temperature. This is the expected behaviour if we use the simple model described in the previous section. The positions of the fields, B_m , at which the maximum in $\Delta W/W_0$ occurs for $B_{||} \langle 001 \rangle$ are plotted in figure 4.16 for different temperatures. We can see an abrupt change in the variation of B_m with temperature for $T \sim 1.4$ K, corresponding to an energy $\sim 5 \text{ cm}^{-1}$. The positions of the peaks in the heat current spectrum \bar{v}_m are also plotted in figure 4.16 versus the corresponding B_m . The behaviour for $T \geq 1.4$ K can then be explained if we assume phonon scattering between a magnetic doublet, with $g(\langle 001 \rangle) \approx 5.6 \pm 0.3$ (figure 4.16). The line through the B_m -versus- T data points is a calculated one for $g \approx 5.6$. However for $T \leq 1.4$ K, the calculated heat current spectrum for this sample does not account for the field behaviour. This indicates another scattering process is becoming important at these low temperatures, which has not been included in the calculation of $f(x,T)$. This process is represented by the change in slope observed at ~ 4 kG in the broad $\Delta W/W_0$ maximum (figure 4.7). From figure 4.19 the g -values describing the phonon scattering within the magnetic doublet, along other crystallographic directions, can be evaluated:

$$g(\langle 1\bar{1}1 \rangle) = 7.2 \pm 0.4 \text{ and } g(\langle 1\bar{1}0 \rangle) = 4.6 \pm 0.2.$$

These g -values are rather large and it is not clear whether the splittings are due to Cr^{2+} or Cr^{3+} ions. (We note that Krebs and

Stauss (1977a) report a g -value along $\langle 001 \rangle$ of 5.154 but the anisotropy we observe is completely different to theirs).

From the total area of the $f(x,T)$ curves we should expect that the change in $\Delta W/W_0$ would decrease with temperature (if $\Delta\omega_0$ does not change with field), which is observed in figure 4.10.

The simple model does not however explain the decrease in $\Delta W/W_0$ (increase in conductivity relative to the zero-field value) at high fields. This behaviour can be accounted for if we assume (Berman 1976) that a band of phonons is scattered even in the absence of field and this band is moved to high frequencies in large fields. It could be possible to identify this zero-field splitting with the 0.7 cm^{-1} value already deduced in Chapter 3. It is possible to draw a line, for the $\bar{\nu}_m$ -versus- B_m data points in figure 4.16, starting at $\bar{\nu}_m \sim 0.7 \text{ cm}^{-1}$ for $B_m = 0$. This would allow us then to attribute the field effects in this sample to the same centre which is responsible for the 0.7 cm^{-1} resonant scattering.

4.4.3 Application to TI#4

In Chapter 3 it was shown that the zero-field conductivity of this sample was largely determined by resonant scattering in the temperature range 1 - 4 K. The heat current spectrum, $f(x,T)$, calculated for TI#4 is shown in figure 4.17, where the effect of resonant scattering is clearly seen. Now to account for the magnetoresistance results it is necessary to have a knowledge of the effect of magnetic field on the energy levels of the paramagnetic centres and hence on the resonance frequency. Let us

suppose for a moment that the magnetic field does not appreciably change the resonance frequency, i.e. the heat current spectrum in zero-field is a good approximation to $f(x,T)$ for all fields.

Most of the features of figure 4.8 can correctly be accounted for using the zero-field $f(x,T)$. The variation of thermal resistance with field is just a 'trace' of the heat current spectrum curves.

The sharp increase in thermal resistivity at low fields and the non-variation of the first 'line' with temperature is well described by the first maximum in the heat current. This maximum occurs at $\sim 1.9 \text{ cm}^{-1}$ ($xT = 3.0$) and shifts insignificantly with temperature. The 'dip' in the heat current spectrum also appears in the magnetothermal resistance curves. Its position remains unchanged as the temperature is increased. The second maximum in $\Delta W/W_0$ corresponds to the second peak in $f(x,T)$ and the variation of its position with temperature follows closely the shift to higher temperatures observed for the second maximum of $f(x,T)$. The relative size of the two maxima in $\Delta W/W_0$ (figure 4.8) is also easily interpreted if we consider the relative size of the maxima in the heat current spectrum.

The fact that the magnetothermal resistance effects can qualitatively be interpreted using the heat current spectrum in zero-field could mean that the $\sim 5 \text{ cm}^{-1}$ phonon resonance frequency found in zero-field does not vary very much with applied field. However for large fields the thermal conductivity is actually higher than the zero-field one and this might be due to an appreciable change in the resonant frequency and the basic heat

current spectrum is no longer a good approximation to the heat current with the application of a magnetic field.

It is very unlikely that the 'ruler' which is tracing out the heat current spectrum curves is a residual impurity or other defect since there is no such observable effect in any of the two n-type samples or in the undoped sample. It seems probable that the magnetic ion responsible for these magnetic field effects is a Cr ion in a Cr^{2+} or Cr^{3+} charge state. There is, however, no clear evidence, at this stage, of which ion (or both ions) is causing these effects and further detailed analysis is needed.

4.4.4 Crossing Effects

The term 'frequency crossing' is used to describe the situation where two resonant scattering frequencies are made equal by the application of an external perturbation such as a magnetic field. If a system has two such frequencies, that are well separated, the net reduction in the heat current is the sum of the contributions from each scattering process. The crossing occurs when the separation of the two resonant frequencies is reduced until overlap occurs. The result of this is a reduction in the total phonon scattering, giving rise to a local minimum in the thermal resistance whose field position is independent of temperature. The observation of a frequency crossing signal is of interest since the field at which it occurs provides spectroscopic information about the energy levels of the scattering centres (e.g. Anderson and Challis 1975). The height and width of a signal should provide a measure of the concentration of the centres (e.g. Challis and Williams 1978).

The frequency crossing signals observed in TI#4 are superimposed on a steep background making it difficult to estimate the size of the lines. As mentioned earlier the lines are completely isotropic for all field directions in the (110) plane. This clearly shows these frequency crossings do not arise from the Cr^{2+} or Cr^{3+} centres for which the local symmetry as seen by EPR is D_{2d} and C_{2v} respectively (Krebs and Stauss 1977b). This is not surprising since the selection rules (section 4.2) would not allow phonon transitions within the EPR levels. A possibility for the origin of the signals would be a crossing between pairs of levels of Cr^{2+} and Cr^{3+} but this seems unlikely if we consider the energy levels derived by EPR. Finally the assignment of the crossings to other impurities or defects is improbable since they do not appear in the undoped or n-type samples.

We note that similar behaviour has been observed in a GaP:Cr sample. Also two APR lines which are thought to be due to Cr, are completely isotropic (Bury et al 1980b). This behaviour is still a mystery.

4.4.5 The Anisotropy of the Magnetoresistance

All the large effects presented earlier were for one field direction ($\vec{B} \parallel \langle 001 \rangle$) in a (110) plane and for the heat current perpendicular to the field. In figure 4.18 are shown the size effects for GA735(e) when the field is swept away from $\langle 001 \rangle$. $(\Delta W/W_0)_{\text{max}}$ is the fractional change of the thermal resistance at the maximum. Some idea of the anisotropy which shows the overall symmetry has already been given in figures 4.4 to 4.6 in which $\Delta W/W_0$ is shown over a wide range of angles but at a particular value of field.

Similar anisotropy in the thermal magnetoresistance of paramagnetic ions has already been observed (e.g. Challis et al 1969) and discussed in terms of the changes in the attenuation of phonons along different crystallographic directions as the field is rotated. The authors used the attenuation coefficients derived by Dobrov (1964) and assumed the heat to be carried predominantly by phonons travelling along the crystal axis. Good qualitative interpretation was achieved for the different transitions involved. The same model might be used here to explain our observation if the transitions involved in the phonon scattering were identified.

Another type of anisotropy observed in GA735(e) is shown in figure 4.19 where the position at which the maximum in $\Delta W/W_0$ occurs varies with the field angle. This behaviour can be interpreted as a change of the g-values characterizing the transitions responsible for the thermal resistance (section 4.4.2).

4.5 CONCLUSION

Different field effects have been observed in the samples under investigation. While the undoped and n-type samples did not show any field dependence, large effects were seen in the SI samples. A simple model using the zero-field heat current spectra has been used to qualitatively account for most of the features. It is thought that the magnetic scattering arises from the Cr^{2+} or/and Cr^{3+} ions but no detailed analysis using existing models has been attempted. Isotropic frequency crossing lines were detected in TI#4 and TI#5, which are thought to be due to Cr ions but no model is presently available to explain the observed isotropy.

<i>lines</i> <i>T(k)</i>	1	2	3	4	5
1.12	4.03	6.01	7.30	10.31	
1.15	4.08	5.90	7.29	10.41	13.17
1.52	3.94	6.01		10.29	12.91
1.99	4.13	6.03	7.23	10.33	
3.09	3.96	6.04	7.24	10.35	

Table 4.1 *Field positions (kG) of the frequency crossing lines seen in TI#4.*

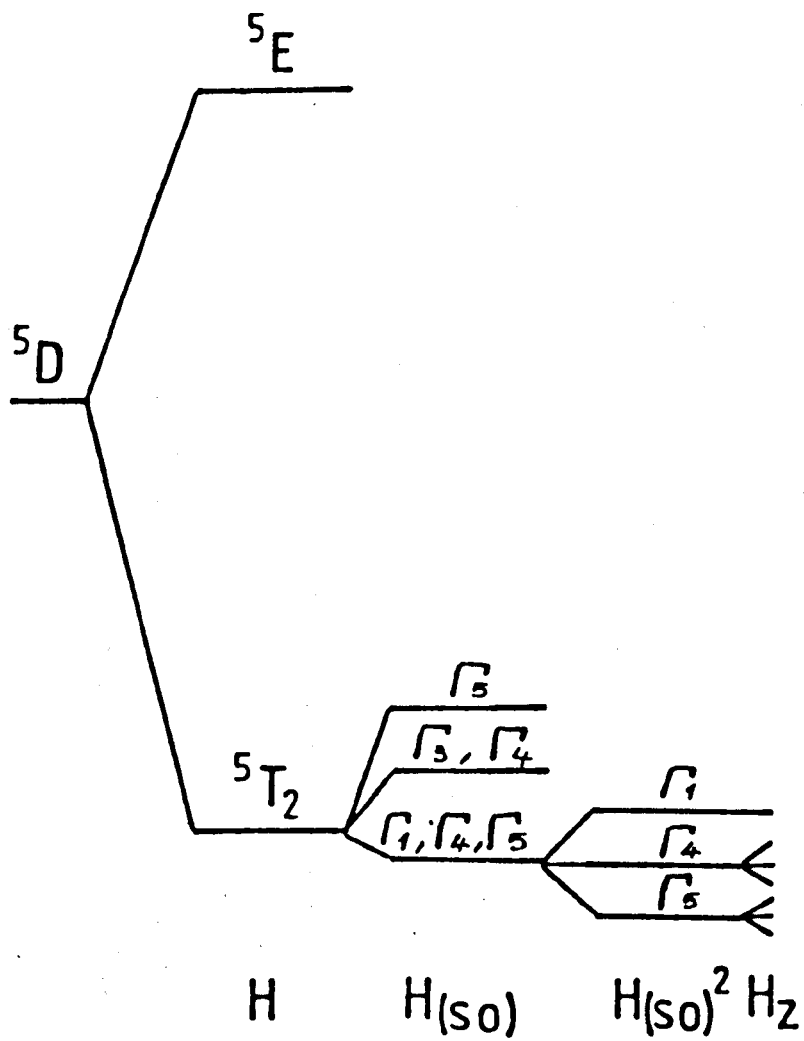


FIGURE 4.1 Ground state structure of Cr^{2+} (T_d) from APR measurements.

(After Ganapol'skii 1975).

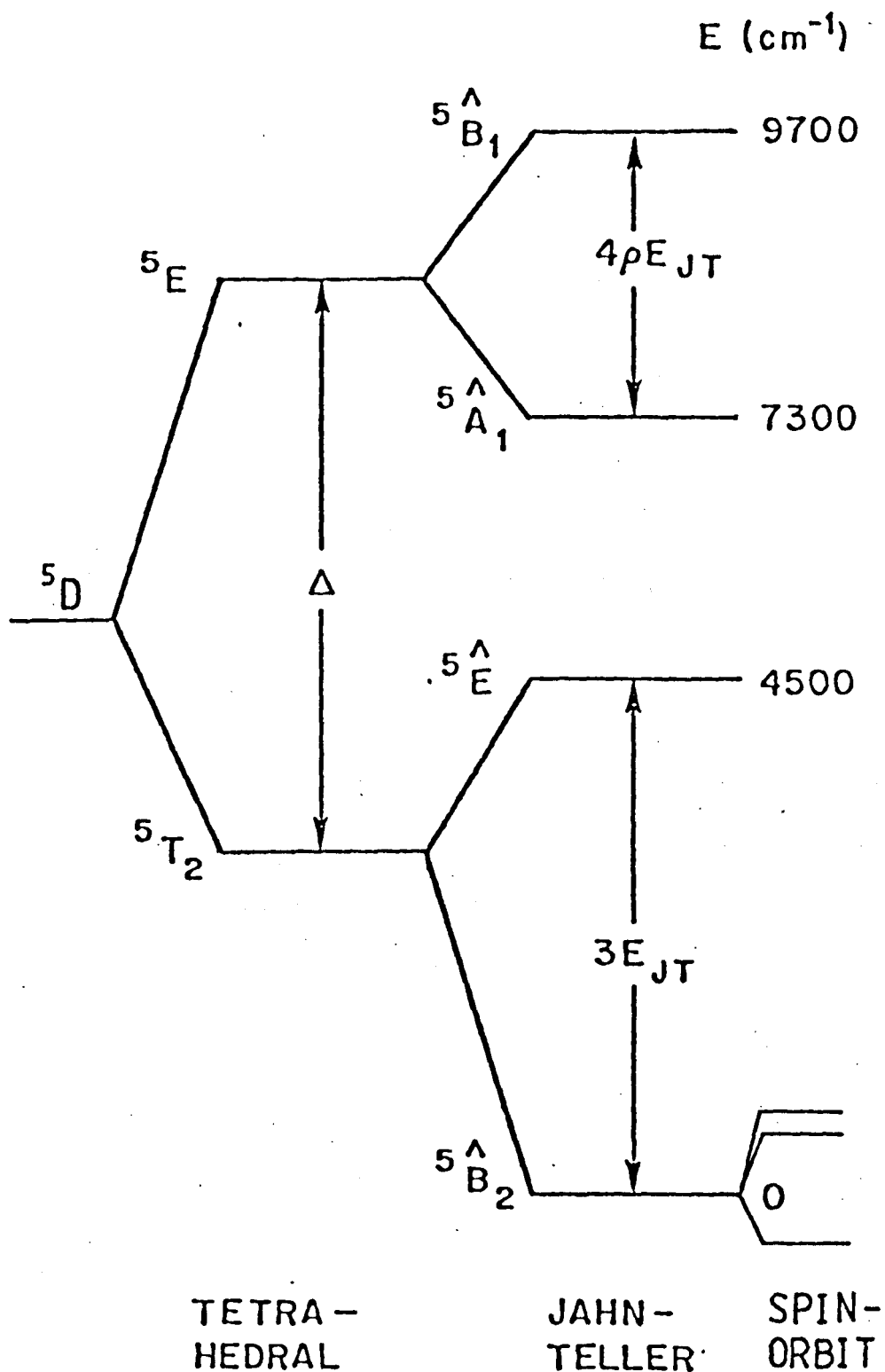


FIGURE 4.2 Energy level diagram of Cr^{2+} (D_{2d}) from EPR measurements.

(After Krebs and Stauss 1977b, 1979a).

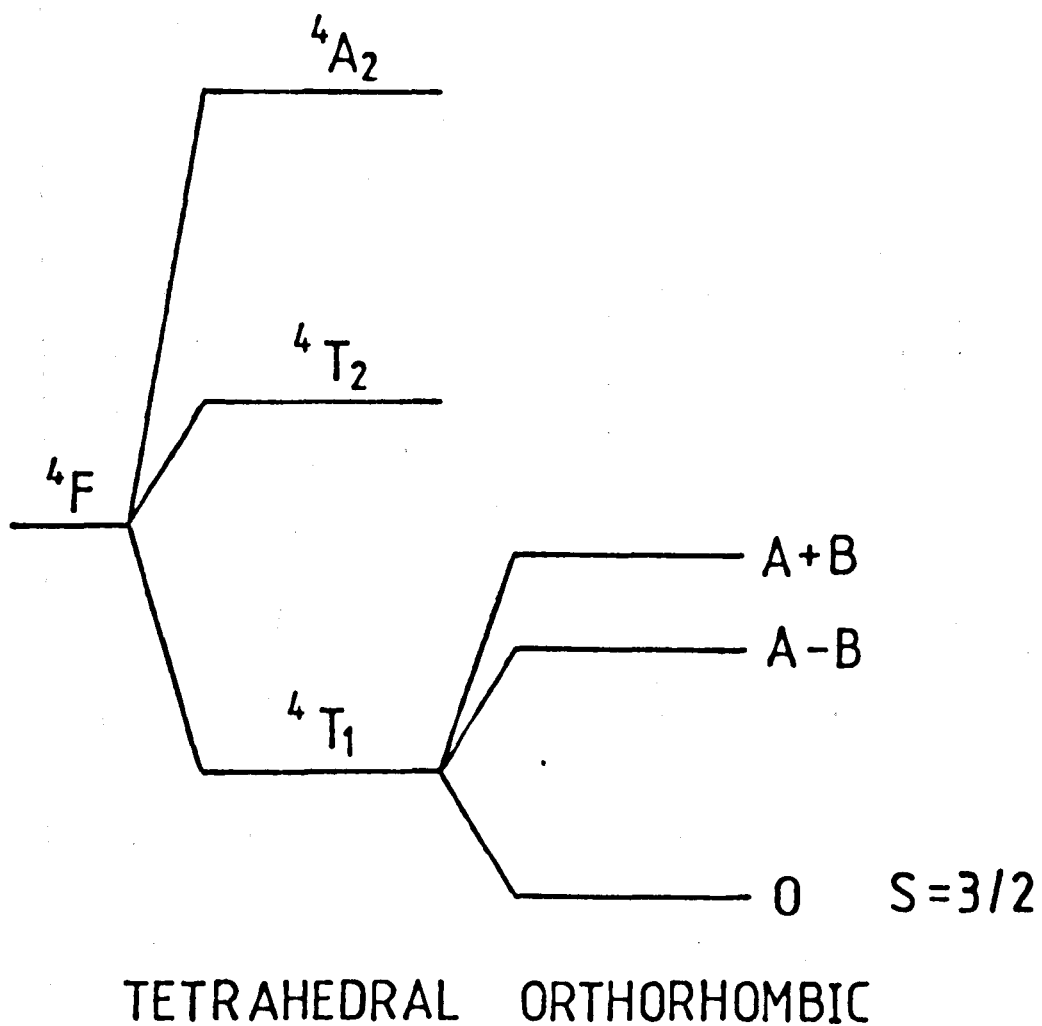


FIGURE 4.3 Ground state structure of Cr^{3+} (C_{2v}) from EPR measurements.

(After Krebs and Stauss 1977a).

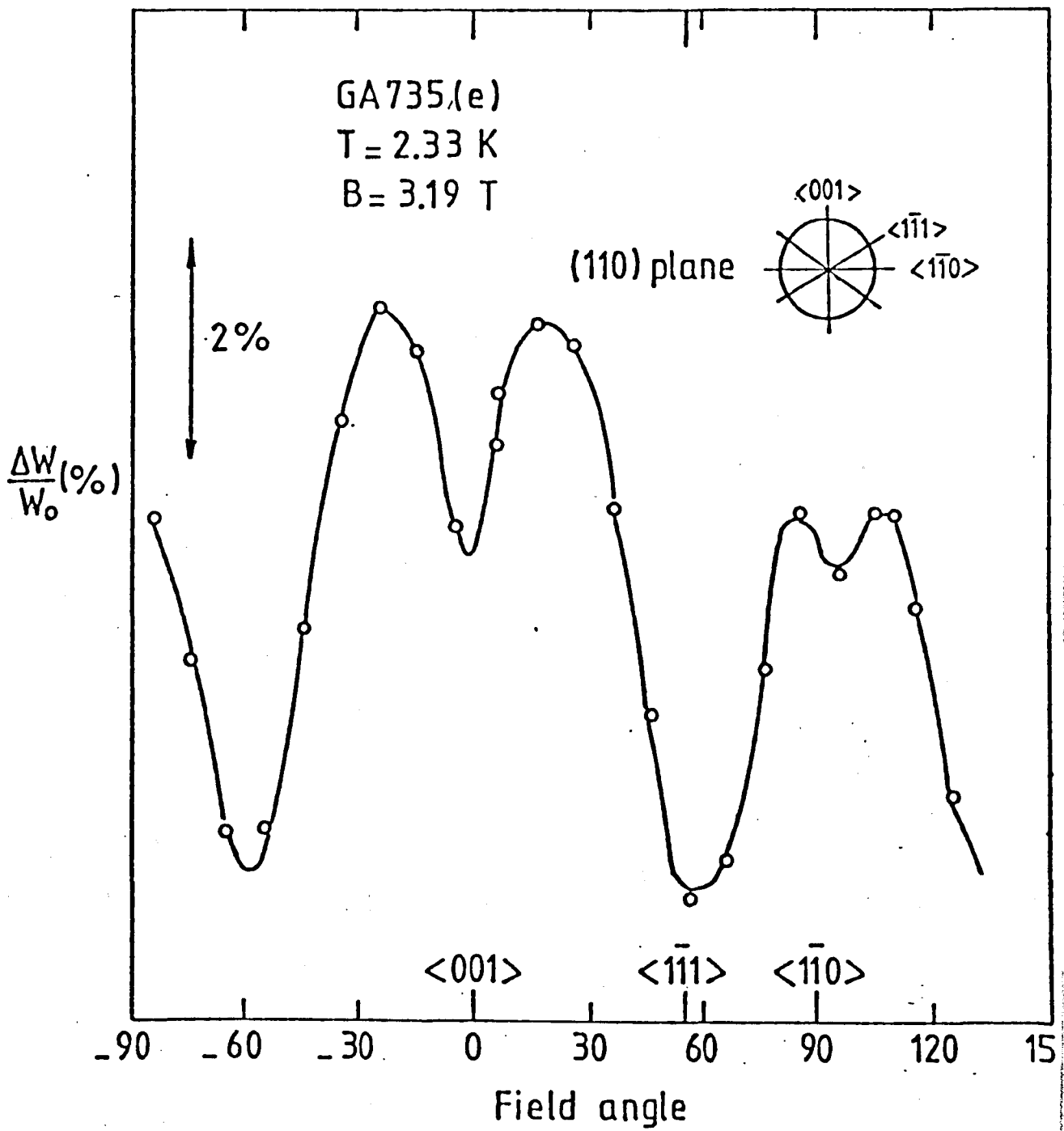


FIGURE 4.4 Anisotropy of thermal resistivity of GA735(e).

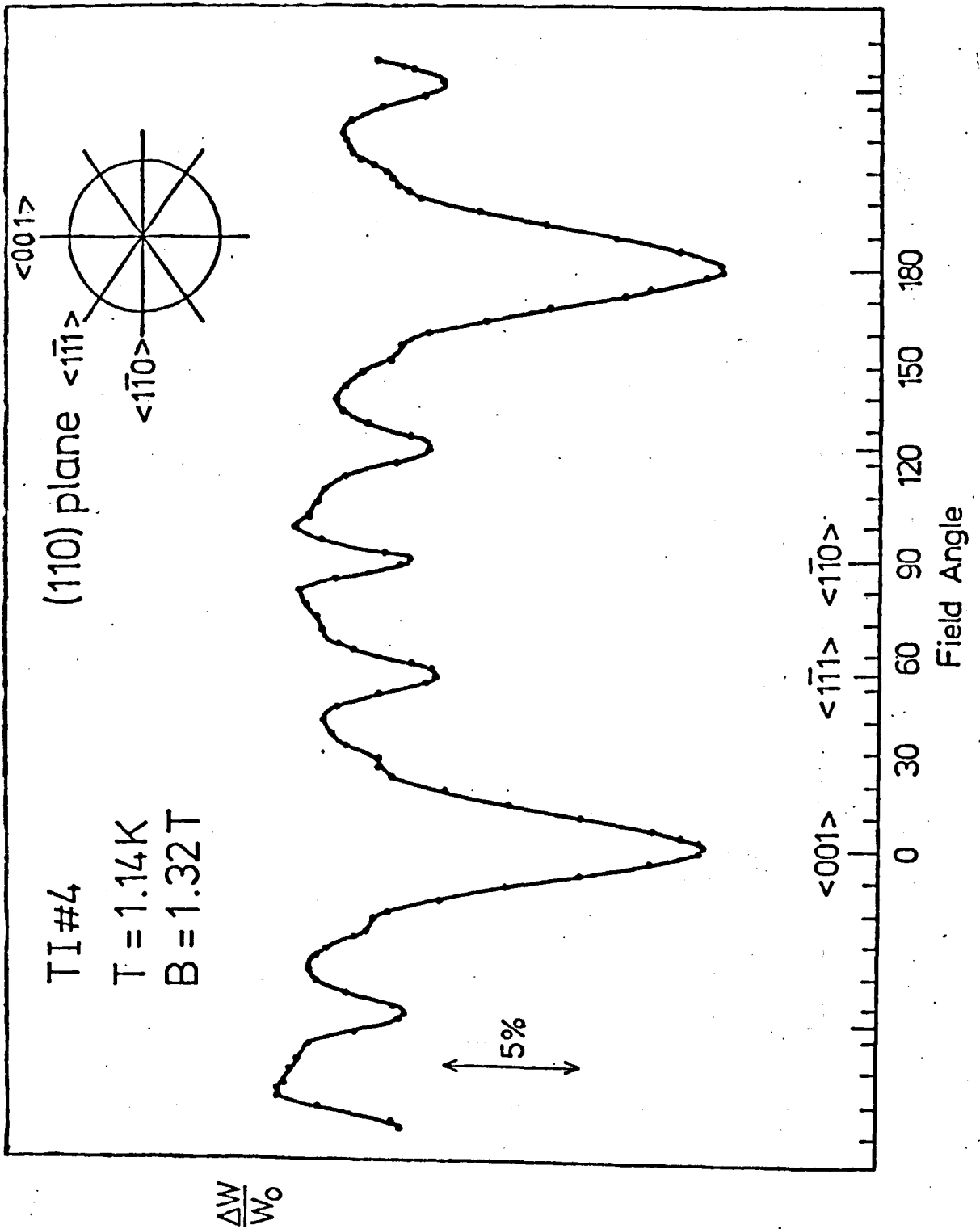


FIGURE 4.5 Anisotropy of thermal resistivity of TI#4.

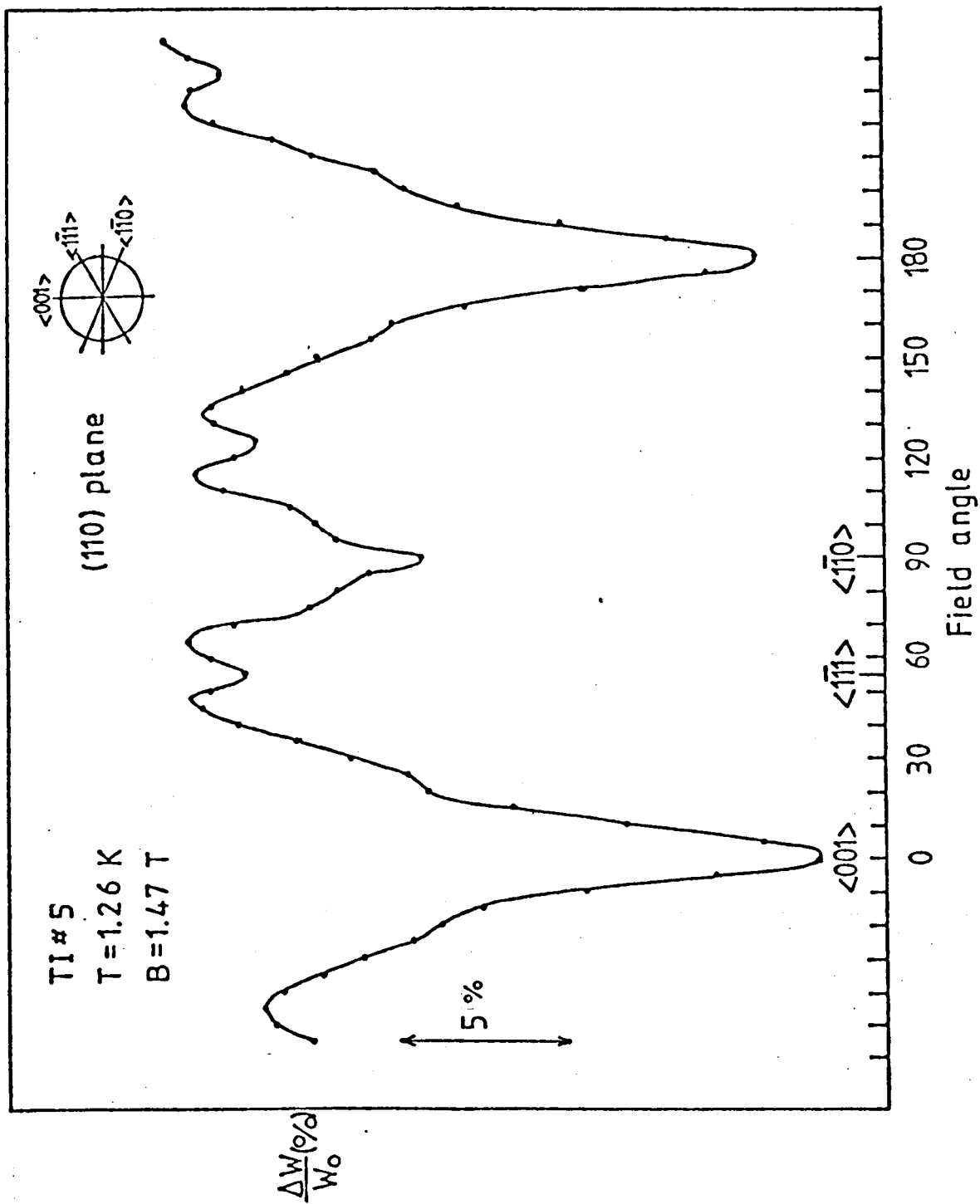


FIGURE 4.6 Anisotropy of thermal resistivity of TI#5.

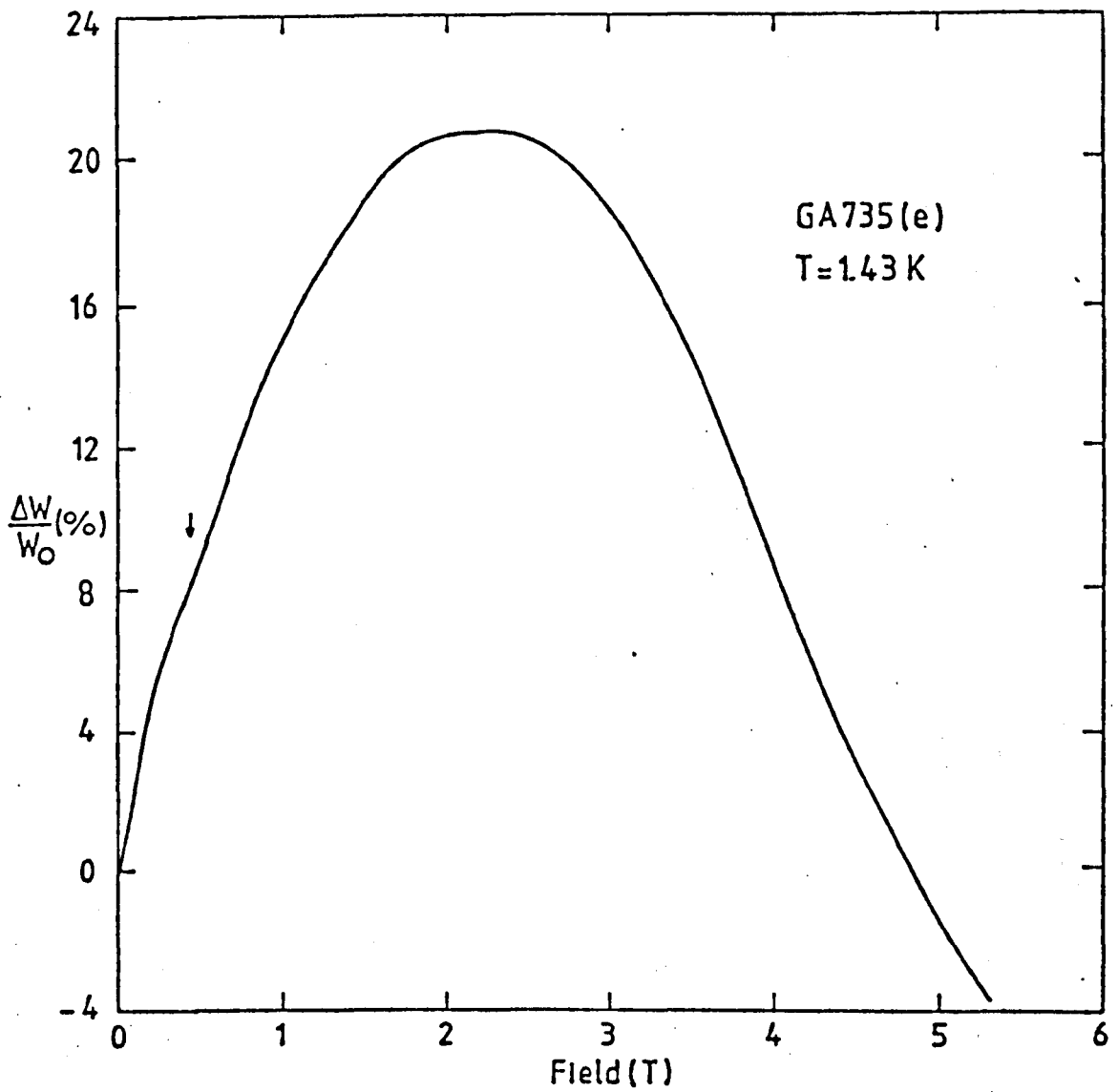


FIGURE 4.7 Change of resistivity of GA735(e) with field
($B \parallel \langle 001 \rangle$).

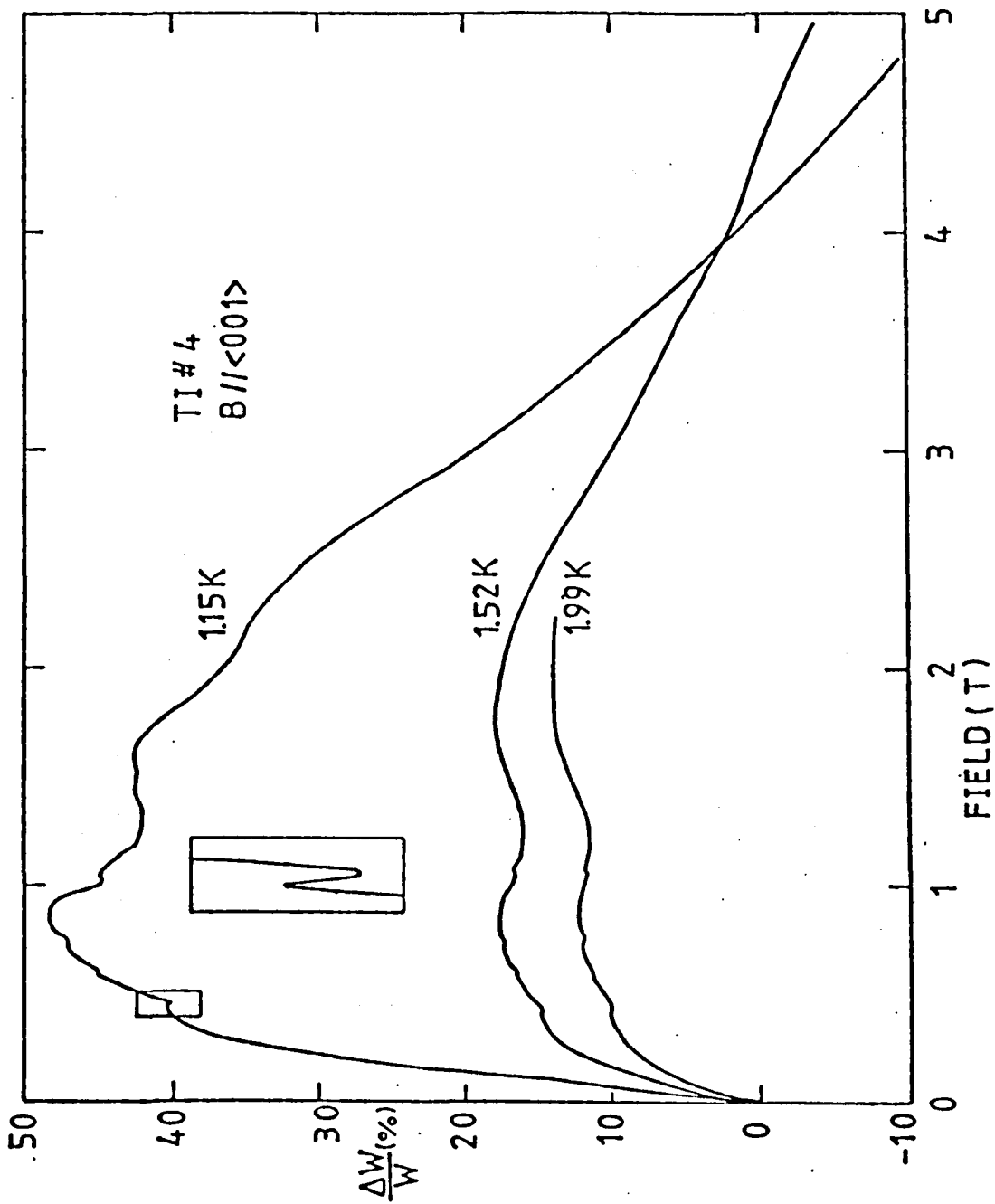


FIGURE 4.8 Change of resistivity of TI#4 with field.
The insert shows the detail of a frequency crossing line.

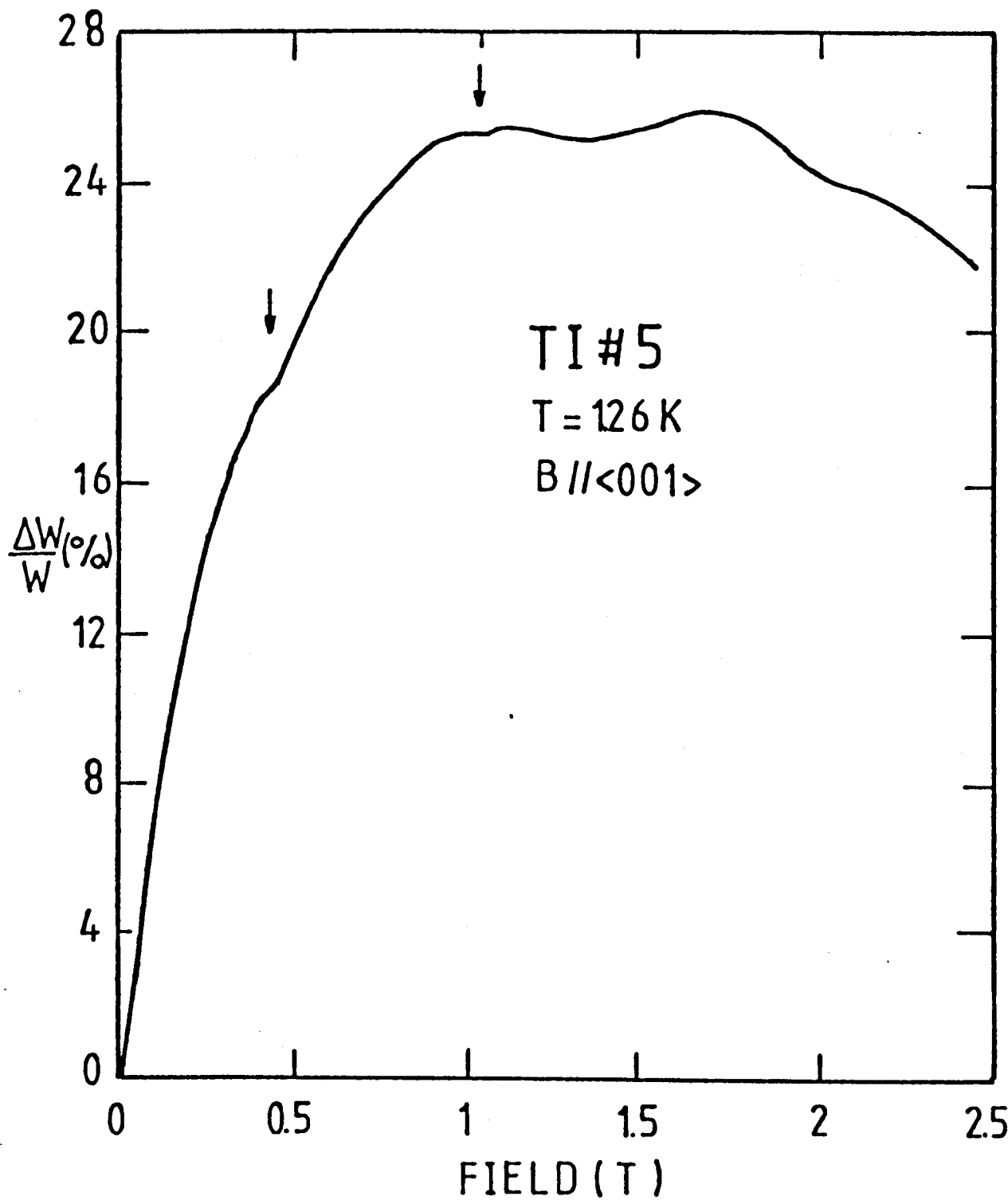


FIGURE 4.9 Change of resistivity of TI#5 with field.

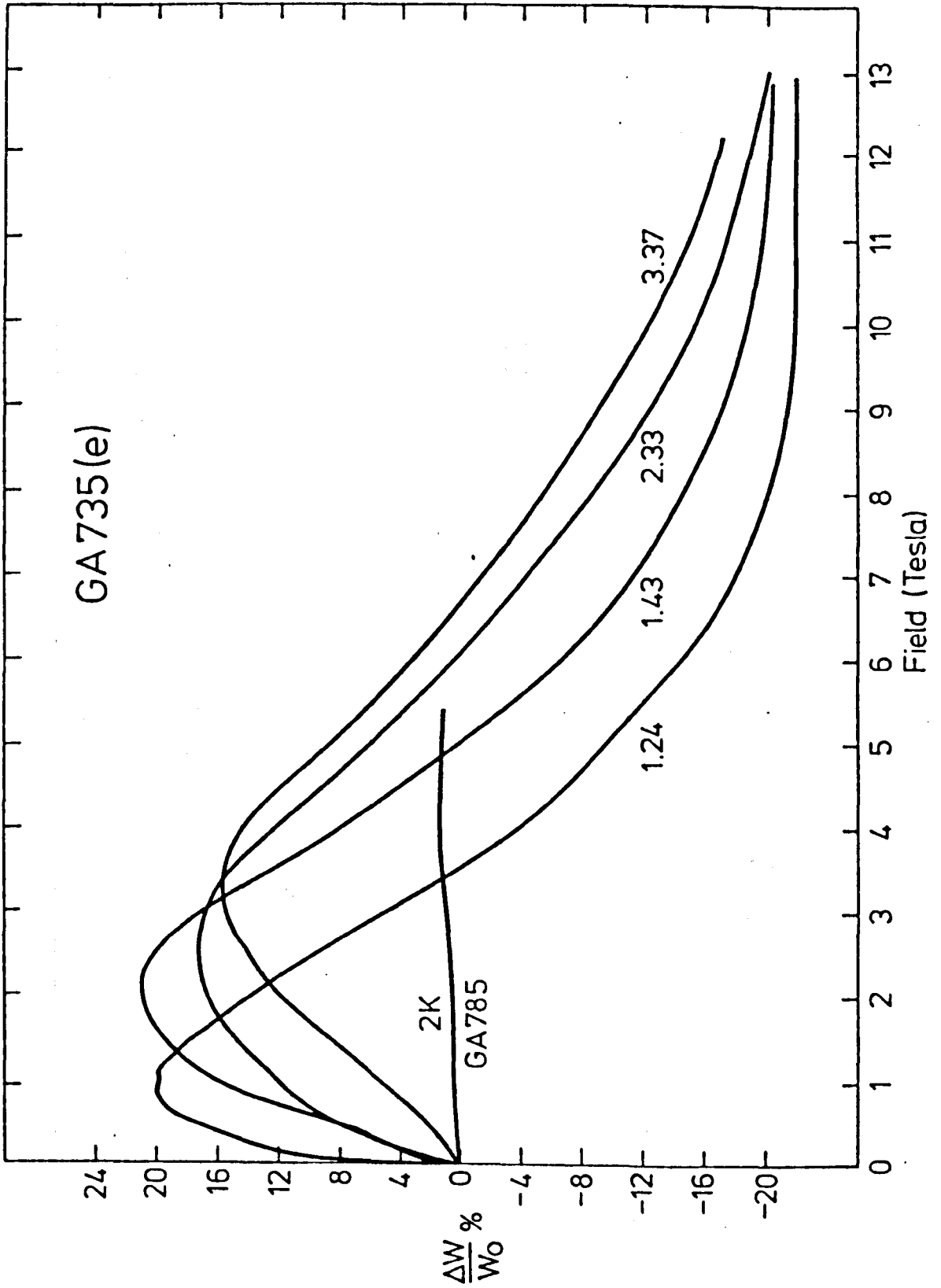


FIGURE 4.10 High field thermal resistivity of GA735(e)
 $(B_{||} \langle 001 \rangle)$.

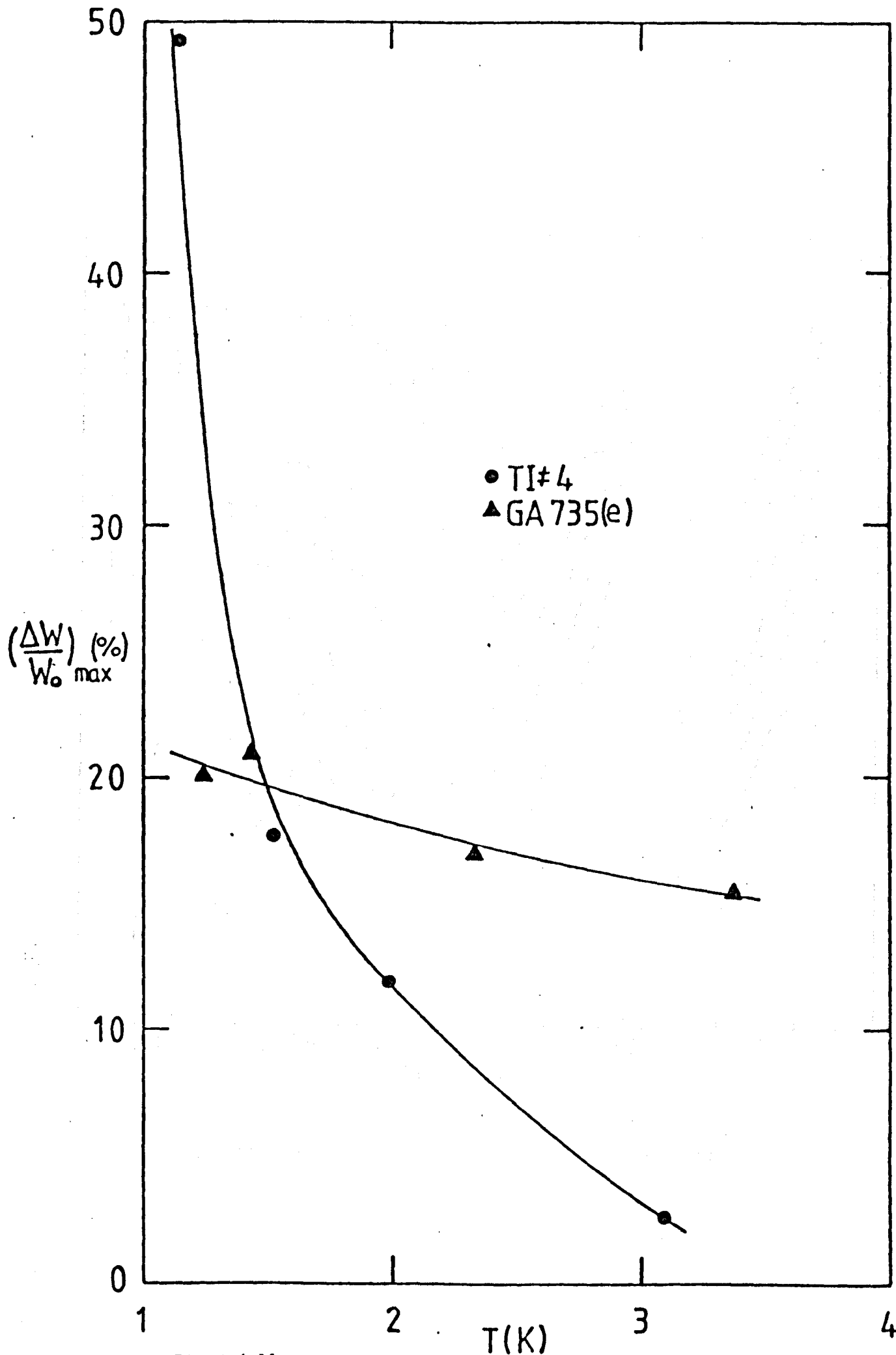


FIGURE 4.11

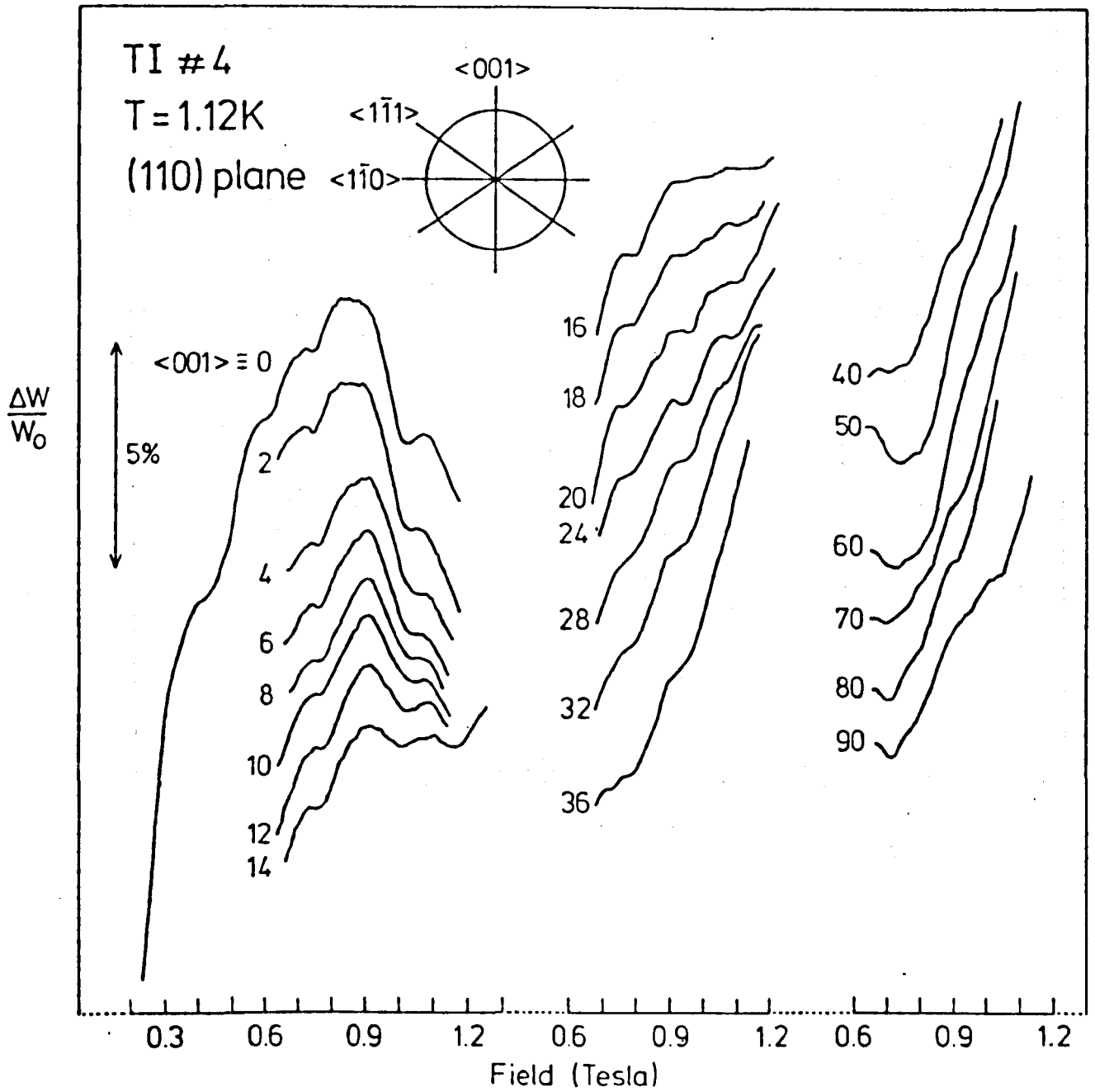


FIGURE 4.12 Isotropy of frequency crossing lines in TI#4.

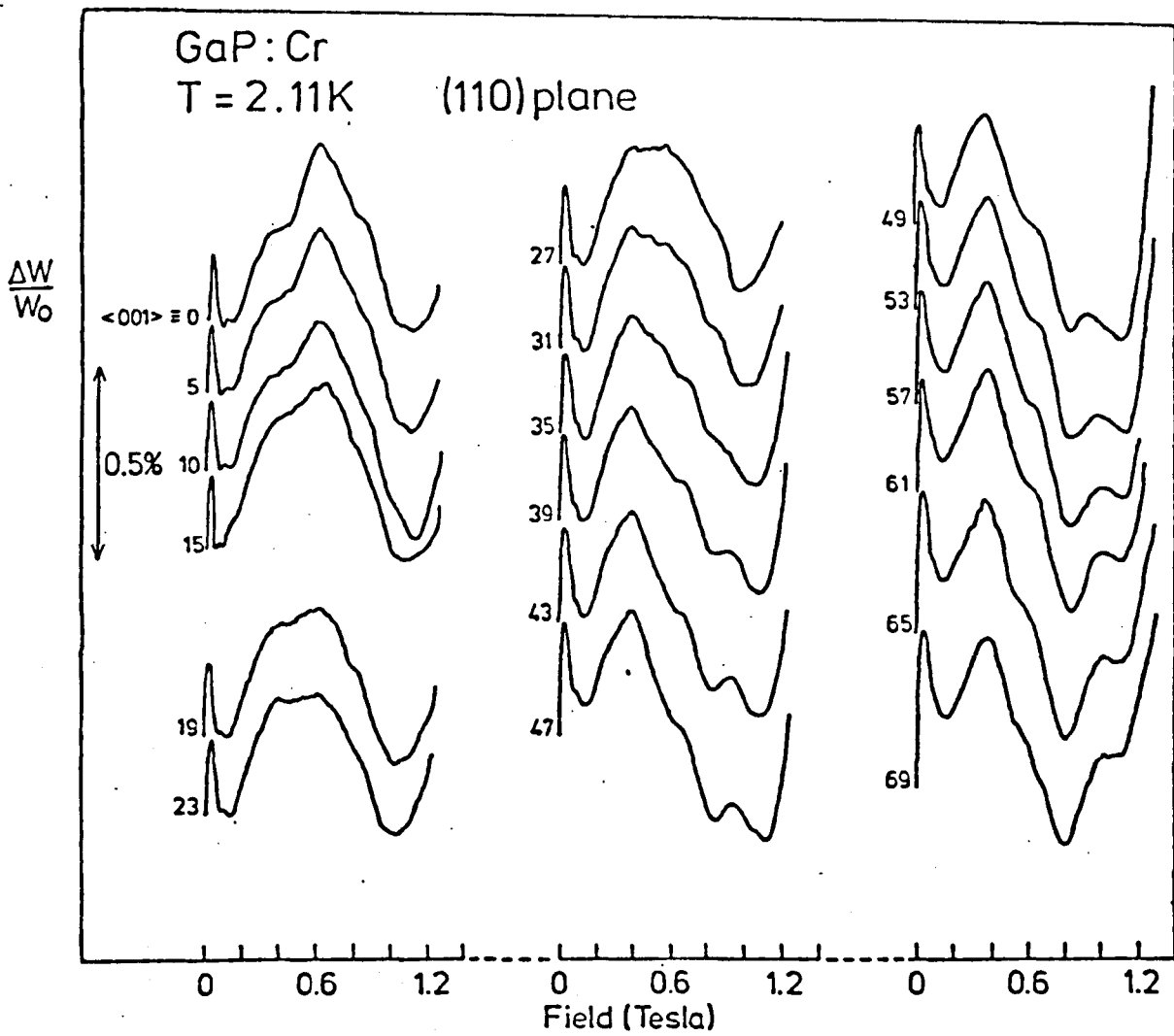


FIGURE 4.13 . Isotropy of frequency crossing lines in GaP:Cr.

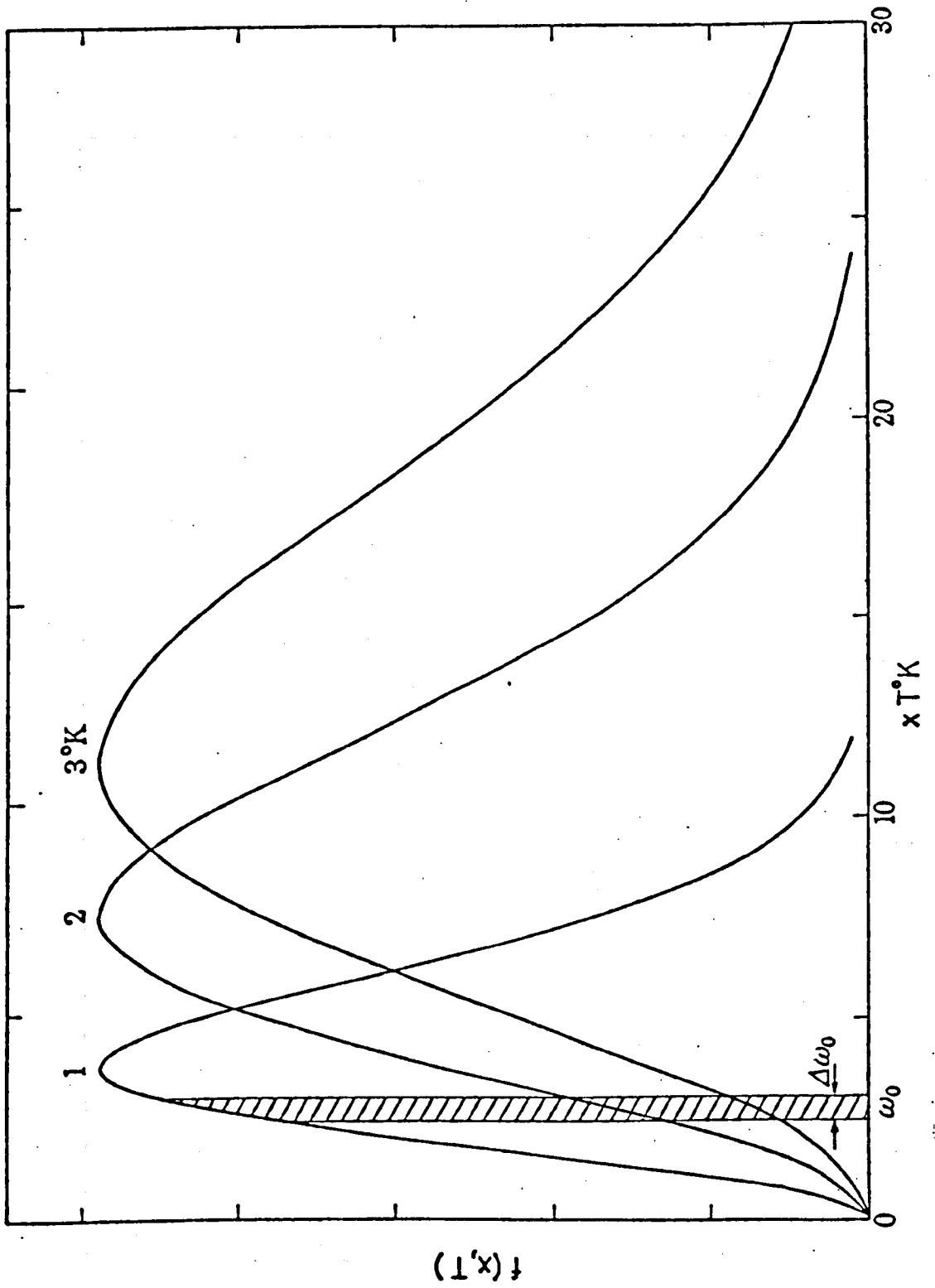


FIGURE 4.14 Heat current spectrum with boundary scattering only.

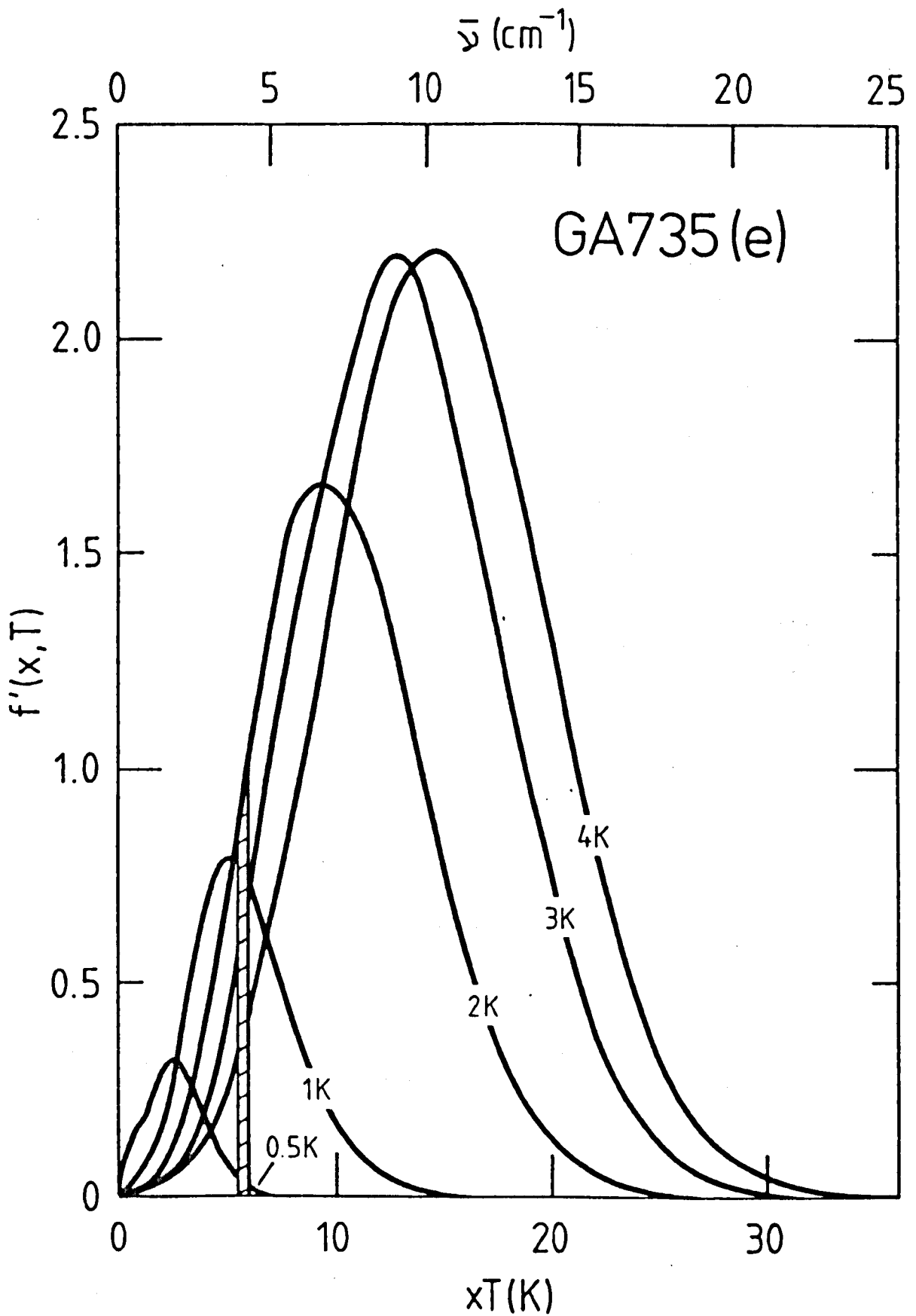


FIGURE 4.15 Calculated heat current spectrum of GA735(e)

$$f'(x,T) = c^{te} \cdot x f(x,T).$$

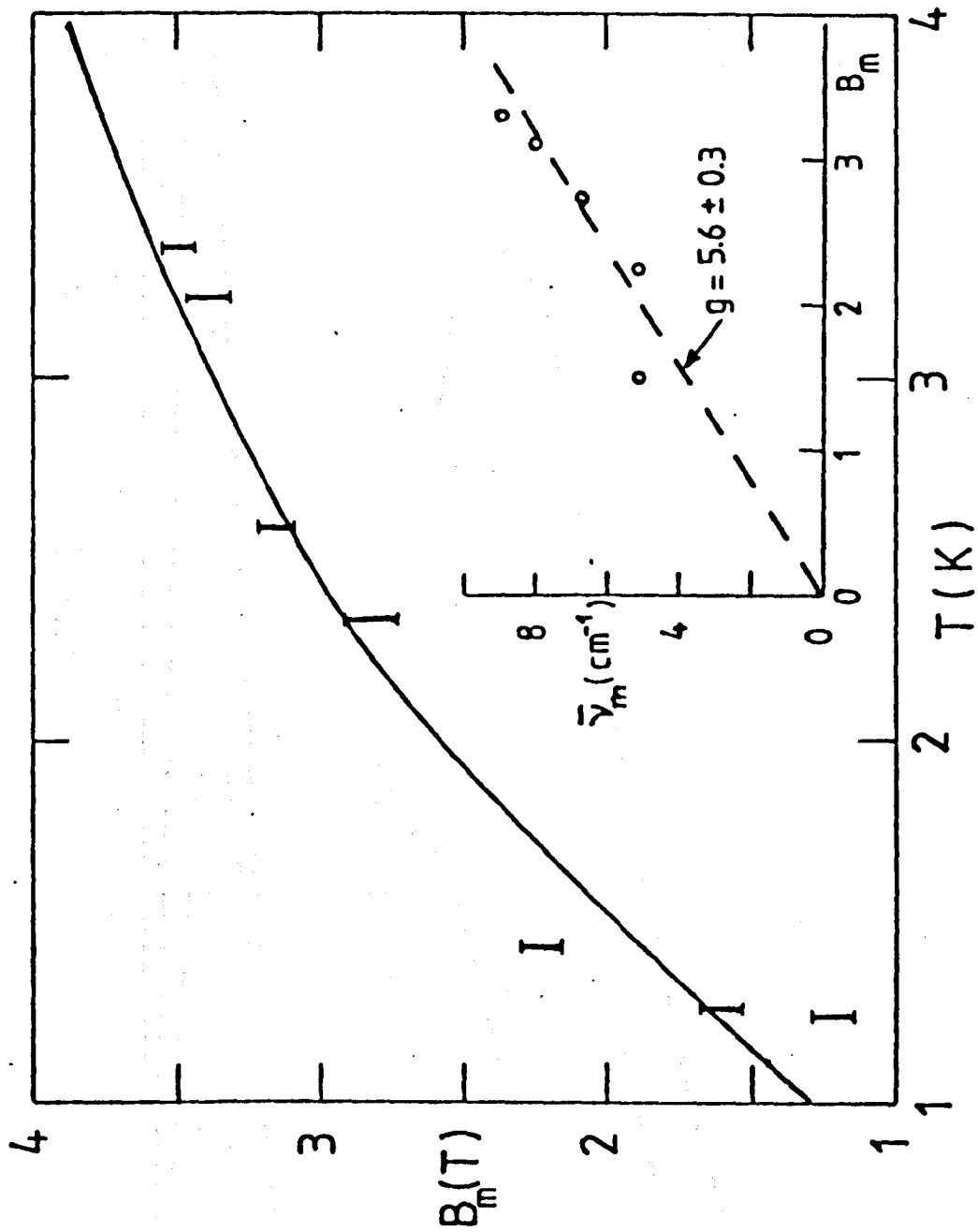


FIGURE 4.16

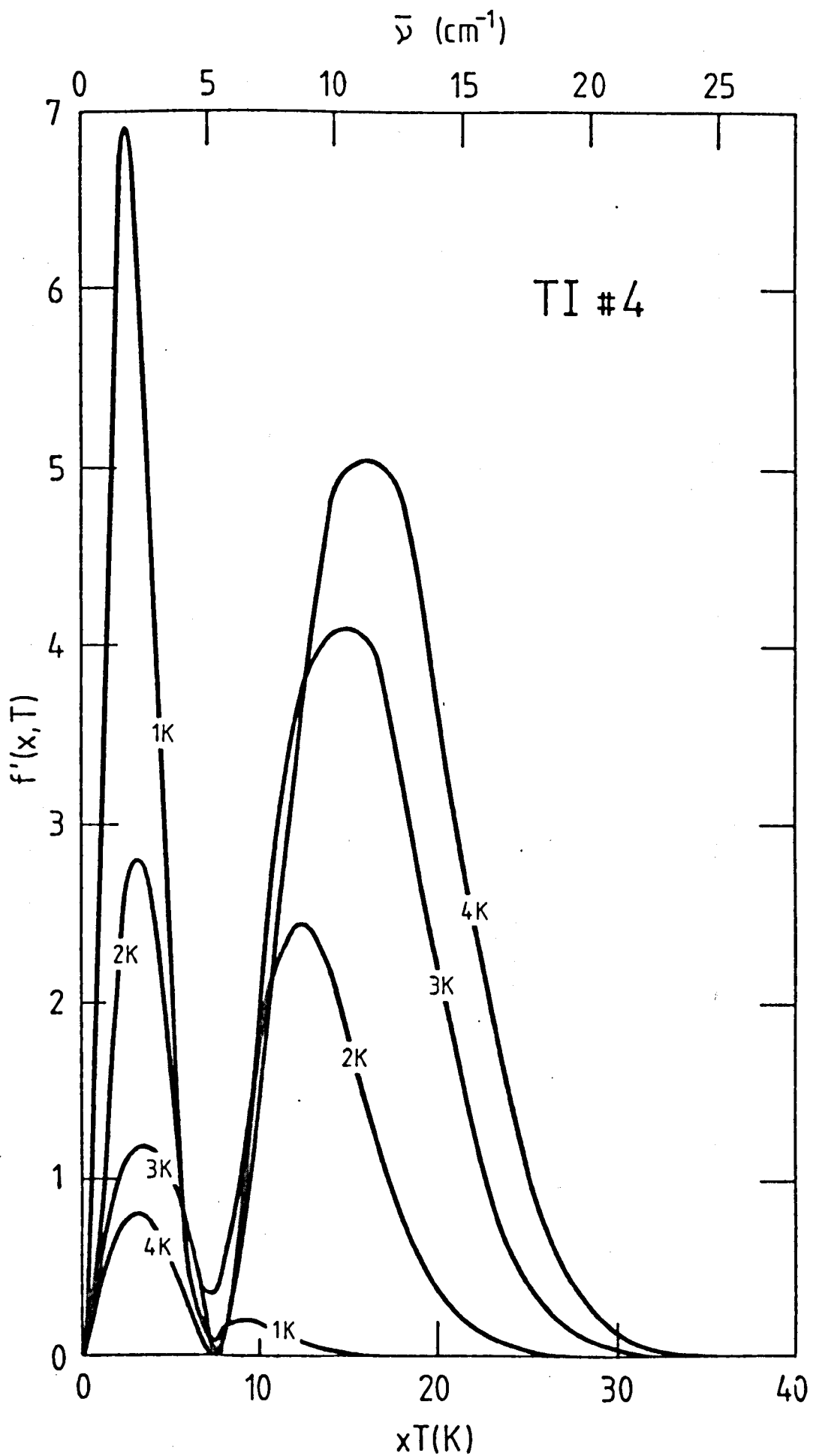


FIGURE 4.17 Calculated heat current spectrum of TI#4

$$f'(x,T) = c^{te} x f(x,T)$$

FIGURE 4.18

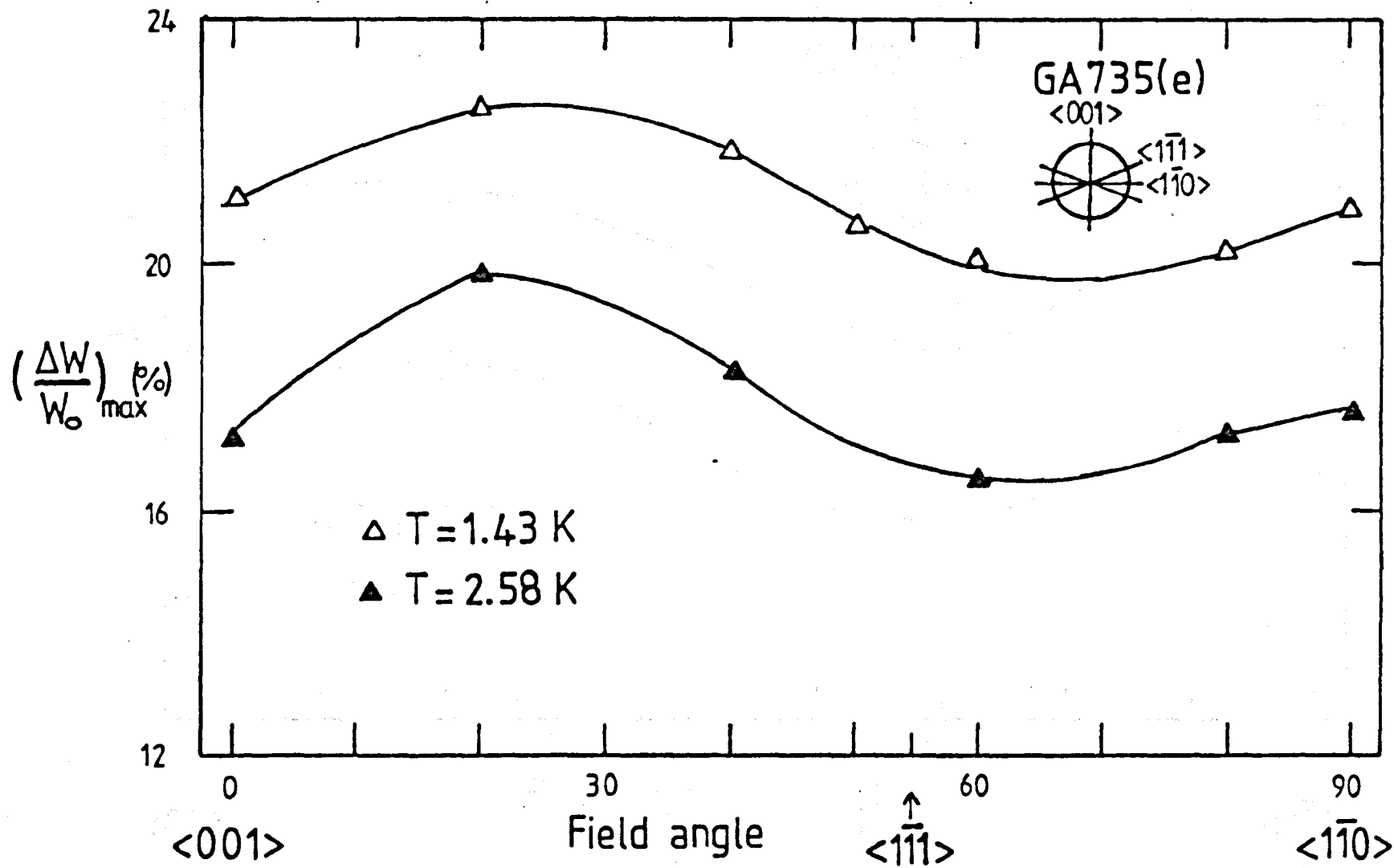
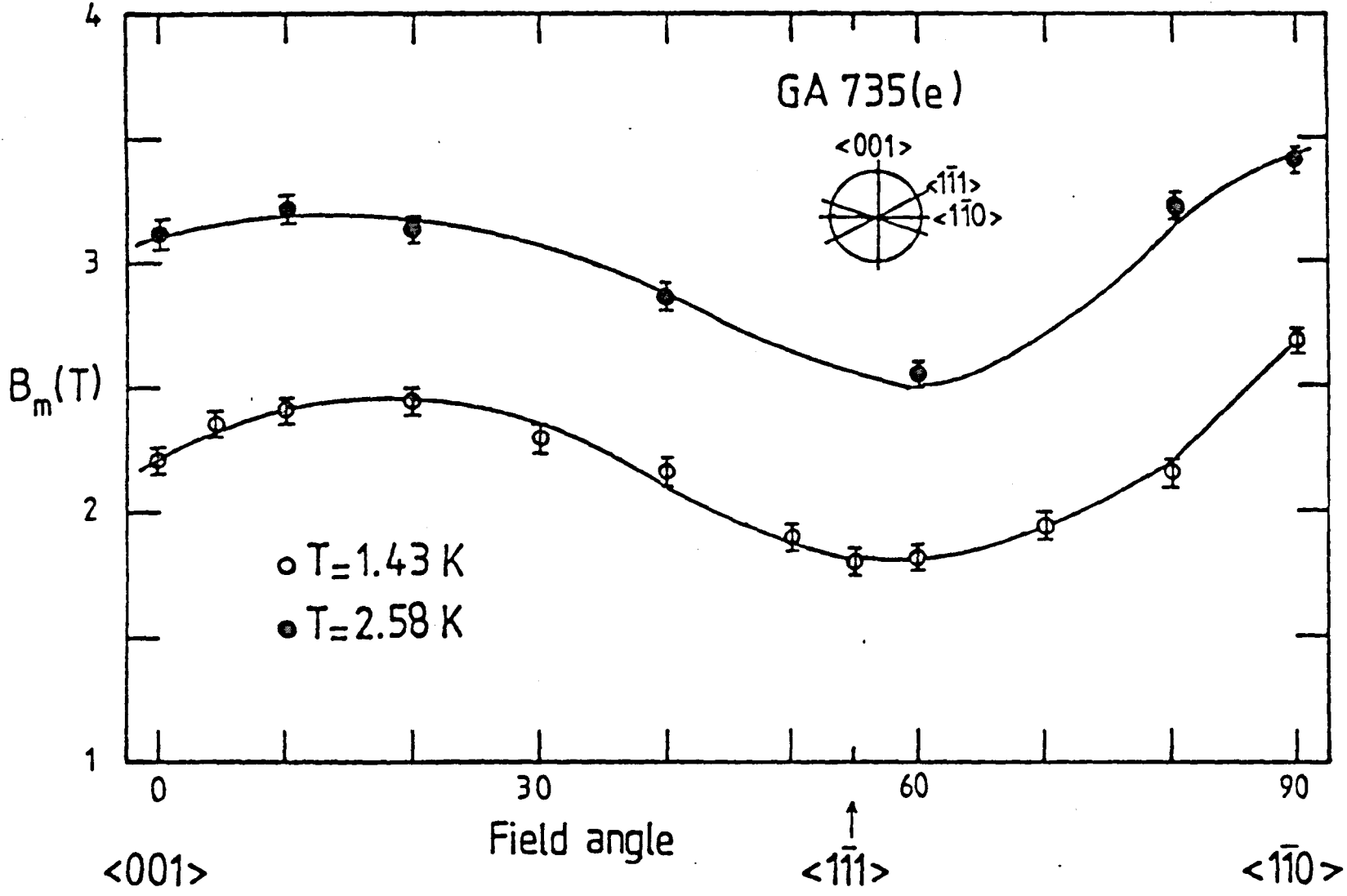


FIGURE 4.19



CHAPTER 5

PIEZOTHERMAL CONDUCTIVITY

5.1 INTRODUCTION

In this chapter we present work undertaken in collaboration with Dr. B. Salce of Centre d'Études Nucléaires de Grenoble. The thermal conductivity under applied uniaxial stress has been measured for several GaAs:Cr samples. This study was prompted by a desire to make a comparison with recent EPR measurements under stress (Krebs and Stauss 1979a) which showed that the lowering of the local symmetry of the $\text{Cr}^{2+}/\text{Cr}^{3+}$ ions was indeed due to Jahn-Teller effects. The ground state of these systems would then be sensitive to applied strain and the effect on the phonon scattering at low temperature could be a useful probe to check on the occurrence of a static Jahn-Teller effect. The experimental results are described in the next section.

5.2 THE EXPERIMENTAL DATA

The measurements were made at fixed temperature between ~ 2 K and 15 K. A typical stress sweep at one temperature was very lengthy and took ~ 8 hours. However the time for equilibrium for each value of stress decreased as the strain was increased thanks to the improved thermal bond to the helium bath. The variation of the thermal conductivity with stress is plotted as $(K(\sigma) - K(0))/K(0) \equiv \Delta K/K_0$ for GA735(e) which is SI in figure 5.1. This was the first sample to be measured and the precision on the data at low stress ($\sigma \leq 300 \text{ kg/cm}^2$) is not believed to be good. We found

we had a poor thermal contact with the helium bath for low stresses. In subsequent runs the two ends of the samples were thermally 'shunted' to the bath and to the lower copper piece (figure 1.4) using copper foils. Unfortunately this sample cleaved on two occasions while being mounted and it became impossible to repeat the measurements because of its reduced size. A specimen cut from a neighbouring slice, GA735(i), was later on tried by Salce but a very surprising phenomenon occurred: when the stress was increased to its highest value, the sample literally exploded and was reduced to powder. For these reasons figure 5.1 shows the only set of presently available data on GA735(e) with an axis along $\langle 110 \rangle$. It is thought that the reason why GA735(i) 'exploded' was because it was highly strained. We learned later that reports of similar behaviour when GaAs single crystals are being cut have been made at GaAs meetings (D.J. Stirland - Private communication). We did not experience any mechanical problem with the remaining samples.

In figure 5.2 are shown the results for GA781 $\langle 001 \rangle$ the axis of which was along $\langle 001 \rangle$. This sample is a 'brother' of GA781 used in the $K(T)$ measurements and their conductivities in zero-stress are roughly the same. The stress effects are huge compared with the effects seen in GA735(e). $\Delta K/K_0$ is characterized by a 'dip' which occurs at low stresses and shifts to higher stress as the temperature is increased. For large enough stresses the fractional change in conductivity reaches a saturation value and at 2.5 K, the lowest temperature, $K(\sigma_{\max}) \approx 10.5 K(0)$. The data are plotted for $\sigma \leq 500 \text{ kg/cm}^2$ in figure 5.3. It shows the limit on the accuracy of a stress measurement. Changes in conductivity of $\sim 1\%$ can be resolved. The main errors are those arising from temperature instability and inaccuracies in the measurement of absolute

temperature (and hence temperature difference) using the germanium thermometer. There is less precision in the measurement (figure 5.2) for high stresses where the conductivity is increased, i.e. the gradient of temperature across the sample has become smaller. The precision could be improved by averaging the readings of the DVM giving the values of R_{Ge} .

The results for GA785 (n-type) and GA803 (undoped) are shown in figure 5.4. The effects are small ($\lesssim 10\%$) but the precision on these measurements is thought to be rather poor. The thermal conductivity of these two samples in zero stress is relatively high so that the temperature differences involved in the stress sweep are small.

The SI sample TI#5 showed a different behaviour than the p-type GA781 $\langle 001 \rangle$ (figure 5.5). The effects here again are small ($\lesssim 30\%$) but a pronounced minimum in $\Delta K/K_0$ occurs at low stress. The conductivity reaches a maximum and decreases again, and seems to be approaching a very broad second minimum. TI#5 had the biggest cross-section and at the highest value of stress we could reach ($\sigma \approx 1300 \text{ kg/cm}^2$), the second minimum was not defined.

Finally the data for TI#4 are presented in figure 5.6 and the conductivity is not altered very much by the application of uniaxial stress. A small change ($\lesssim 10\%$) can be seen at low stress, for the lowest temperature (2.45 K) only.

At this stage the results seem rather puzzling since they are different for each sample. The greatest difference is between GA781 $\langle 001 \rangle$ in which the stress was applied along $\langle 001 \rangle$ and the rest of the samples in which the stress is along $\langle 110 \rangle$, and to test whether this difference was primarily due to the difference in

stress direction an experiment was carried out by B. Salce on a 'brother' of GA781 <001> cut along <110>. The new sample had a thermal conductivity comparable to GA781 <001>. The results are shown in figure 5.7. The behaviour is quite similar to that of T1#5 confirming the importance of the stress direction.

In section 5.5 a tentative model is presented which can account qualitatively for all the features of the data. In order to compare the results with published stress work on the EPR spectra of the GaAs:Cr system, a brief summary of the static Jahn-Teller effect in crystals is presented in section 5.4. The definitions of stress and strain tensors are summarized in the next section.

5.3 STRESS AND STRAIN: DEFINITIONS

For a general crystalline solid, Hooke's law takes the form

$$T_i = \sum_{j=1}^6 C_{ij} e_j \quad (i = 1,6)$$

where T_i are the six independent stress components

e_j are the six independent strain components

C_{ij} are the elastic stiffness constants

(e.g. Brown 1967, p. 109)

Using symmetry arguments it can be shown that for a cubic crystal the number of independent stiffness constants is reduced to 3: C_{11} , C_{12} and C_{44} . In matrix form, Hooke's law is then written:

$$\begin{bmatrix} T_1 \\ T_2 \\ T_3 \\ T_4 \\ T_5 \\ T_6 \end{bmatrix} = \begin{bmatrix} C_{11} & C_{12} & C_{12} & & & \\ C_{12} & C_{11} & C_{12} & & & \\ C_{12} & C_{12} & C_{11} & & & \\ & & & C_{44} & & \\ & & & & C_{44} & \\ & & & & & C_{44} \end{bmatrix} \begin{bmatrix} e_1 \\ e_2 \\ e_3 \\ e_4 \\ e_5 \\ e_6 \end{bmatrix}$$

The stress and strain components are here referred to cartesian axes, and the subscripts 1 2 3 4 5 6 correspond to

xx yy zz yz zx xy

T_{ij} refers to a stress in the i direction applied to a plane the normal of which is in the j -direction.

e_{ii} refer to uniaxial strains along the i axis

e_{ij} refer to shear strains produced by stresses T_{ij} .

The inverse form of Hooke's law is:

$$\begin{bmatrix} e_1 \\ e_2 \\ e_3 \\ e_4 \\ e_5 \\ e_6 \end{bmatrix} = \begin{bmatrix} S_{11} & S_{12} & S_{12} & & & \\ S_{12} & S_{11} & S_{12} & & & \\ S_{12} & S_{12} & S_{11} & & & \\ & & & S_{44} & & \\ & 0 & & & S_{44} & \\ & & & & & S_{44} \end{bmatrix} \begin{bmatrix} T_1 \\ T_2 \\ T_3 \\ T_4 \\ T_5 \\ T_6 \end{bmatrix}$$

where $[S_{ij}]$ is the elastic compliance tensor.

In our experiments the applied stress is uniaxial stress, normal to the (001) and (110) planes. It can readily be shown (e.g. Schawlow et al 1961) that for a stress σ ($\sigma > 0$) in the $\langle 001 \rangle$ direction, the stress tensor is

$$\begin{bmatrix} 0 \\ 0 \\ -\sigma \\ 0 \\ 0 \\ 0 \end{bmatrix} \quad \text{The strains are therefore} \quad \begin{bmatrix} -S_{12}\sigma \\ -S_{12}\sigma \\ -S_{11}\sigma \\ 0 \\ 0 \\ 0 \end{bmatrix}$$

For a stress in the $\langle 110 \rangle$ direction, the stress components are given as follows:

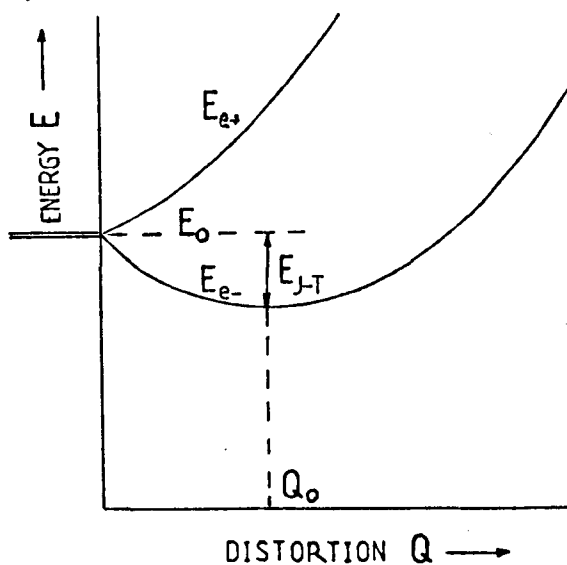
$$\begin{bmatrix} -\sigma/2 \\ -\sigma/2 \\ 0 \\ 0 \\ 0 \\ -\sigma/2 \end{bmatrix} \quad \text{and the strain tensor is} \quad \begin{bmatrix} -(S_{11}+S_{12})\sigma/2 \\ -(S_{11}+S_{12})\sigma/2 \\ -S_{12}\sigma \\ 0 \\ 0 \\ -S_{44}\sigma/2 \end{bmatrix}$$

5.4 JAHN-TELLER EFFECT

5.4.1 The Jahn-Teller Theorem

The theorem (Jahn and Teller, 1937) states that, if a molecule or crystalline defect has an orbital electronic degeneracy due to its local symmetry, then there exists a spontaneous distortion of the lattice which lowers the symmetry and lifts the degeneracy.

The theorem is illustrated in the case of two-fold orbital degeneracy (Ham 1972):



If E_0 denotes the energy of a doubly degenerate electronic state in the symmetric configuration, then, there exists a distortion Q that lifts the electronic degeneracy. The lower split-off state has an energy E_{e-} given by:

$$E_{e-} = -VQ + \frac{1}{2}KQ^2$$

which has a minimum at $Q_0 = V/K$ where V is a coupling constant and K is an elastic modulus. Thus a distortion of Q_0 results in a stable configuration having a stabilization, or 'Jahn-Teller', energy of

$$E_{J-T} = \frac{V^2}{2K}$$

The system would occupy a potential well with vibrational states of energy $(n + \frac{1}{2})\hbar\omega$ where $\omega = \sqrt{K/\mu}$ and μ is the reduced mass for the lattice motion. ω is usually taken as the frequency of the dominant phonon mode. The Jahn-Teller coupling is said to be strong (weak) if $E_{J-T} \gg \hbar\omega$ ($\ll \hbar\omega$).

In general the lattice distortion Q_0 may take place in one of several equivalent directions resulting in several configurations of stable equilibrium. The system can reorient from one distorted configuration to another, by tunnelling or by thermal activation. The Jahn-Teller effect is said to be static (Ham 1972) if the lifetime of the experimental measurement is short compared to the time for reorientation. The measurements then describe the properties of the system corresponding to one of the stable, distorted configurations. A measurement taking a longer time may give an average over the configurations and the effect is said to be dynamic.

Strong static Jahn-Teller effects have already been reported in the case of II-VI compounds doped with Cr (Vallin, Slack, Roberts and Hughes 1970).

The stress effects in the low temperature thermal conductivity of GaAs:Cr are tentatively ascribed to the Cr^{2+} ions which are Jahn-Teller distorted (section 5.5). In the next section we briefly summarize the main results for the theory of the static Jahn-Teller effect for the Cr^{2+} centres in GaAs.

5.4.2 Jahn-Teller Effects in an Orbital Triplet T_2

Cr^{2+} in GaAs has a $3d^4$ - electronic configuration and its ground state in a tetrahedral crystal field T_d is an orbitally degenerate triplet state 5T_2 . The EPR studies (Krebs and Staus 1979b) have

shown that only the E modes were coupled to the Cr^{2+} ions. The splitting of the orbital degeneracy of a triplet electronic state in cubic symmetry by a pair of lattice distortion coordinates Q_θ and Q_ϵ which belong to the E representation is described by the Hamiltonian (Ham 1972):

$$H = H_0 I + V_E (Q_\theta U_\theta + Q_\epsilon U_\epsilon) \quad (5.1)$$

$$\text{where } H_0 = E_0 + (1/2\mu) [P_\theta^2 + P_\epsilon^2 + \mu^2 \omega^2 (Q_\theta^2 + Q_\epsilon^2)] \quad (5.2)$$

ω is the angular frequency appropriate to the (Q_θ, Q_ϵ) mode of vibration, μ is the effective mass appropriate to this mode. E_0 is the electronic energy in the absence of Jahn-Teller coupling. P_θ and P_ϵ are the momenta conjugate to Q_θ and Q_ϵ respectively. In the case of a static Jahn-Teller effect, the term $(P_\theta^2 + P_\epsilon^2)$ is neglected. V_E is the coupling coefficient, I is the 3 x 3 unit matrix, and U_θ and U_ϵ are two electronic orbital operators belonging to E and taking the matrix form with respect to the basis functions $\psi\xi, \psi\eta, \psi\zeta$ (which transform as yz, zx and xy respectively) (Ham 1972):

$$U_\theta = \begin{bmatrix} \frac{1}{2} & 0 & 0 \\ 0 & \frac{1}{2} & 0 \\ 0 & 0 & -1 \end{bmatrix}; \quad U_\epsilon = \begin{bmatrix} -\sqrt{3}/2 & 0 & 0 \\ 0 & \sqrt{3}/2 & 0 \\ 0 & 0 & 0 \end{bmatrix} \quad (5.3)$$

Because the operators U_θ and U_ϵ are diagonal in terms of the electronic states $\psi\xi, \psi\eta$ and $\psi\zeta$, these states will also be eigenstates of H for any Q_θ, Q_ϵ (Ham 1972). The energy surfaces describing the static Jahn-Teller effect are then three disjointed paraboloids (figure 5.8) corresponding to $\psi\xi, \psi\eta, \psi\zeta$. The three stable energy minima in Q space lie at

$$Q_{\theta i} = -V_E b_{i\theta} / \mu \omega^2, \quad Q_{\epsilon i} = -V_E b_{i\epsilon} / \mu \omega^2$$

where $b_{i\theta}$ and $b_{i\epsilon}$ are the diagonal matrix elements of U_θ and U_ϵ ,

respectively, corresponding to $i = \xi, \eta, \zeta$. The Jahn-Teller energy is

$$E_{J-T} = V_E^2 / 2\mu\omega^2 \quad (5.4)$$

The stable configurations correspond to pure tetragonal distortions along each of the cubic axes. The local symmetry is reduced to D_{2d} and the ground state is a singlet ${}^5\hat{B}_2$ (see figure 4.2).

5.4.3 The Effect of Uniaxial Strain on the Jahn-Teller Centres

For D_{2d} symmetry, the effect of applied uniaxial stress can be written:

$$\Delta E = V_E \Delta Q_\theta \quad (5.5)$$

where the term for the coefficient of strain belonging to the A_1 representation of T_d is ignored, since it results in the same energy shift for all Cr^{2+} centres for a uniform strain (Krebs and Stauss 1979a). ΔQ_θ is the additional component of mode Q_θ , referred to the local z-axis, due to the applied stress. Assuming a local cluster model, ΔQ_θ can be written (Vallin and Watkins 1974):

$$\Delta Q_\theta = \frac{2\sqrt{2}}{3} R e_\theta \quad (5.6)$$

$$\text{where } e_\theta = e_{zz} - \frac{1}{2}(e_{xx} + e_{yy}) \quad (5.7)$$

R is the nearest neighbour distance.

At any distorted site, the probability p_i that the Jahn-Teller distortion will occur with its tetragonal axis (z-axis) oriented along a cubic axis (i), is given by the Boltzmann distribution

$$p_i \sim \exp(-\Delta E^i / k_B T)$$

$$\text{where } \Delta E^i = V_E \frac{2\sqrt{2}}{3} R e_\theta^i \quad (5.8)$$

and e_θ^i is the component of tetragonal strain defined along the i th axis.

5.5 INTERPRETATION OF EXPERIMENTAL RESULTS

5.5.1 Qualitative Analysis

5.5.1.1 Effect of stress along <001>

GA781 <001> is the only sample which shows big positive effects when the stress is increased (figure 5.2). In all other samples, the stress effects are relatively small. The results for GA781 <001> are plotted as $K(\sigma)$ in figure 5.9 and $K(T)$ at fixed stress in figure 5.10. Figure 5.10 is interesting in such that two different effects are clearly seen. With a relatively small stress, most of the low temperature phonon scattering observed in this sample is suppressed while the high temperature scattering is practically unaffected. For higher values of stress the conductivity approaches that of GA735(064) for $T \lesssim 5$ K. The small extra thermal resistance in this sample is believed to be due to defects and micro-precipitates (section 3.6). The resonant scattering dip observed at $T \approx 9$ K in zero stress appears now very clearly and its position is slightly shifted to higher temperatures with increasing stress.

This behaviour for a stress parallel to the <001> direction can be explained by assuming that the low frequency phonon scattering (0.7 cm^{-1}) is due to Cr^{2+} centres undergoing a tetragonal Jahn-Teller distortion. In the previous section we have seen there exists three equivalent stable configurations which are particularly sensitive to strain. In the absence of any strain, the three configurations are equally populated, resulting in an 'orientational degeneracy'. We recall that the $5\hat{B}_2$ ground state of an individual Cr^{2+} centre is split by spin-orbit interaction in second order (see figure 4.2) but in this discussion we neglect scattering between these spin-orbit levels and assume that the predominant

scattering is between splittings due to the displacement of the three equivalent 'wells' relative to each other by strains. The zero stress phonon scattering at 0.7 cm^{-1} may be interpreted as arising between splittings caused by built-in random strains. These splittings are not connected with any real energy level splitting of individual centres but are due only to a different shift of levels in the centres which are oriented differently, i.e. a phonon at 0.7 cm^{-1} causes a reorientation.

Applying stress along an $\langle 001 \rangle$ cubic axis favours one configuration (see section 5.5.2) relative to the two others and the scattering is quenched. The same behaviour was reported by Krebs and Stauss (1979a) who could preferentially populate one type of distorted Cr^{2+} site by applying uniaxial stress along one of the cube edges at low temperature.

The dip seen in $\Delta K/K_0$ at low stress corresponds to a splitting of energy of the two, now different sets of Cr^{2+} centres, which is equal to the energy of the dominant phonons in the heat current (section 5.5.2). Then the separation in energy between the two different 'populations' takes place very rapidly when the stress is increased. This is seen as a sharp increase in conductivity at low temperature (figure 5.2). For high enough stresses, the conductivity reaches a saturation value and this occurs when the difference in energy between the stress-split configurations is much larger than the energy of the dominant phonons.

A direct comparison of the value of stress at which saturation occurs can be made with the results of Krebs and Stauss (1979a) where the saturation value of the EPR line intensity is reached at $\sigma \approx 500 \text{ kg/cm}^2$ (for $\vec{\sigma} // \langle 001 \rangle$ at 4.2 K). For the same temperature

the thermal conductivity of GA781<001> reaches a saturation value at $\sigma \approx 1800 \text{ kg/cm}^2$. However, the condition for saturation in EPR ($I \approx I_S$) is $3\alpha\sigma \gg k_B T$ (Krebs and Stauss 1979a) while in our case the condition is $3\alpha\sigma \gg \sim 3.8 k_B T$ where $3.8 k_B T$ is taken as the energy of the dominant phonons. Thus the values of stress for saturation are consistent with the preceding conditions.

The effects for <110> stress are also easily interpreted using the same picture.

5.5.1.2 Effect of a stress along <110>

The large stress effects seen in GA781<001> do not occur in GA781<110> which is a sample cut from a neighbouring slice, with its axis along <110>. This is consistent with the model proposed earlier. A stress along <110> lowers two 'wells' relative to the third (section 5.5.2) and these two 'wells' are displaced relatively to each other by random strains resulting in a distribution of splittings. The thermal conductivity is then kept at a low level because of phonon scattering between the splittings and the stress effects are small. The behaviour observed in TI#5 (figure 5.5) for which the stress was also applied along <110> can be explained in the same way. The pronounced dip occurring at low stress indicates that the strain-split wells are separated by an energy equal to the energy of the dominant phonons. In both samples a second very broad dip (~ -20 to -30%) is traced out for stresses $\geq 1500 \text{ kg/cm}^2$. This dip is very well defined in GA735(e) where it occurs at $\sigma \approx 1000 \text{ kg/cm}^2$ (figure 5.1). A priori this could indicate the presence of individual Cr^{2+} ion levels which are split by applied strain (e.g. splitting of degeneracies left after spin-orbit coupling of $5\hat{B}_2$). However, in this case, some effect should have been seen in GA781

$\langle 001 \rangle$ due to these extra levels, which is not the case. It seems unlikely therefore that the decrease in conductivity for high stresses is due to scattering within the $5\hat{B}_2$ levels. It is much more likely that the applied stress is not *exactly* uniaxial (section 5.5.2.2) so that the two lowest wells are gradually split towards the dominant phonon energy as the stress is increased.

We should mention that the low stress dip in $\Delta K/K_0$ is not clearly observed in GA735(e). We have already noted that the low stress data for this sample was not reliable and it was impossible to repeat the measurement. The only indication of a possible dip in the stress sweep is one (!) data point for $\sigma \approx 100$ kg/cm² at $T = 2.3$ K.

In summary the experimental data for GA781 (both $\langle 001 \rangle$ and $\langle 110 \rangle$ samples), T1#5 and GA735(e) are qualitatively explained by assuming a static Jahn-Teller effect for the Cr^{2+} centres. The phonon scattering occurs between levels due to the displacement of the three configurations of stable energy relative to each other, by the applied strain. The 0.7 cm⁻¹ phonon scattering in zero-stress is ascribed to levels due to the effects of residual strains in the samples. However there is a possibility of splitting of the low lying energy levels by tunnelling between the three equivalent configurations (Dynamic Jahn-Teller effect). This, also, might induce low frequency phonon scattering. We have not considered in detail the theoretical possibility of this situation. It is not clear at the moment whether the very small effect seen in T1#4 at $T = 2.45$ K is related to Cr^{2+} (No effect is observed at $T = 4.1$ K). In the next section the levels of the different centres are described and an estimate of the Jahn-Teller energy is made.

5.5.2 Effect of Strain on the Ground State of Cr²⁺ The Jahn-Teller Energy

5.5.2.1 Estimate of the Jahn-Teller energy

In the last section we have seen that the stress alignment of the different defects is determined by the difference between the tetragonal components of strain e_{θ} along the z axis of each defect, where, for the ith defect

$$e_{\theta}^i = e_{zz}^i - \frac{1}{2}(e_{xx}^i + e_{yy}^i)$$

Let a, b and c be the Cr²⁺ centres distorted along the <100>, <010> and <001> cubic axes, respectively.

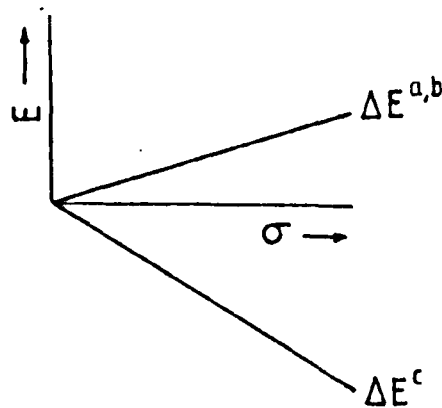
For a stress along <001>:

$$e_{xx} = e_{yy} = -S_{12}\sigma$$

$$e_{zz} = -S_{11}\sigma \quad (\text{section 5.3})$$

and $e_{\theta}^c = -2e_{\theta}^{a,b}$ (e.g. Krebs and Stauss 1979a)

Using these relations and equation (5.8), we can obtain the energy of the different distorted centres as:



$$\Delta E^c = -V_{ES}(S_{11} - S_{12})\sigma$$

$$\Delta E^{a,b} = \frac{1}{2}V_{ES}(S_{11} - S_{12})\sigma$$

(5.9)

where $V_{ES} = \frac{2}{3} \sqrt{2} R V_E$.

The energy difference between the $\langle 001 \rangle$ distorted centres and the other distorted ones, $\langle 100 \rangle$ and $\langle 010 \rangle$, is given by

$$\Delta_{\langle 001 \rangle} = \frac{3}{2} V_{ES} (S_{11} - S_{12}) \sigma \quad (5.10)$$

To make a direct comparison with Krebs and Stauss, we consider the constant $\alpha = \frac{1}{2} V_{ES} (S_{11} - S_{12})$. We assume that the dip observed in GA781 $\langle 001 \rangle$ occurs at a stress σ_m , where $\Delta_{\langle 001 \rangle} \approx x k_B T$ where T is the temperature at which the stress is swept; x characterizes the energy of the dominant phonons and is taken from the heat current spectra in zero stress. The values of x used for GA781 are those found for T1#5 which is a sample with about the same zero-stress conductivity over the whole temperature range (figure 3.2.b) The heat current spectra of the two samples should not then be too different. The results are summarized in the table below:

sample	T(K)	σ_m (kg/cm ²)	x	$\alpha (x 10^{-30} \text{ m}^3)$
GA781 $\langle 001 \rangle$	2.5	90 ± 10	4.5	5.9 ± 0.9
	4.2	155 ± 20	3.2	4.1 ± 0.6
	6.4	170 ± 20	2.25	4.0 ± 0.6

The total estimated error on α is about 15%.

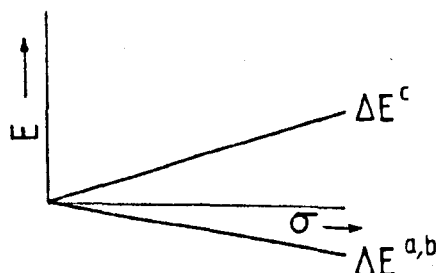
For a stress along $\langle 110 \rangle$

$$e_{xx} = e_{yy} = -\frac{1}{2} (S_{11} + S_{12}) \sigma$$

$$e_{zz} = -S_{12} \sigma \quad (\text{section 5.3})$$

and $e_{\theta}^c = -2e_{\theta}^{a,b} \quad (\text{Krebs and Stauss 1979a})$

The energy diagram for the different centres is shown below:



where $\Delta E^C = \frac{1}{2} V_{ES} (S_{11} - S_{12}) \sigma$ (5.11)
 and $\Delta E^{a,b} = -\frac{1}{4} V_{ES} (S_{11} - S_{12}) \sigma$

The difference in energy is given by

$$\Delta_{\langle 110 \rangle} = \frac{3}{4} V_{ES} (S_{11} - S_{12}) \sigma \quad (5.12)$$

i.e. half that for $\Delta_{\langle 001 \rangle}$. The values obtained for α are given in the table below:

sample	T(K)	σ_m (kg/cm ²)	x	α (x10 ⁻³⁰ m ³)
TI#5	2.5	130 ± 15	4.5	8.1 ± 1.2
	4.1	140 ± 15	3.3	9.1 ± 1.4
	6.3	163 ± 20	2.3	8.3 ± 1.2
GA781<110>	1.95	85 ± 10	4.9	10.6 ± 1.6
	4.04	125 ± 15	3.35	10.2 ± 1.5

A striking feature of the results is the value of σ_m , which is about the same, for the two stress directions, at the same temperature, while from (5.10) and (5.12) we would expect $\sigma_m(\langle 110 \rangle) = 2\sigma_m(\langle 001 \rangle)$. (This is also shown by the fact that experimentally $\alpha_{\langle 001 \rangle} \sim \frac{1}{2} \alpha_{\langle 110 \rangle}$ whereas theoretically they should be equal). This seems to imply there is no anisotropy when the stress is applied, which is in contradiction with the invoked symmetry (D_{2d}) for explaining the data. Although Krebs and Stauss found no stress effects for the $\langle 111 \rangle$ direction, their results are not reliable for $\vec{\sigma} // \langle 110 \rangle$ (Krebs and Stauss 1979a). It would be very interesting to measure the change in thermal conductivity for stresses along $\langle 111 \rangle$. This should be very useful in checking on the proposed model.

There are roughly two values of α depending on the stress direction. The value of $\alpha = 2.3 \times 10^{-30} \text{ m}^3$ given by Krebs and Stauss

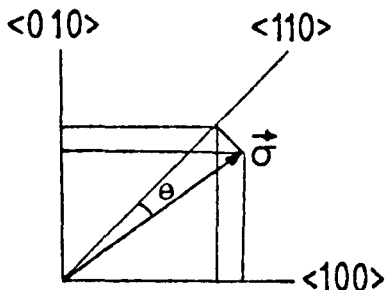
for stress parallel to $\langle 001 \rangle$ is about half the value we find for the same stress direction ($\alpha \approx 5 \times 10^{-30} \text{ m}^3$). Using this value, the Jahn-Teller coupling coefficient V_E is found to be $V_E = 1.9 \pm 0.3 \text{ eV}/\text{\AA}$, where the values of R and $(S_{11} - S_{12})$ are the same as those used by Krebs and Stauss (1979a), $R = 2.443 \text{ \AA}$ and $S_{11} - S_{12} = 1.47 \times 10^{-12} \text{ cm}^2/\text{dyne}$. This then is twice the value $V_E \sim 0.85 \pm 0.09 \text{ eV}/\text{\AA}$ of Krebs and Stauss. We can then estimate the Jahn-Teller energy E_{J-T} using equation (5.4): $E_{J-T} \approx 3850 \text{ cm}^{-1}$ where $\hbar\omega_E = 78 \text{ cm}^{-1}$ (Krebs and Stauss 1979a). The value of E_{J-T} estimated in this way is again twice as high as the value deduced by EPR measurements. However this value would be about four times the value of Krebs and Stauss if we use the results for stress along $\langle 110 \rangle$ ($\alpha \approx 9.3 \times 10^{-30} \text{ m}^3$). Recently, Tokumoto and Ishiguro (1979) determined the Jahn-Teller coupling coefficient for Cr^{2+} in GaAs by ultrasonic attenuation. They measured the relaxation time for the reorientation of the Cr^{2+} centres and from the stress dependence of the attenuation they obtained $V_E = 0.4 \text{ eV}/\text{\AA}$. However the elastic compliance constants used in their analysis were taken as $S_{11} - S_{12} = 5.4 \times 10^{-13} \text{ cm}^2/\text{dyne}$. We have calculated the values of S_{11} and S_{12} from the measured values of C_{11} and C_{12} at low temperature (Garland and Park, 1962) and we find $S_{11} - S_{12} = 1.53 \times 10^{-12} \text{ cm}^2/\text{dyne}$, which is about the same value used by Krebs and Stauss, and taken from the data of Carlson and Mott (1963). The Jahn-Teller energy estimated from the ultrasonic attenuation work, and using the same S_{ij} constants as Krebs and Stauss, is then $E_{J-T} \approx 630 \text{ cm}^{-1}$. This is about three times less than the EPR value. This shows the three estimates give the same order of magnitude for E_{J-T} . Our estimate is however rather approximate since we use the relation $\hbar\omega_d \approx xk_B T$ determined from the zero-stress heat current spectrum, for the phonons which are responsible for the low stress dip in $\Delta K/K_0$. A detailed computer

analysis should be made to precisely determine the energy of the dominant phonons with applied stress.

In the preceding analysis the effect of internal strains (e_{θ}^{int}) or inhomogeneities in the applied strains (Δe_{θ}) has not been considered. We know however (section 5.5.1) that the effect of internal strains is not negligible. It can give rise to energy separation of the Jahn-Teller distorted centres of $\sim 0.7 \text{ cm}^{-1}$. From figure 6 of Tokumoto and Ishiguro's paper the tetragonal component of internal stress in their samples can be estimated to be $\sim 20 \text{ kg/cm}^2$. (They actually estimate $\sim 10 \text{ kg/cm}^2$). For this, the expressions for the ground state energy with applied stress, (5.9) and (5.11) are not really valid and any proper treatment should consider averages over the distributions of internal and inhomogeneous applied strain (Vallin and Watkins 1974).

5.5.2.2 Effect of misalignment of stress

For stresses along $\langle 110 \rangle$, $\Delta K/K_0$ shows broad minima at high stress values ($\sigma \geq 1500 \text{ kg/cm}^2$ for GA781 $\langle 110 \rangle$ and T1#5, and $\sigma \approx 1000 \text{ kg/cm}^2$ for GA735(e)). This can be explained if we assume the strain is not exactly along $\langle 110 \rangle$ but has a small component along $\langle 100 \rangle$ as it must in practice.



The effect of this component is to split the $\langle 100 \rangle$ and $\langle 010 \rangle$ levels. If the component is small, this splitting varies very slowly with stress and the second dip occurs when the splitting becomes equal to $\hbar\omega_d$ (figure 5.11). If θ is the angle between the $\langle 110 \rangle$ direction

and the sample axis, the component of stress along $\langle 110 \rangle$ is $\sigma \cos^2 \theta$ giving rise to a splitting $\delta_{110} = (3/4)V_{ES}(S_{11} - S_{12})\sigma \cos^2 \theta$ (section 5.5.2.1). Due to misalignment the effective stress component along $\langle 100 \rangle$ is

$$\sigma' = \sigma[\cos^2(45-\theta) - \cos^2\theta \cos^2 45]$$

The splitting of the two lowered wells is then

$$\delta_{100} = (3/2)V_{ES}(S_{11} - S_{12})\sigma'$$

The two minima occur (figure 5.11) when the ratio of the two splittings equals the ratio of the two stresses:

$$\frac{\delta_{001}}{\delta_{110}} = \frac{\sigma_1}{\sigma_2}$$

$$\therefore \frac{\sigma_1}{\sigma_2} \approx 2\theta$$

where we have taken $\cos\theta \approx 1$ and $\sin\theta \approx \theta$ ($\theta \ll \frac{\pi}{2}$).

The stress at which the second minimum occurs will depend on the misalignment of the sample. From the data for TI#5 and GA781 $\langle 110 \rangle$ $\sigma_1 \approx 130 \text{ kg/cm}^2$ and $\sigma_2 \approx 1500 \text{ kg/cm}^2$, giving $\theta \approx 2^\circ$. This emphasizes the splitting of the Cr^{2+} centres is very sensitive to the direction of strain and any slight misalignment of stress can be seen in the experimental data. It seems that GA735(e) may be most misaligned as the second minimum here occurs at $\sigma \approx 1000 \text{ kg/cm}^2$. A careful check on the orientation of this sample has indeed shown that the axis was $\sim 4^\circ$ away from $\langle 110 \rangle$.

5.6 CONCLUSION

All the stress effects in the thermal conductivity of GaAs:Cr have been attributed to the Cr^{2+} charge state of the Cr ions. The piezothermal conductivity has been explained assuming a tetragonal Jahn-Teller distortion of the Cr^{2+} centres. An approximate value of the Jahn-Teller energy has been deduced from the experimental data. The effect of internal strains may not be negligible and from the stress data, the low frequency (0.7 cm^{-1}) phonon scattering in zero stress has tentatively been attributed to strain removal of orientational degeneracy although tunnelling may also be the case. At the time of writing steps are being taken to anneal the samples to try to reduce the residual strains. Measurements under stress for samples cut along $\langle 11 \rangle$ (no stress effect should occur) are also planned.

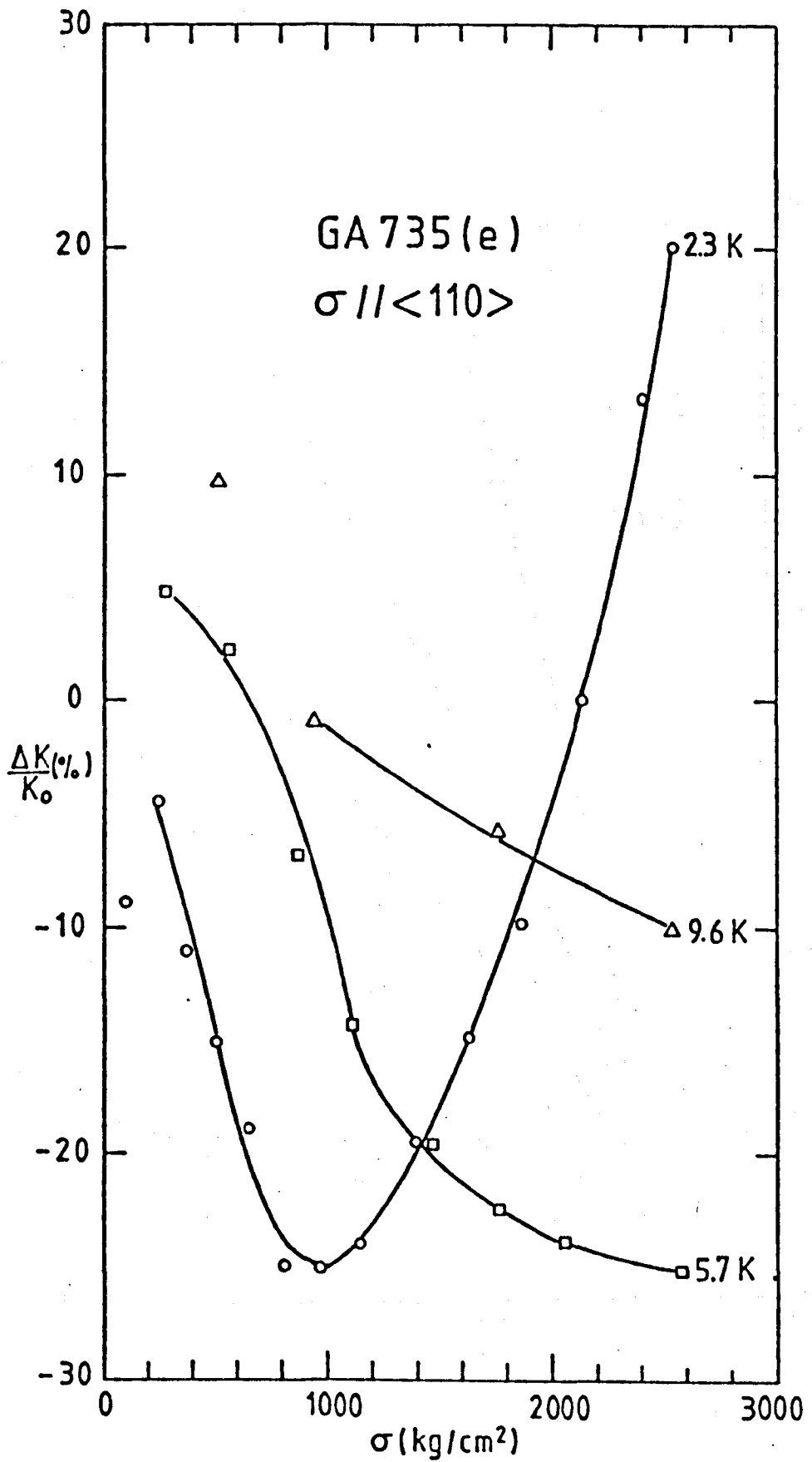


FIGURE 5.1 Effect of applied stress on the thermal conductivity of SI GA735(e).

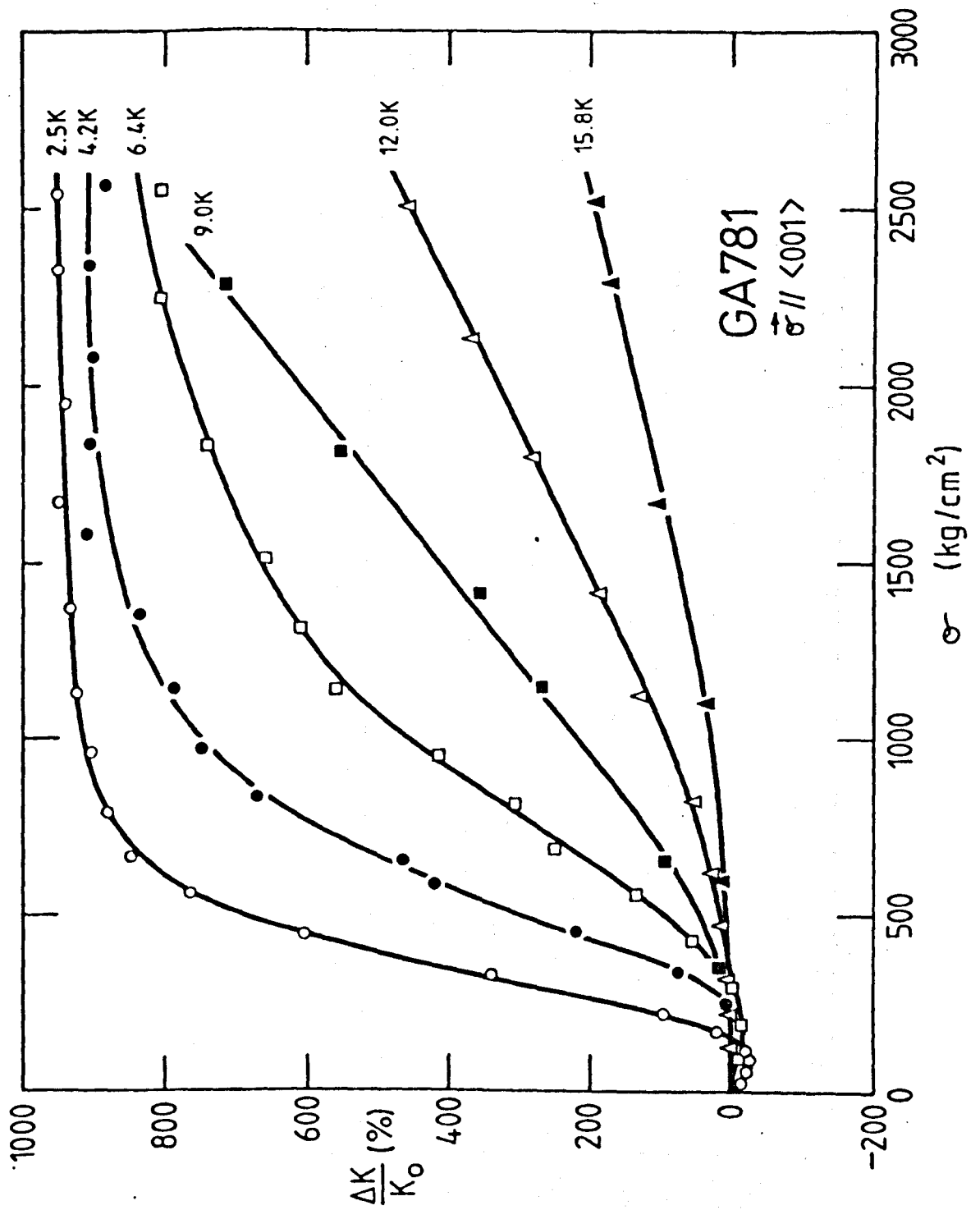


FIGURE 5.2 Effect of applied stress on the thermal conductivity of p-type GA781 $\langle 001 \rangle$.

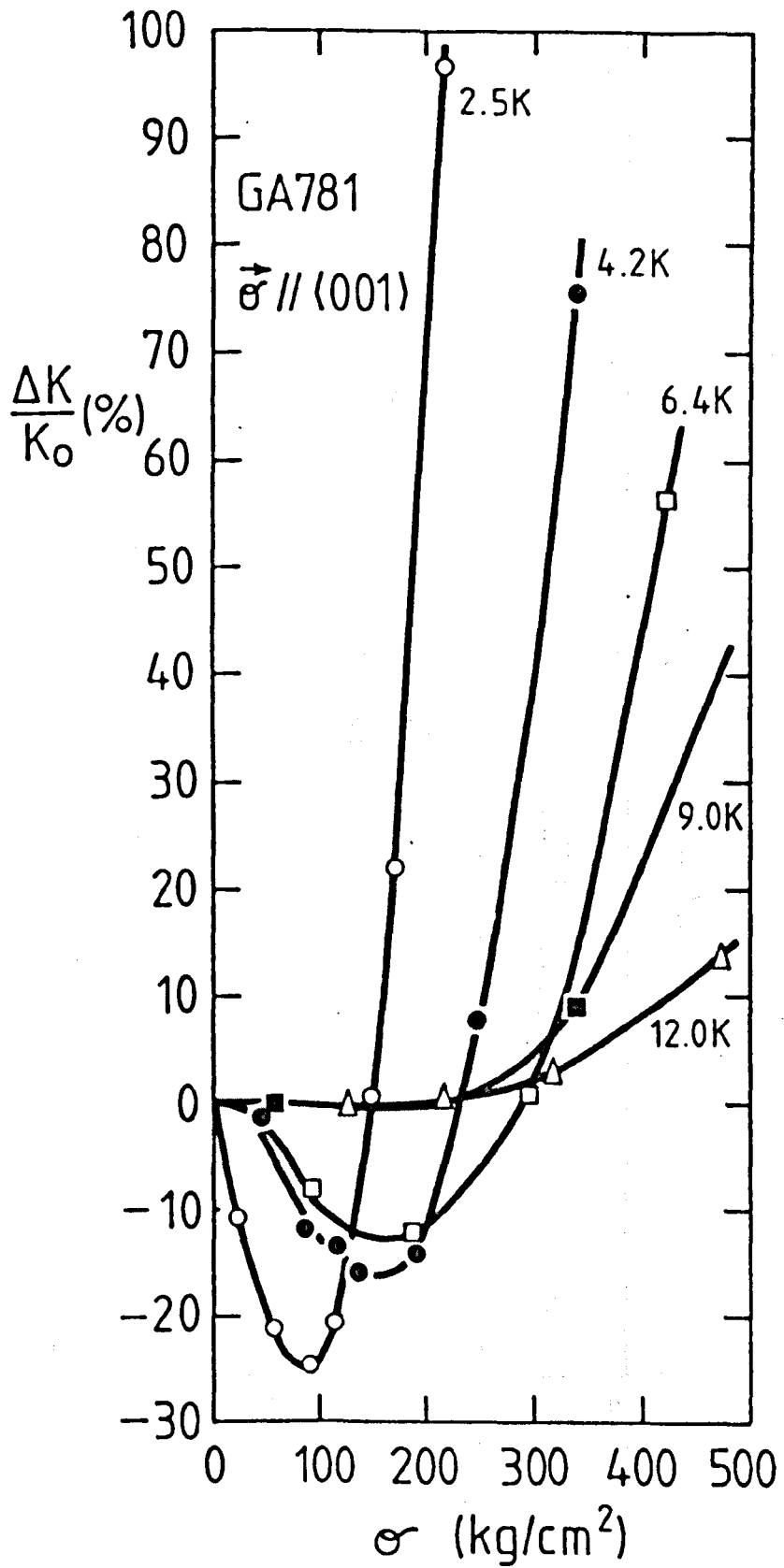


FIGURE 5.3 Detail of low stress data (GA781 <001>).

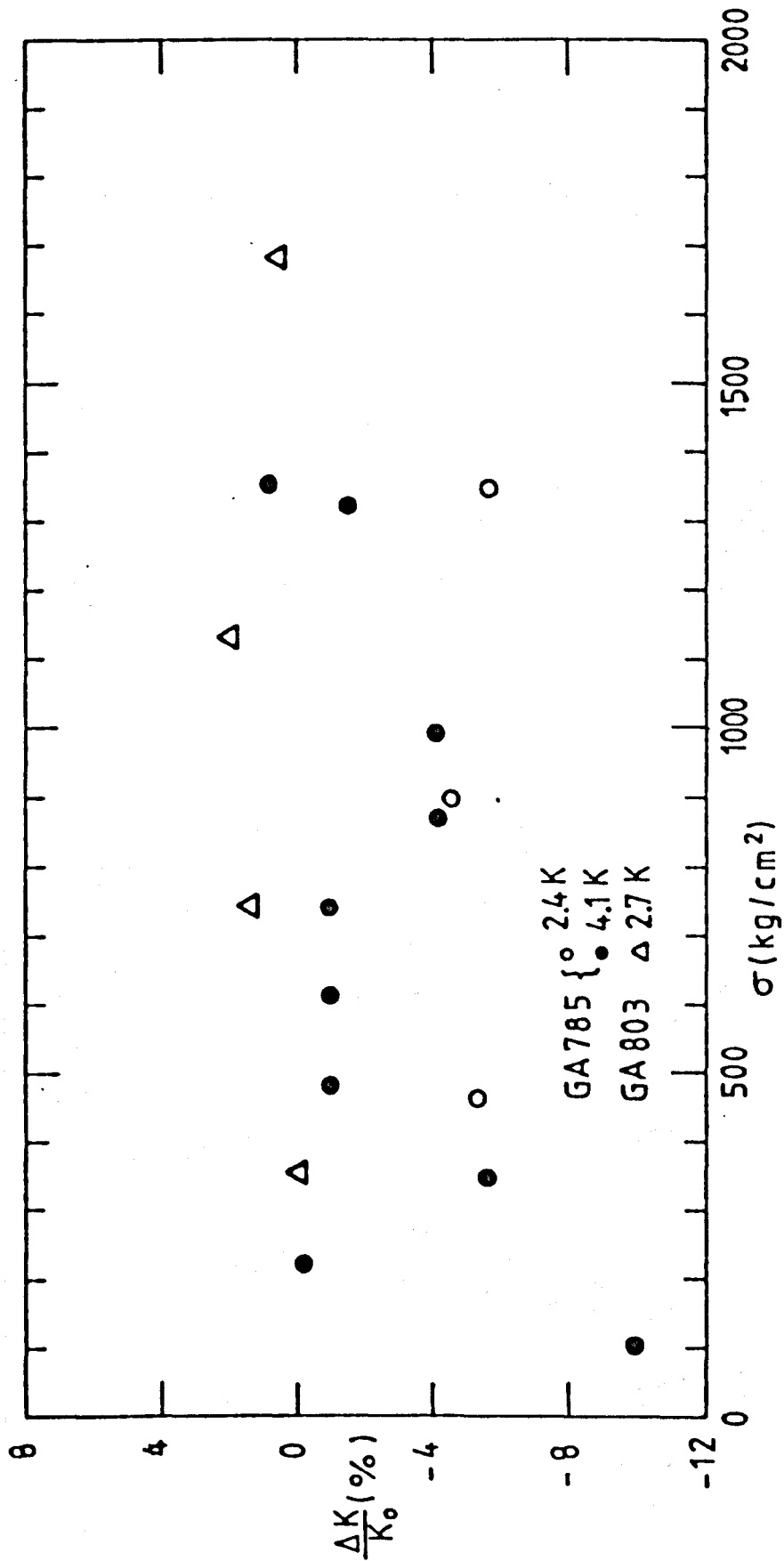


FIGURE 5.4 Thermal conductivity of GA785 (n-type) and GA803 (undoped) under applied stress.

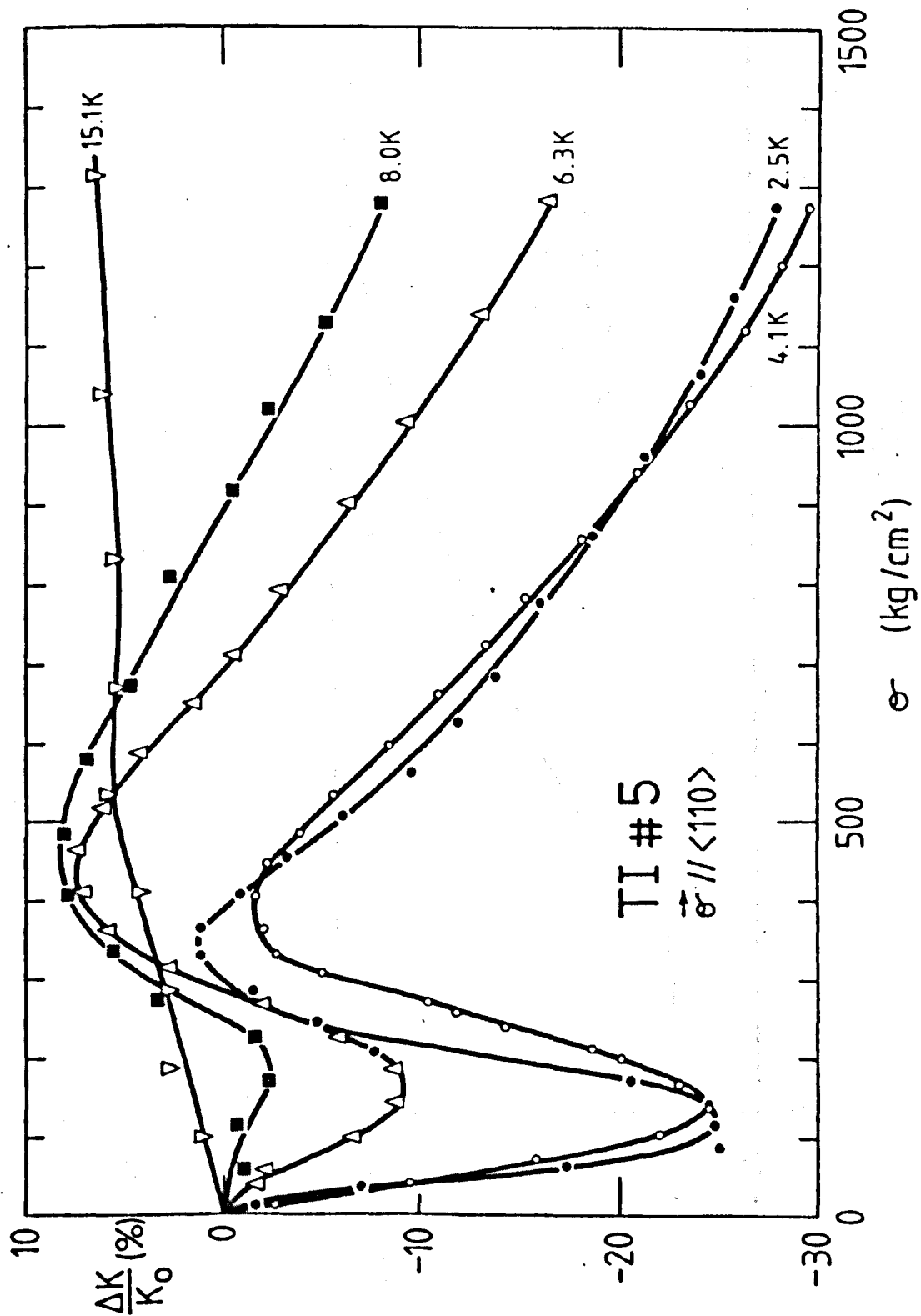


FIGURE 5.5 Effect of applied stress on the thermal conductivity of SI TI#5.

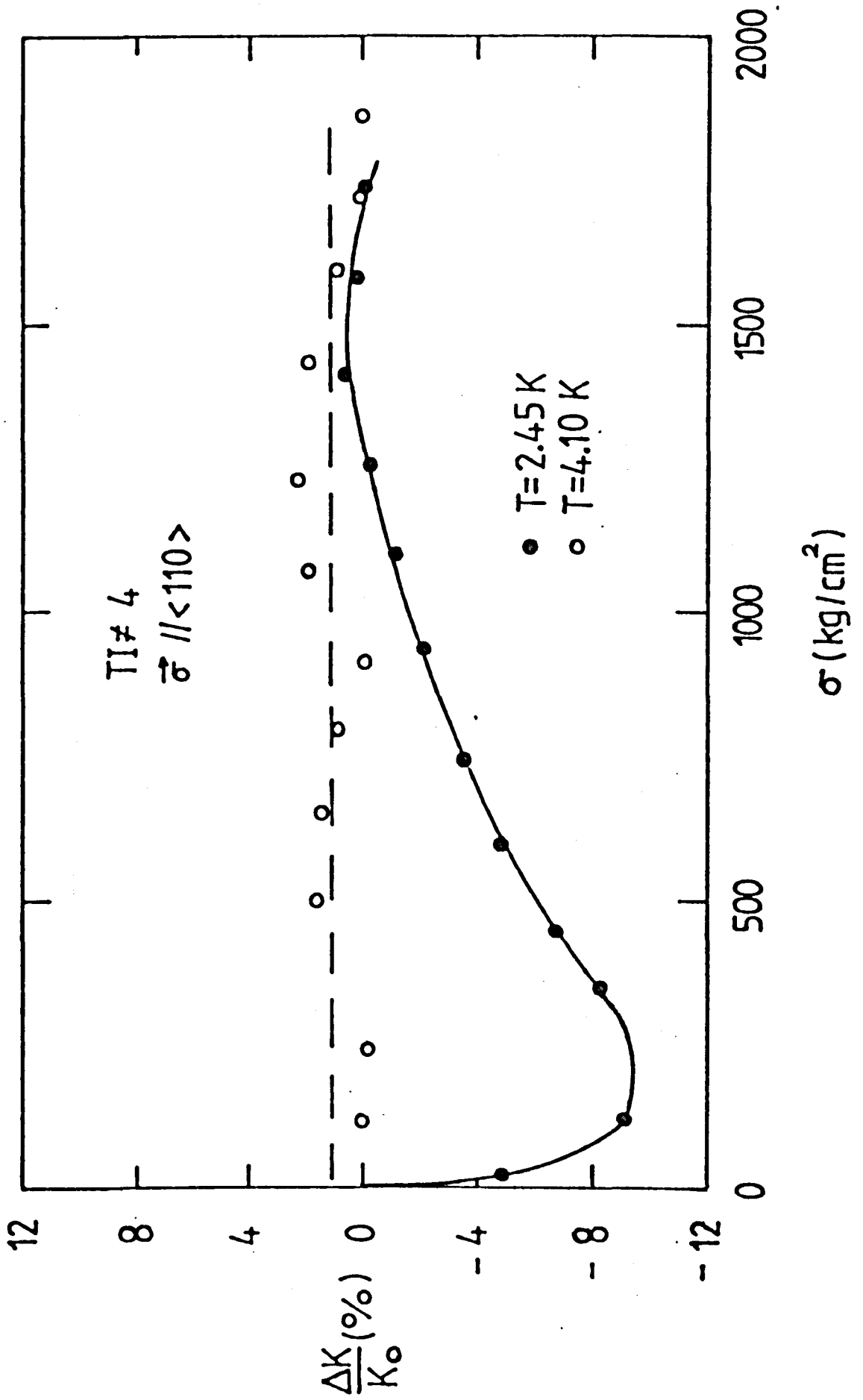


FIGURE 5.6 Thermal conductivity of SI TI#4 under applied stress.

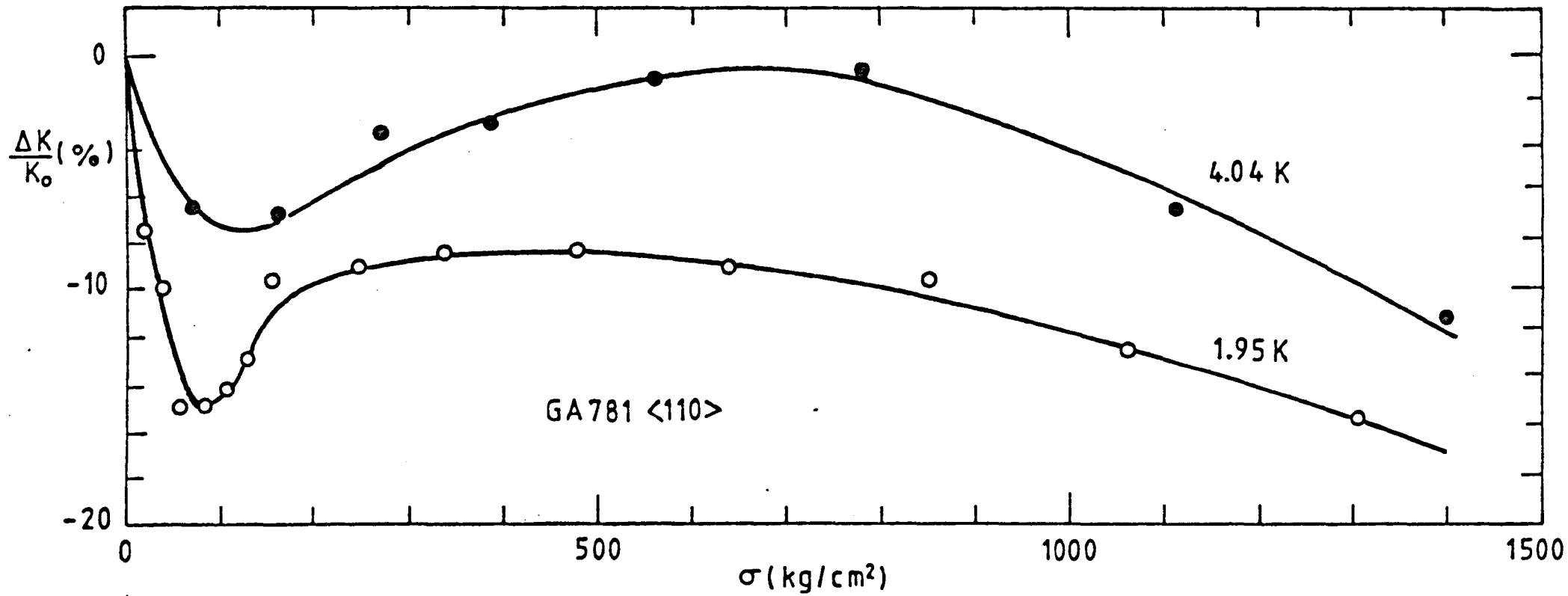


FIGURE 5.7 Effect of applied stress on the thermal conductivity of p-type GA781 <110>.

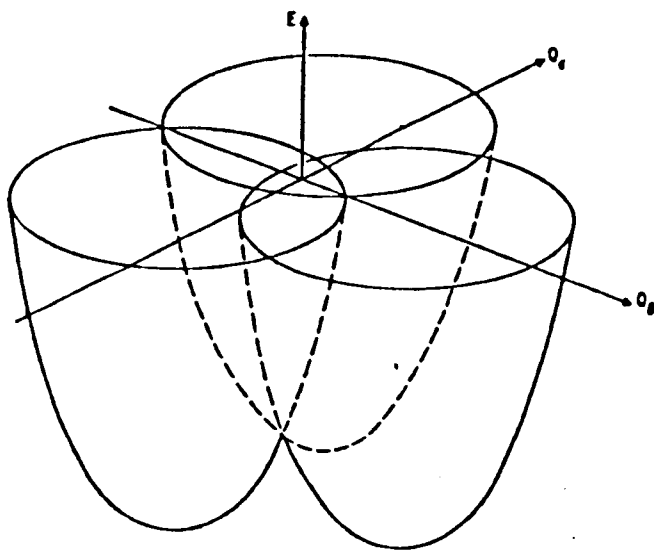


FIGURE 5.8 Energy surfaces describing the static Jahn-Teller effect for a triplet state coupled to E vibrational modes.
(After Ham 1972).

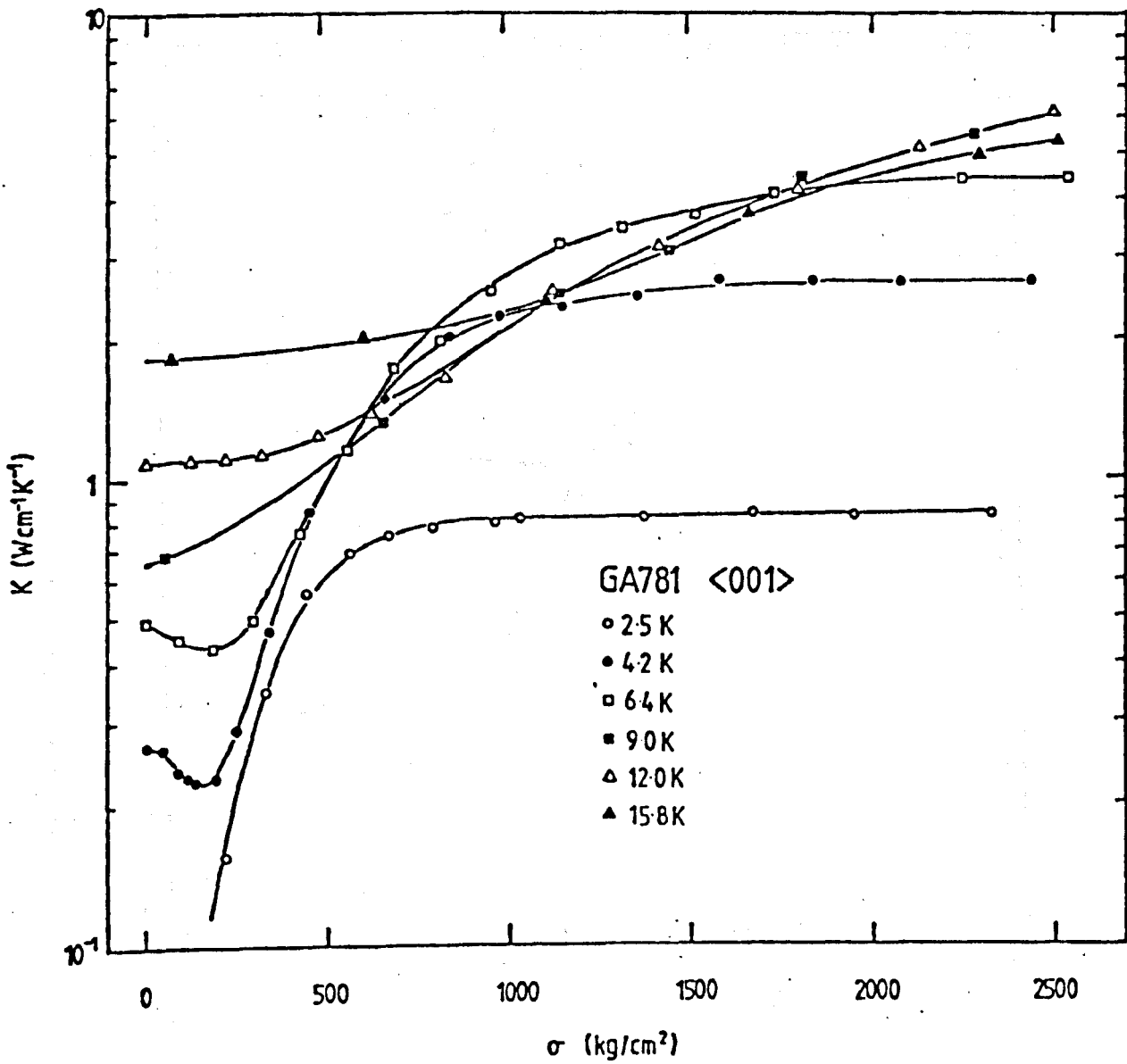


FIGURE 5.9 $K(\sigma)$ of GA781 <001>.

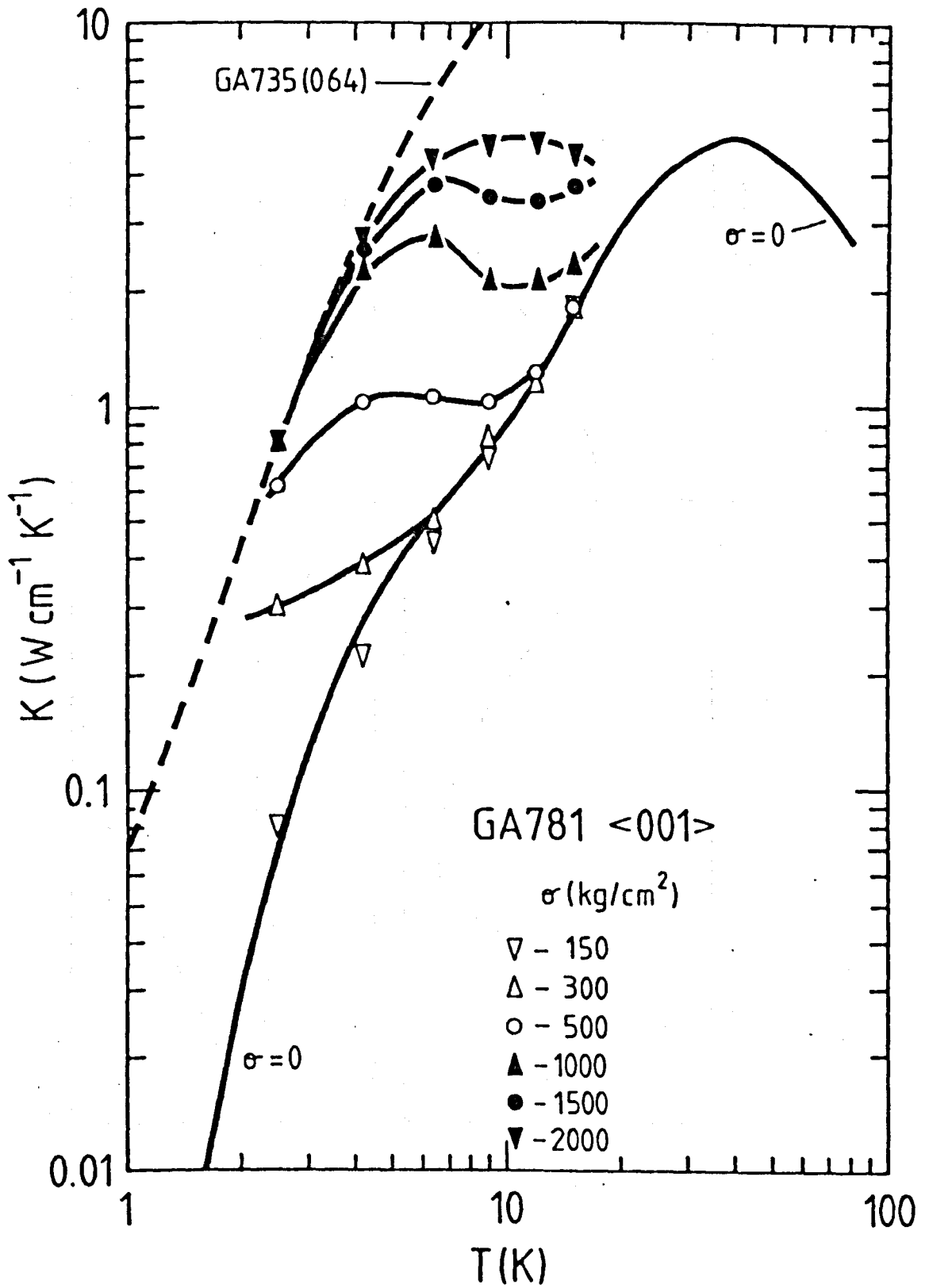


FIGURE 5.10 Thermal conductivity of GA781 <001> at fixed values of stress.

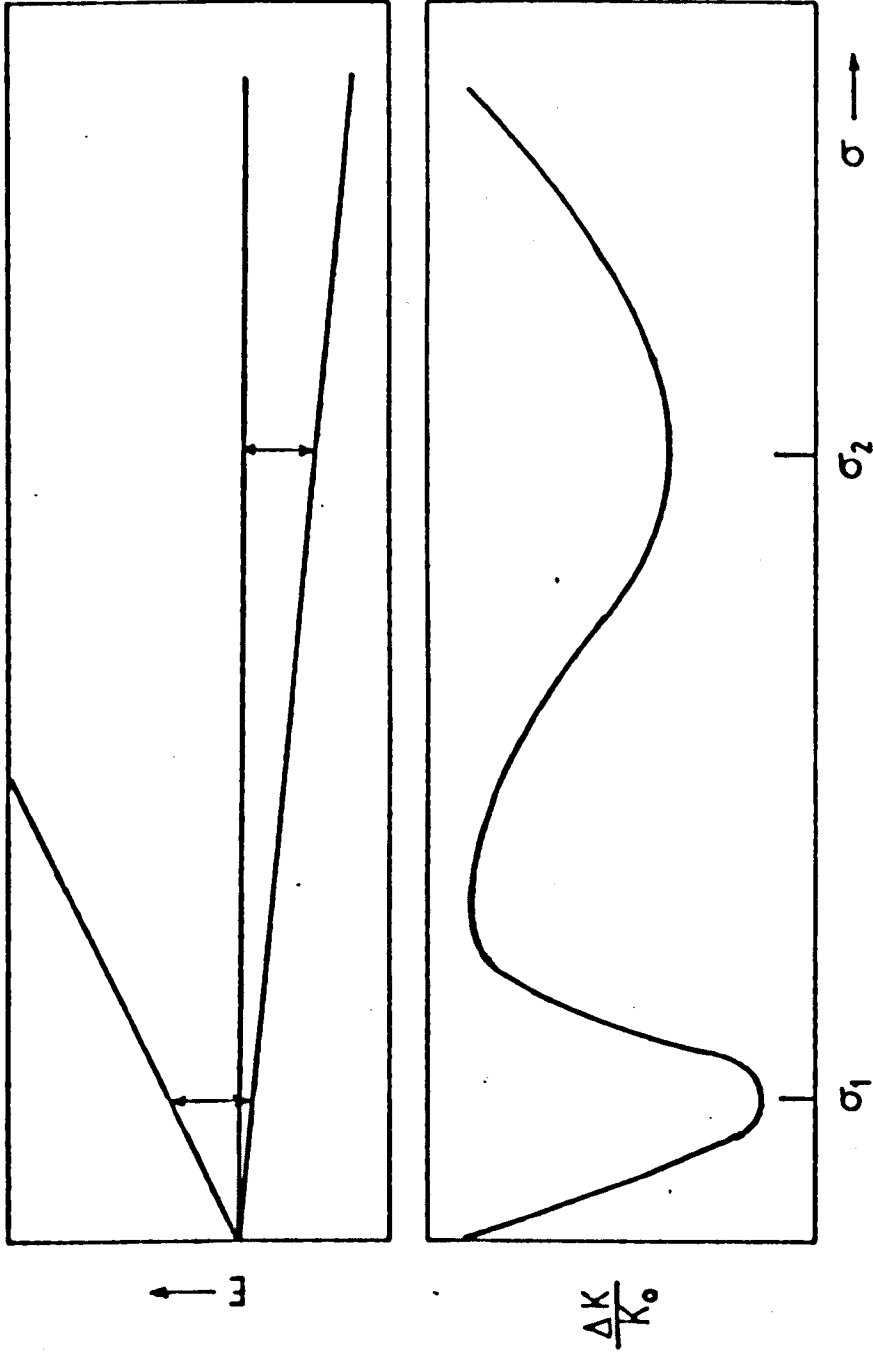


FIGURE 5.11 Effect on K of misalignment of applied stress.

CHAPTER 6

PHOTO-INDUCED EFFECTS IN GaAs:Cr

6.1 INTRODUCTION

Light with $h\nu < E_g$, where E_g is the band gap, can alter the concentration of the charge states of Cr in GaAs (e.g. Stauss and Krebs 1977). In Chapter 3 we have seen that the phonon scattering in GaAs:Cr, at low temperature, was very much dependent on the charge state of the Cr ions. The aim of the work described in this chapter was to change the concentration of the different charge state ions, in a controlled way, by sub-band-gap illumination. The possibility of selecting a particular charge state would have allowed us to conduct spectroscopic investigations using an additional external perturbation such as magnetic field or stress. A simple experimental arrangement for photoexcitation was mounted in the sample cell. It consists of an ordinary torch bulb enclosed in a copper shield to minimize heating effects (figure 6.1). A silicon filter is used to cut-off any high frequency radiation with $h\nu \geq 1.1\text{eV}$ and the bulb glass cuts-off radiation with $h\nu \leq 0.4\text{eV}$. Any radiation falling on the sample is then of energy $0.4\text{eV} \leq h\nu \leq 1.1\text{eV}$. The room temperature spectrum from this optical set up, which should only differ slightly from that at helium temperature, is also shown in figure 6.1.

We could monitor changes in thermal resistivity due to illumination as well as changes of electrical conductivity, in the

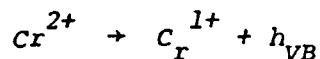
same sample. It was hoped this would facilitate the interpretation of possible transitions induced by the light.

The preliminary results of this investigation are presented in section 6.3. Previous work on light induced charge state conversion in GaAs:Cr is briefly reviewed in the next section.

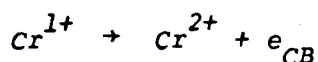
6.2 OPTICALLY INDUCED CHARGE STATE CONVERSION IN GaAs:Cr

We mention first the effect of optical excitation on the populations of the different Cr charge states in GaAs, as seen by EPR. We base our discussion at this stage on the work reported before ~1980. More recent results are discussed in section 7.3.

Kaufmann and Schneider (1976) reported the observation, in semi-insulating GaAs:Cr, of an isotropic line with $g \sim 2$ presumed to be the Cr^{1+} centre (6S), after sub-band-gap illumination. No signal was observed in the dark. The excitation and quenching of the chromium EPR signal were studied as a function of light wavelength at 20 K. In their interpretation they proposed that for phonon energies $h\nu > 0.75eV$

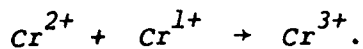


where h_{VB} is a hole, free in the valence band. This process converts Cr^{2+} into Cr^{1+} and locates the Cr^{2+} ground state at $\sim 0.75eV$ above the valence band. To explain the quenching of the EPR signal by photons of energy $h\nu > 0.45eV$, they assumed the process



in which one electron is taken from a Cr^{1+} centre to the conduction band. However the level diagram for GaAs:Cr proposed in their paper is now generally believed to be incorrect since it implies it would be possible to promote an electron from the valence band to the conduction band, via the two processes described earlier, by expending only $\sim 1.35\text{eV}$, whereas the band gap of GaAs is $\sim 1.52\text{eV}$ at 20 K.

Stauss and Krebs (1977), Krebs and Stauss (1977a, b; 1979b) observed the three charge states of Cr (Cr^{3+} , Cr^{2+} and Cr^{1+}) in semi-insulating GaAs and studied the effect of light on the populations of the three centres, in the temperature range 5 - 30 K. Again Cr^{1+} was only seen after illumination. Their results are shown in figure 6.2. They conclude that for $h\nu > 0.83\text{eV}$, Cr^{3+} is converted to $\text{Cr}^{2+} + \text{Cr}^{1+}$ while for $0.45\text{eV} \lesssim h\nu \lesssim 0.83\text{eV}$, the concentrations of Cr^{1+} and Cr^{2+} fall and that of Cr^{3+} rises, or schematically



For $h\nu < 0.75\text{eV}$, the Cr^{1+} signal is completely quenched.

The general shape of the spectrum of the photo-induced interconversion between the three Cr charge states was found to be the same for different samples but the magnitude of the effects varied from sample to sample and this was thought to be due to the differences in concentration of Cr and other impurities (Stauss and Krebs 1977). A modified version of a model first presented by Lin and Bube (1976) to explain their dark and photo-induced properties of GaAs:Cr, was proposed by Stauss and Krebs for the interpretation of their results. Levels other than that of Cr ions

were required to account for the optical transitions. These extra levels, within the gap, were thought to be related to oxygen impurities present in bulk-grown GaAs (Lin and Bube 1976).

A more recent study of the change of EPR spectra of the charge states of Cr in GaAs during and following optical excitation was reported by White et al (1980). Semi-insulating and p-type samples were used and again no Cr^{1+} was seen in the dark. Following application of light at 1.1eV, the Cr^{2+} and Cr^{1+} signals rise to a saturation value with time constants dependent on the light intensity. After switching off the optical excitation the signals decay to some equilibrium level with a non-exponential transient but with a time scale of seconds to minutes at 4.5 K (in p-type material the Cr^{2+} signal decays to zero). The intensity of the Cr^{3+} signal reflects the behaviour of Cr^{1+} and Cr^{2+} signals, increasing when these signals are decreasing. From the quenching effects of application of light at low energies ($\sim 0.5\text{eV}$) at a fixed delay after removal of the pump radiation at 1.1eV, the authors postulated the existence of hole traps with hole liberation energies of 0.45eV. The transient phenomena were qualitatively explained in terms of exchange of holes with traps.

Hence the EPR studies have shown the possibility of modifying the equilibrium-populations of the three chromium charge states by optical excitation of energy less than E_g .

Light effects in GaAs:Cr, using other techniques, have also been reported in the literature. Photoconductivity measurements by Lin and Bube (1976) have shown the existence of two levels

related to Cr, in the band gap, but these levels were not thought to be associated with different charge states of the same centre. Szawelska and Allen (1979) reported the photoionization spectra for transitions from two levels associated with different charge states of the same Cr centre. More recently, the effect of illumination on the APR spectra of Cr-doped GaAs has been investigated and the observed behaviour discussed in terms of the Cr^{3+} , Cr^{2+} and Cr^{1+} charge states model (Bury et al 1980b).

6.3 PERSISTENT PHONON-SCATTERING CENTRES IN n-GaAs:Cr,Si

6.3.1 Experimental Procedure

Most of the runs were carried out in the 4 - 20 K dipstick apparatus (Chapter 2). The Oxford Instruments Co. cryostat was also used which allowed magnetic fields to be applied. The main experimental problem we were faced with was the heating effect by the incident radiation. We observed a direct heating of the thermometers, probably due to absorption in the copper-stycast bond, which resulted in very fast transients (figure 6.6). Heating of the sample itself resulted in transients with a larger characteristic time (~ 30 s).

Four point probe techniques were used in the measurement of the photoconductivity. Ohmic contacts were made by alloying indium spots on to the samples in a nitrogen atmosphere, using HCl as a flux. A constant-current method was used for the DC photoconductivity. Figure 6.3 shows a block-diagram for the photo-thermal and photo-electrical conductivity measurements. It was possible to store the transient effect signals and analyse

their variation with time using a Datalab DL400DB microprocessor system.

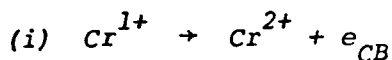
The samples were always cooled down in the dark. Following optical illumination, the variation of f_{12} (Chapter 1) with time is monitored. The experimental results are presented in the next section.

6.3.2 Experimental Results and Discussion

In Chapter 3 it was found that the phonon-scattering by Cr^{1+} ions was very small compared to the scattering by $\text{Cr}^{2+}/\text{Cr}^{3+}$ ions. To study light effect we first selected a sample which was supposed to contain mostly Cr^{1+} in the dark, hoping to change this charge state to $\text{Cr}^{2+}/\text{Cr}^{3+}$ and observe the resulting phonon scattering. GA735 (064) (Appendix 1) which has the highest thermal conductivity amongst the Cr-doped samples was first investigated and a typical curve for the photoresponse is shown in figure 6.4 for $T = 2$ K.

The reduced resistivity W/W_0 is plotted versus time, starting ~ 15 s after ~ 1 s pulse of light from the torch bulb. W_0 is the thermal resistivity before illumination. The effect of light is to increase the thermal resistivity, showing the creation of phonon-scattering centres. When the light is switched off the resistivity decreases and from 6.4, two types of decay of these centres are observed. One is slow with a characteristic time of ~ 1 hour, the second is persistent with decay times too long to detect.

A tentative interpretation of the first decay was given in Challis and Ramdane (1980). Before illumination, most of the Cr present in GA735 (O64) is the Cr^{1+} charge state (assuming Brozel et al model - see Appendix 1) and the effect of light is to ionize Cr^{1+} through the processes



which result in an increase of the concentration of free electrons (e_{CB} is an electron free in the conduction band). After removal of optical excitation, neutral Cr^{3+} can capture an electron back to form Cr^{2+} and this process should be fast because of coulombic attraction. If this is so it is unlikely that we could observe the effect of this process in the phonon scattering, using the present experimental set up: the thermometers response times are only a few ms but the time for the sample to cool after illumination provides a dead-time of ~ 15 s before measurements can be made. The first decay time of ~ 1 hour was then interpreted as arising from the reverse of process (i), in which electrons are slowly trapped at Cr^{2+} ions, which are negatively charged relative to the lattice.

A very similar decay curve was observed in the photo-conductivity of samples cut from neighbouring slices (Eaves and Williams 1979). The decay with a life-time 3×10^3 s was attributed to electron-capture at Cr^{2+} . However, in a later experiment, we observed the same type of decay of the photo-conductivity (figure 6.5) of GA803 which is not Cr-doped but comes from the same source (Allen Clark Research Centre, Plessey Co.). No detectable change in thermal resistivity was observed

however following illumination (figure 6.6). This poses the question of whether the photoconductivity effects seen in the Cr-doped n-type sample are related to the presence of the Cr ions. Oxygen contamination for example was found to influence the photoelectronic properties of GaAs:Cr (Lin and Bube 1976) and it seems necessary to investigate other n-type Cr-doped samples, from different origins, to ascertain the assignment of the observed photo-induced effects. The second part of the decay is discussed in section 6.3.3.

The photothermal conductivity of GA781<110> (p-type) was also investigated at low temperatures. We did not observe any light induced effect. This was rather surprising since we would expect charge state conversion in this sample which is similar to the p-type ones used for EPR work by White et al (1980). Extrinsic light at 1.1eV should convert Cr^{3+} (which is supposed to be the dominant charge state in this sample) to Cr^{2+} and Cr^{1+} . This might suggest that the light intensity available from the torch bulb is too small to induce a significant change in concentration. Alternatively it could be connected with the fact that our illumination covers a broad range, including the range ~ 0.5eV which drives the charge transfer in the opposite direction to that at higher energies. The next step planned for a thorough investigation is to provide an optical path from room temperature by the use of fibre optics, thus allowing monochromatic radiation of different intensities, to be shone on the samples.

6.3.3 Persistent Effects

A large amount of the photo-induced thermal resistivity ($W \sim 1.9 W_0$) seen in figure 6.4 remains unaltered even after 10 hours, suggesting the characteristic time for this process is $\gg 10^5$ s. Thermal conductivity data in this state are shown in figure 3.1. When we warmed up the sample to room temperature and then cooled again we found that the persistent phonon scattering had completely disappeared, although no measurements were made to determine the quenching temperature more precisely. The photoconductivity persistent level is quenched by warming the sample to about 100 K (Eaves and Williams 1979) and in the case of GA803, we found that the persistent photoconductivity is quenched at 55 ± 10 K.

To try to identify these stable phonon scattering centres, measurements were made in a magnetic field. We did not find any detectable change ($\lesssim 1\%$) in the phonon scattering, which presumably implies that these stable scattering centres are not Cr^{2+} ions. (We recall that we did not observe any field effect in GA735 (O64) in the dark where the Cr is believed to be in the Cr^{1+} state, but large effects were detected in TI#4, GA735(e) and TI#5 which are believed to contain Cr^{2+}).

These persistent effects have already been observed in several compound semiconductors (e.g. Lang and Logan 1977). To explain this phenomenon these authors have proposed a configuration coordinate model in which the coupling between the electronic and vibrational systems of the defects is very strong (figure 6.7). In the diagram, curves C and V correspond to the total system

energy of an unoccupied defect with a delocalized electron in either the conduction or valence band, respectively. $E_{\infty}(E)$ is the thermal barrier to electron-capture (-emission). E_0 is the net binding energy. After optical excitation of an electron from the minimum of curve D (see arrow), this electron relaxes to the bottom of curve C by emission of phonons. In this model where the minimum of curve C does not overlap with any vibrational states of curve D ('large-relaxation-limit'), electron capture can only occur by thermal excitation of the system to near the C-D crossing point (Lang and Logan 1977), and hence quenching of the persistent effect occurs after warming up the sample.

The defects responsible for this persistent effect are thought to be some sort of a complex of a donor atom with a native defect or ubiquitous impurity. Lang et al (1979) have proposed that the most likely model for these centres in $\text{AlGa}_{1-x}\text{As}$ and perhaps in other compound semiconductors, is a complex involving a donor and an anion vacancy.

We note that another interpretation of persistent photoconductivity in semiconductors exists, which assumes macroscopic potential barriers due to sample inhomogeneities (e.g. Sheinkman and Ya. Shik 1976).

6.4 CONCLUSION

This preliminary investigation has shown that light with energy less than the band gap can induce transitions from deep traps, the effect of which is observed on the phonon scattering at helium temperatures. The transient photothermal resistivity has

been measured in an n-type Cr-doped GaAs sample. Two types of decay were observed. One is slow with a decay time of ~ 1 hour which we have tentatively attributed to electron-capture at Cr^{2+} ions. The other is persistent with a decay time of $\gg 10^5$ s. To our knowledge, this is the first report of persistent effects in a semiconductor observed by thermal conductivity techniques. The centres responsible for this effect are not magnetic. Similar effects have been attributed to complexes of a shallow donor and a native defect, although if this is the explanation here we need to explain why this distortion produces so much stronger phonon scattering than a donor in T_d symmetry; so this could provide a test of the model.

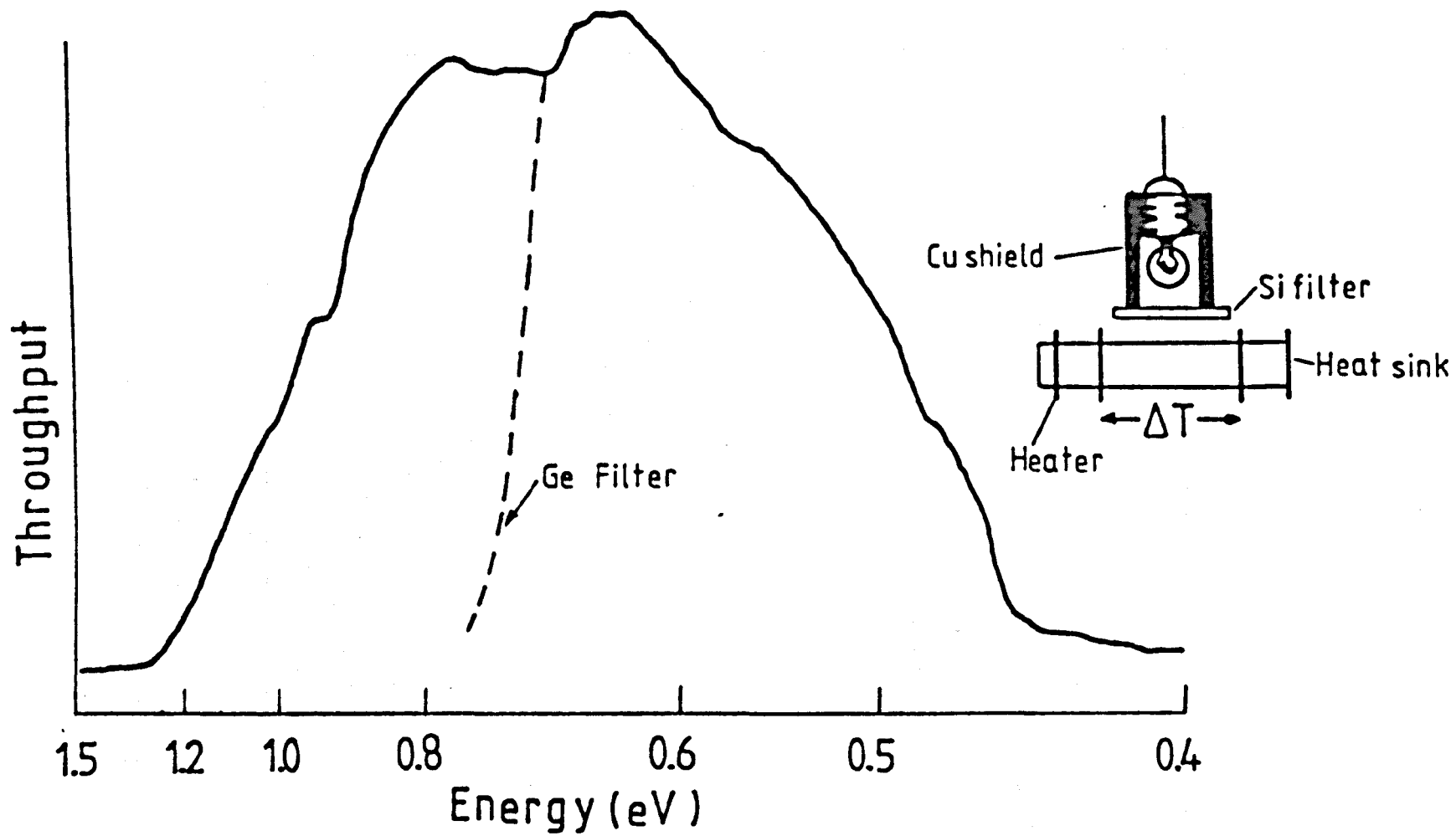
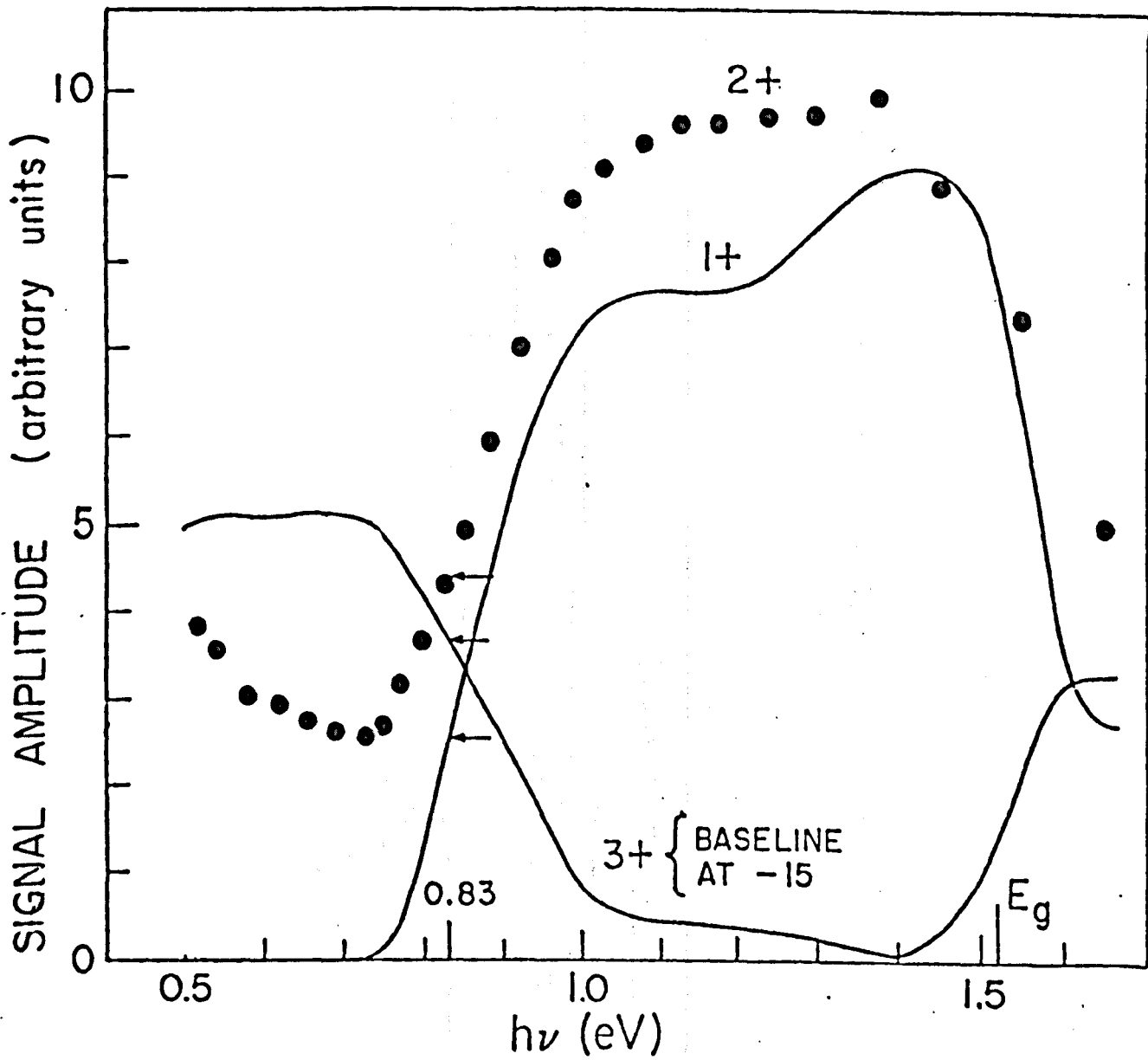


FIGURE 6.1 Optical set-up used for photo-excitation.



Effect of light on Cr^{n+} centers

FIGURE 6.2 Effect of light on Cr^{n+} centres.
(After Krebs and Stauss 1979b).

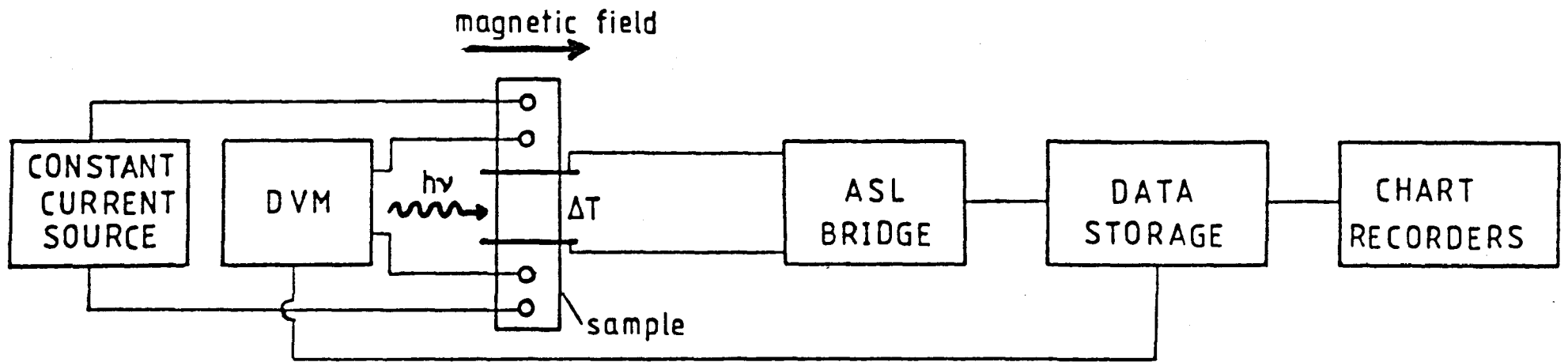


FIGURE 6.3 Block diagram of electrical and thermal photoconductivity experiments.

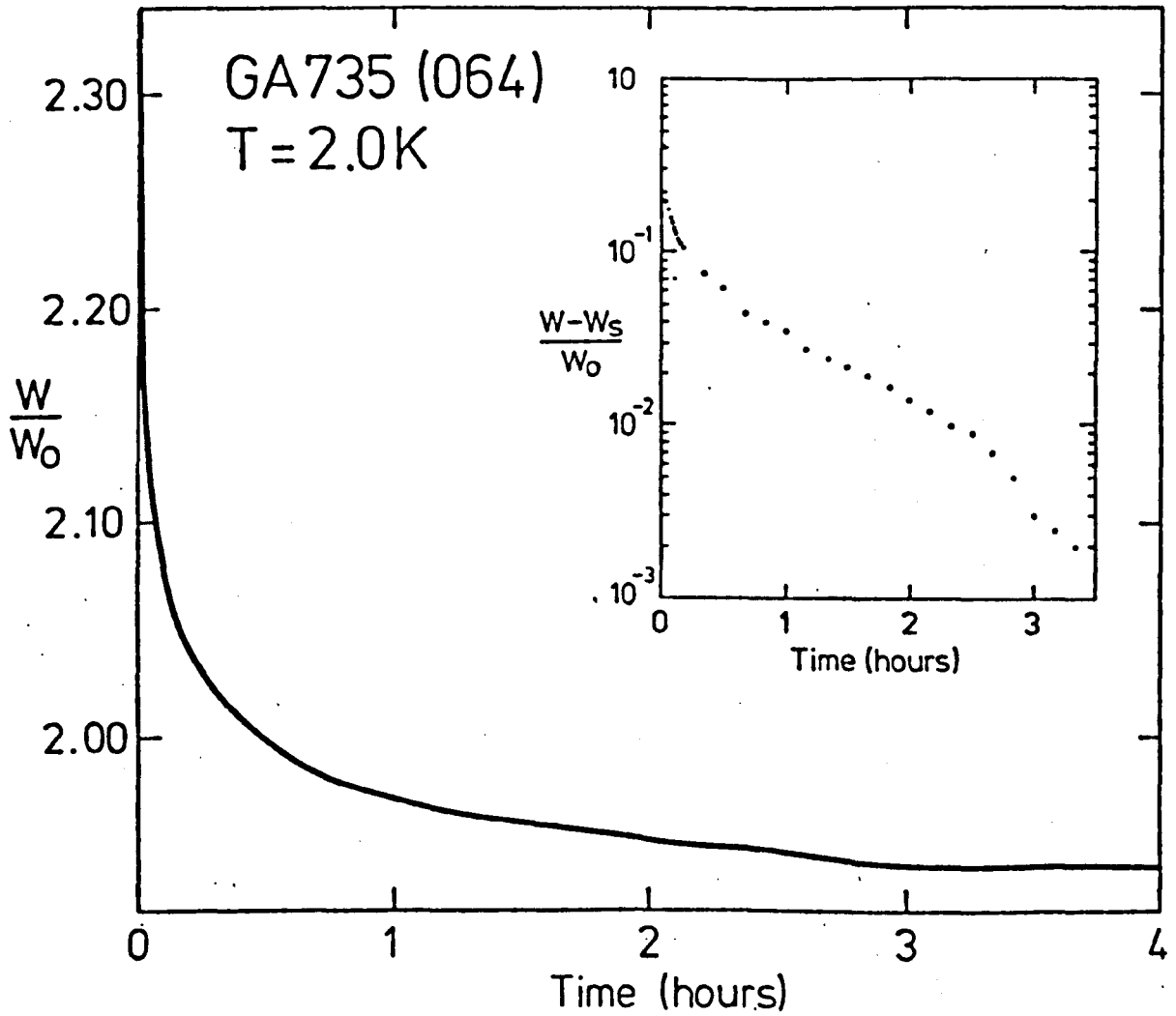


FIGURE 6.4 Decay of the photoinduced thermal resistance in n-type GA735 (064).

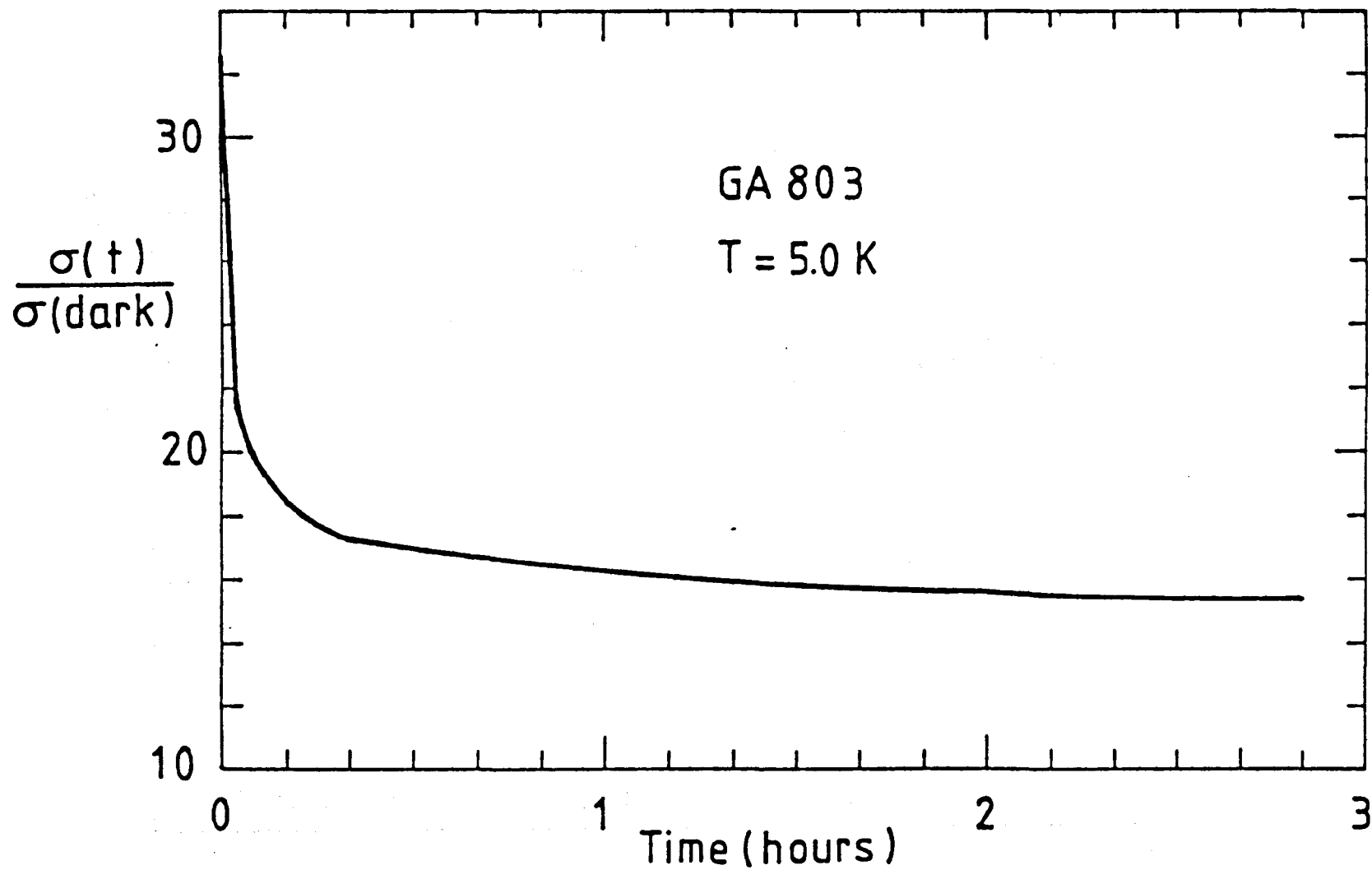


FIGURE 6.5 Decay of the photoconductivity $\sigma(t)/\sigma(\text{dark})$ of n-type GA803 following the switching-off of sub-band-gap illumination.

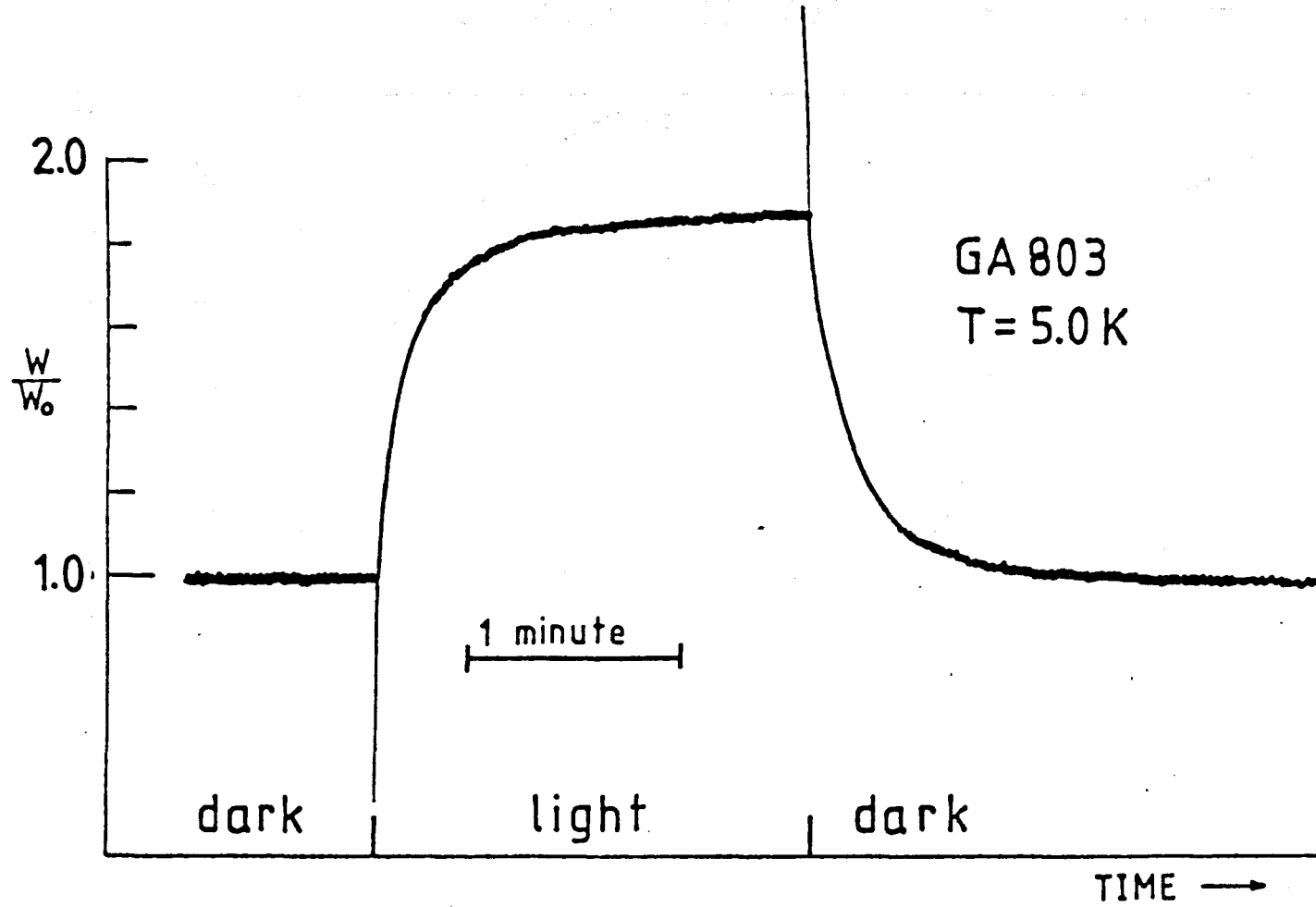


FIGURE 6.6 Effect of light on the thermal resistivity of n-type GA803.

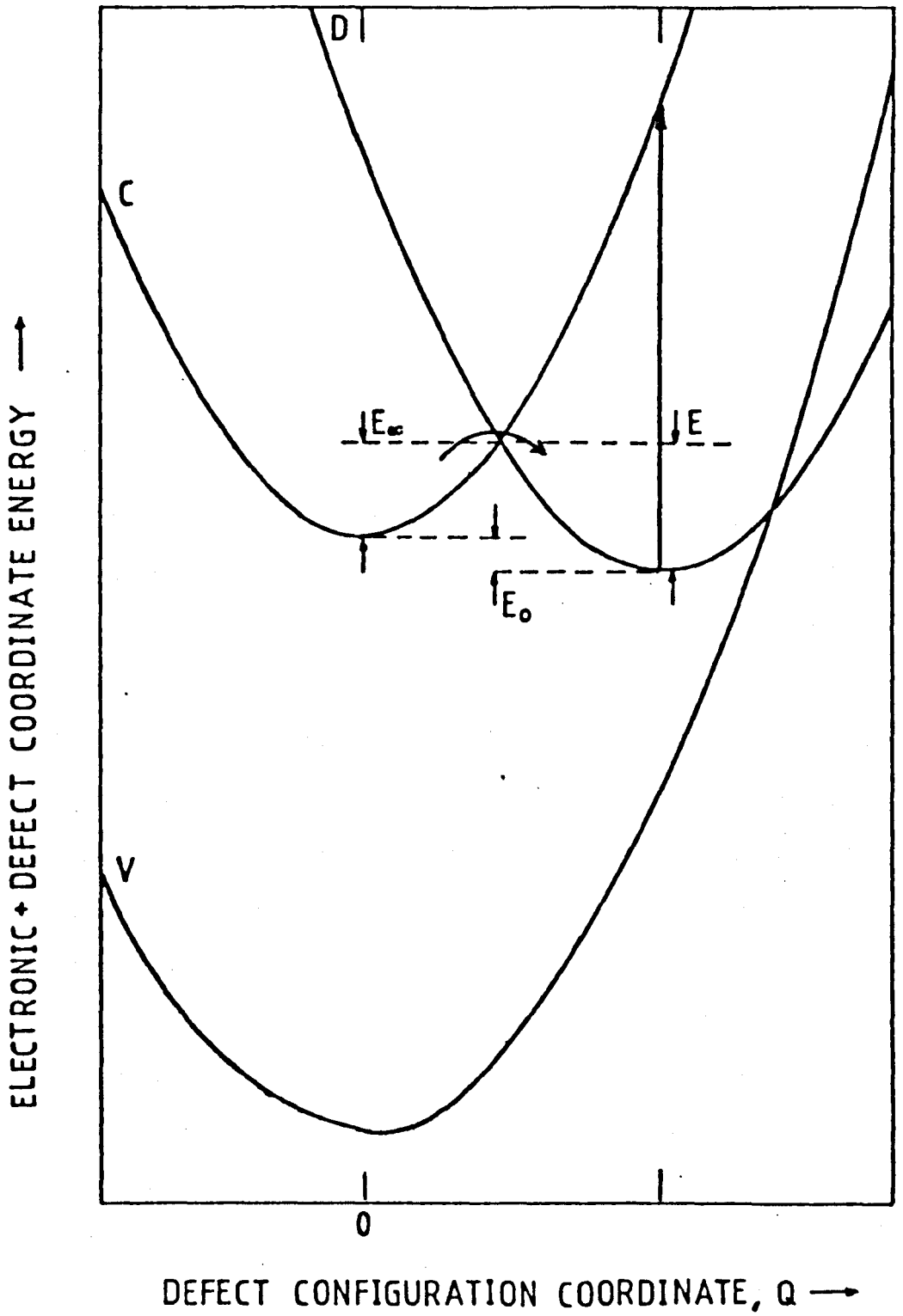


FIGURE 6.7 Diagrammatic representation of large-lattice-relaxation configuration model for persistent photoconductivity.

(After Lang and Logan 1977).

CHAPTER 7

DISCUSSION

7.1 INTRODUCTION

The zero-field low temperatures phonon scattering in all the samples studied (Chapter 3) was found to be consistent with the model proposed by Brozel et al for the charge states of Cr in GaAs if we assume that Cr^{2+} and Cr^{3+} ions scatter phonons strongly and Cr^{1+} ions (6S) do not. This model is described in Appendix 1. Thus resonant phonon scattering was observed in samples supposed to contain $\text{Cr}^{2+}/\text{Cr}^{3+}$ charge states ions (SI and p-type) while those believed to contain mostly Cr^{1+} ions (n-type) showed little scattering. This behaviour was also reflected in the magneto-thermal conductivity where the effect of magnetic fields on the low temperature thermal conductivity of samples believed to contain mostly Cr^{1+} was very small (Chapter 4). The same samples did not show any effect with applied stress (Chapter 5). We recall that all the stress effects could be attributed to Cr^{2+} ions in a tetragonal symmetry due to static Jahn-Teller effects. Another model for the charge states of Cr in GaAs is presented in section 7.3. In the next section a comparison is made of all the present results concerning the ground state of Cr ions in GaAs.

7.2 GROUND STATE SPLITTING OF $\text{Cr}^{2+}/\text{Cr}^{3+}$ IONS IN GaAs

The results for different techniques are summarized in Table 7.1. The assignment of charge state and local symmetry is that of the authors given in the references.

7.2.1 Ground State Splitting of Cr^{3+} Ions

We first consider the splitting of $23 \pm 5 \text{ cm}^{-1}$ seen in all our SI and p-type samples. If we assume the Brozel et al model, Cr^{3+} is the dominant charge state in p-type material and could also be present in SI samples. It seems likely then that the 23 cm^{-1} resonance is due to Cr^{3+} .

About the same splitting ($\sim 18 \text{ cm}^{-1}$) (Table 7.1) was observed by Chaudhuri et al (1973) in one SI sample. Very recently Bankovskis et al (1980), of this Department, have observed a peak in the 1 GHz ultrasonic attenuation at $\sim 2 \text{ K}$ which occurs strongly in p-type samples and more weakly in SI samples. For this reason they attribute this peak to Cr^{3+} , (they also observe a peak at 20 K (1 GHz) which was detected in SI samples and attributed to Cr^{2+} by Tokumoto and Ishiguro (1979)) and from their analysis they calculated the ground state splitting to be $18.5 \pm 3 \text{ cm}^{-1}$. Thus the two techniques using phonons seem to agree on this value of the ground state splitting of Cr^{3+} . This is certainly very different from the value of $7 \pm 2 \text{ cm}^{-1}$ reported by Krebs and Stauss (1977a) for the zero-field splitting of Cr^{3+} ions. However they obtain this result from the relative intensities of EPR lines in the two doublets, which is not always reliable and lead for example in one case to an error of $\geq 50\%$ for Fe^{2+} in Al_2O_3 (Lewiner et al, 1970).

The best estimate of the ground state splitting from population effects could be obtained from the intensities of two particular lines and was $10.4 \pm 1.5 \text{ cm}^{-1}$. When all the data were taken into account, the average value was then estimated to be $7 \pm 2 \text{ cm}^{-1}$. Nevertheless, even if there is an error, the splitting they are observing cannot be as high as 23 cm^{-1} . If it were, the ratio of intensities of the EPR lines from the two $S' = 1/2$ doublets would vary by a factor of ~ 60 , and the transitions within the upper doublet would probably be unobservable. Now their EPR spectra are attributed to Cr^{3+} centres undergoing an orthorhombic Jahn-Teller distortion. These Jahn-Teller centres are found to reorient rapidly above 5 K, due to tunnelling (Krebs and Stauss 1977a). Probably then the thermal conductivity results are not appropriate to a static Jahn-Teller model for the Cr^{3+} ions as the relevant data are obtained at temperatures higher than 5K. (The resonant phonon scattering dip is observed at ~ 9 K).

7.2.2 Ground State Splittings of Cr^{2+} Ions

In Chapter 5 we attributed the low frequency resonant scattering at 0.7 cm^{-1} to Cr^{2+} ions and suggested that this splitting could arise because of the displacement of the Jahn-Teller configurations relative to each other by internal strains. (We recall we also suggested the 0.7 cm^{-1} scattering could occur between tunnelling split levels but no detailed analysis was attempted).

The Cr^{2+} ground state splitting deduced by EPR measurements at two different frequencies (Krebs and Stauss 1979b, Wagner and White 1979) was $\sim 7.5 \text{ cm}^{-1}$. (This spans three spin-orbit levels separated by 5.6 cm^{-1} and 1.9 cm^{-1}).

We note that these data are not inconsistent since theoretically transitions between equivalent or near equivalent states corresponding to different distortion directions could be strongly coupled to phonons ($\Delta M_S = 0$) while those involving transitions within the multiplet ($\Delta M_S \neq 0$) should be only weakly coupled.

Narayanamurti et al (1978) reported the attenuation of heat pulses in SI GaAs:Cr samples at low temperatures. From their data, for different modes and propagation directions, it is clear that E_g -type distortions are much more strongly coupled than T_{2g} distortions. They argue then that the defects responsible for the observed anisotropic attenuation have tetragonal symmetry although in fact E_g coupling is known to be much more strongly coupled than T_{2g} coupling in a variety of cubic systems, particularly if there is a Jahn-Teller effect (e.g. Bates 1978). By comparing with Krebs and Stauss (1977b) EPR results the authors identified the centres as being Cr^{2+} ions. Their value for the ground state splitting ($\sim 10 \text{ cm}^{-1}$) is reported in Table 7.1, which is broadly consistent with the energy levels of Krebs and Stauss, although not with the selection rules given above. We note that their value is far different from any splitting we report for SI GaAs:Cr samples (4.9 cm^{-1} and 23 cm^{-1}) although the two techniques used are the same in essence. In heat pulse propagation measurements, the heater temperature is used in the analysis and usually this parameter is not known accurately, but even so, the corresponding error should not lead to such a disagreement.

Recently, Narayanamurti (1980) observed the scattering of monochromatic phonons, generated by Sn superconducting tunnel

junctions. Absorption in the range 5.6 to 8.1 cm^{-1} was observed in the Cr-doped GaAs samples and was attributed to Cr^{2+} ions. In Table 7.1 we report the mean of these two values, i.e. $\sim 6.8 \text{ cm}^{-1}$. This splitting is again consistent with the EPR levels but not the selection rules. This technique may be more sensitive but Sn junctions were used which produce monochromatic phonons whose energy can be tuned between ~ 3 and 9 cm^{-1} so that a direct comparison with the 23 cm^{-1} splitting deduced by thermal conductivity measurements is not possible.

At this stage we might consider the value of $\sim 4.9 \text{ cm}^{-1}$ deduced in this work. This value is determined from the computer fit of $K(T)$ of TI#4. It was not found necessary to add a third resonance term at $\sim 2 \text{ K}$ in the fit of GA735(e) although the $K(T)$ curve shows a change in slope at $T \approx 2 \text{ K}$ (Chapter 3). From the magnetothermal conductivity of GA735(e) we also deduce a zero-field splitting of $\sim 5 \text{ cm}^{-1}$ (Chapter 4). Knowing that the dominant charge state in GA735(e) is Cr^{2+} (Appendix 1), it is tempting to attribute this splitting to Cr^{2+} . It might then correspond to the 5.6 cm^{-1} energy difference observed by EPR although again because of selection rules, the assignment to Cr^{2+} may be incorrect. In the next section the Cr^{2+} optical spectroscopy results are discussed.

7.2.3 Optical Spectroscopy Data

The zero-phonon structure of the 0.82 eV absorption line in Cr-doped GaAs has been shown by Clerjaud et al (1980) to be wholly consistent with the model for the substitutional Cr^{2+} ground state proposed by Krebs and Stauss (1979a).

Lightowers et al (1979) showed that the ground state structure of Cr^{2+} derived from the 0.839 eV absorption line was much more complicated than that of the Krebs and Stauss model. Zeeman studies (Killoran et al 1980, Eaves et al 1980) show this ground state to have trigonal symmetry, suggesting a Cr^{2+} complex with a $\langle 111 \rangle$ axis. This has recently been supported by a further study of the fine structure of the 0.839 eV line (Voillot et al 1980). These authors also find a trigonal symmetry for the centres responsible for the line. Their value for the ground state splitting (6.61 cm^{-1}) is also shown in Table 7.1. The question arises then whether the phonon scattering observed in our work might be due to Cr^{2+} -complexes identified by optical measurements.

To throw light on this the infrared absorption of GA735(e) has recently been measured at low temperatures (Eaves and Williams - Private Communication). The 0.82 eV main line reported by Clerjaud et al (1980) was observed but no absorption was seen at ~ 0.839 eV. This presumably suggests that the concentration of $\langle 111 \rangle$ complexes is very small in this sample and it seems unlikely therefore that they are responsible for the strong phonon scattering. Other samples are still being investigated.

The discussion in this section was based on the Brozel et al (1978) model for the Cr charge states. In the next section a different interpretation of the charge states of Cr is discussed.

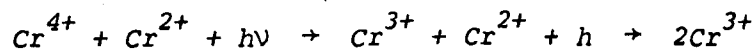
7.3 DOES SUBSTITUTIONAL Cr^{1+} EXIST IN GaAs:Cr?

As of late, some doubt has been expressed about the assignment of the isotropic line at $g \sim 2$ observed in SI samples by EPR, after sub-band-gap illumination. This feature which was reported by different authors (Kaufmann and Schneider 1976; Stauss and Krebs 1977), was always attributed to the Cr^{1+} charge state, and hence it was concluded that Cr ions can act as double acceptors in GaAs.

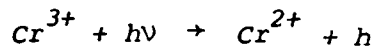
Very recently, Stauss et al (to be published) have reinterpreted their previous EPR results after obtaining new data on GaAs:Cr. They examined n-type, p-type and SI bulk samples. (Their original work was on SI material only.) A strong single isotropic EPR line with $g \sim 2$ is observed in the dark in a very p-type sample, doubly doped with Zn and Cr, with $[\text{Zn}] \gg [\text{Cr}]$. The spectrum does not however show any Cr^{2+} or Cr^{3+} signal. The authors attribute this line to Cr^{4+} (i.e. neutral Cr^{3+} has captured a hole). Another p-type sample, with a higher resistivity and where $[\text{Zn}] < [\text{Cr}]$, shows the same line at $g \sim 2$ and also a Cr^{3+} signal. The ' Cr^{4+} ' line is not detected in a SI sample which shows only Cr^{2+} and Cr^{3+} absorptions. Finally a sample doubly doped with Te and Cr (n-type) does not show any signal which could be attributed to Cr^{1+} even after illumination. Although the sample was too lossy for good EPR measurements, a Cr^{2+} signal could be detected and this allowed the authors to set an upper limit on the concentration of Cr^{1+} (if there was any), of $[\text{Cr}^{1+}] < [\text{Cr}^{2+}]/10$.

These results are then in contradiction with the double acceptor picture which allows the formation of Cr^{1+} and also predicts $[\text{Cr}^{1+}] > [\text{Cr}^{2+}]$ in n-type material.

The authors also report a new type of photoinduced change in the charge states of Cr in GaAs. In samples where $[\text{Cr}^{2+}] > [\text{Cr}^{3+}]$ in the dark, a resonance-like dip in the concentration of Cr^{2+} is observed at 0.87 eV and a broad maximum at about 1.1 eV. The spectral dependence of Cr^{2+} observed previously (e.g. Stauss and Krebs 1977) and which is characterized by a strong transition at ~ 0.7 eV is also reported for samples in which $[\text{Cr}^{2+}] < [\text{Cr}^{3+}]$. All the light induced effects are then reinterpreted in terms of a Cr^{4+} - Cr^{3+} - Cr^{2+} system. The decrease in $[\text{Cr}^{2+}]$ for $0.45 \text{ eV} \leq h\nu \leq 0.7 \text{ eV}$ is attributed to the process



The mid-gap transition is attributed to the process



where the free hole is then trapped at Cr^{3+} to create Cr^{4+} . The resonant effect observed at 0.87 eV is the result of the process



The authors also suggest the EPR transient effects reported in White et al (1980) could also easily be explained using the Cr^{4+} - Cr^{3+} - Cr^{2+} model.

Kaufmann and Schneider (1980) have also suggested that the isotropic feature at $g \sim 2$, previously attributed to Cr^{1+} , could represent a Cr^{4+} signal. From high frequency measurements (35 GHz), the authors also state that in fact that feature represents a

superposition of two lines, the Cr^{4+} signal and possibly the Cr^{1+} signal. They propose that Cr in GaAs could be a four-state system, the isolated neutral Cr being able to trap one electron, two electrons or one hole.

More evidence is brought by Goswaini et al (to be published) who report EPR measurements on n-type and p-type GaAs:Cr. No Cr^{1+} signal was detected in an n-type sample which was first electron-irradiated to reduce the free carriers concentration and thus allow EPR absorption. In the same sample the substitutional Cr^{2+} signal was observed. The $g \sim 2$ line was again detected in a p-type sample and it was suggested that that line could be due to either substitutional Cr^{4+} or interstitial Cr^{1+} .

This seems to be evidence for the non-existence of substitutional Cr^{1+} in n-type Cr-doped GaAs samples, in agreement with the findings of Stauss et al (1980).

Clerjaud et al (1980) also claim that Cr^{2+} is the dominant charge state in n-type GaAs. We note however that their samples are different to those used in the previous investigations as the doping with Cr is obtained by diffusion into n-type GaAs substrates. The concentration of the Cr impurities is also not known so that precise comparison with the 'double acceptor' model is not possible. The same n-type samples show the existence of the Cr^{1+} EPR signal which 'grows under 1.09 μm illumination'. It is not clear from their paper whether this resonance is observed in the dark or appears only after illumination. This is in contradiction with Stauss et al results which do not show any isotropic line in the n-type sample, regardless of illumination.

Clerjaud et al do not state whether they believe their signal arises from interstitial Cr^{1+} .

Bearing in mind these new studies, it would be rather difficult to explain the phonon scattering observed by thermal conductivity measurements. Assuming that the dominant charge state in our n-type samples GA785 and GA735 (O64), in which little phonon scattering was observed, is Cr^{2+} would mean that state is not a phonon scatterer. The only charge state which could then give rise to strong resonant scattering (as observed in the SI and p-type samples) would be Cr^{3+} . All the resonant phonon scattering would then be attributed to different transition frequencies within the Cr^{3+} levels. However this interpretation would be in total disagreement with deductions from other spectroscopic work using phonons. From symmetry arguments, Tokumoto and Ishiguro (1979) attribute the ultrasonic attenuation in SI GaAs:Cr to Cr^{2+} . Narayanamurti et al (1978) interpret the propagation of heat pulses in SI GaAs:Cr in terms of absorption by Cr^{2+} ions. APR measurements (Ganapol'skii 1975 - Bury et al 1980a, b) also show that Cr^{2+} is responsible for the phonon scattering. These studies reveal then that Cr^{2+} ions are efficient phonon scattering centres. Also, the photo-thermal conductivity results for the n-type sample GA735 (O64), seem consistent with the 'double-acceptor' model.

Another support for the 'double-acceptor' picture for Cr in GaAs comes from the photocapacitance measurements of Szawelska and Allen (1979) who show that Cr produces two acceptor levels in GaAs which are associated with different charge states of the same centre.

In the absence of a coherent new model for the Cr charge states in GaAs, we find it possible to interpret our experimental data in terms of the 'double acceptor' model. Any Cr^{4+} present in the p-type samples used in our investigation should be weakly coupled (${}^3\text{A}_2$ in T_d).

Although numerous studies have been devoted to the GaAs:Cr system in the last years, because of its technological importance, there seems there is still more to learn about this intriguing system.

Zero-field splitting (cm^{-1})	Assignment of charge state	Local symmetry	Technique	Reference	Comments
7.5	Cr^{2+}	D_{2d}	EPR (9 GHz) For Infrared EPR (370 GHz) Optical absorption	Krebs and Stauss 1979b Wagner and White 1979 Clerjaud et al 1980	This spans 3 levels
7 ± 2	Cr^{3+}	C_{3v}	EPR	Krebs and Stauss 1979a	
~ 18			Thermal conductivity ($T > 2K$)	Chaudhuri et al 1973	Observed in one SI sample
~ 10	Cr^{2+}	D_{2d}	Heat pulse propagation	Narayanamurti et al 1978	
~ 6.8	Cr^{2+}	D_{2d}	Monochromatic phonons (Tunnel junctions)	Narayamamurti 1980	Average of 5.6 and 8.1
18.5 ± 3	Cr^{3+}		Ultrasonic attenuation	Bankovskis et al 1980	
~ 22	Cr^{2+}	T_d	Luminescence and absorption	Lightowlers et al 1979	This spans 5 levels
6.61	Cr^{2+}	C_{3v}	Luminescence	Voillot et al 1980	This spans 6 levels
0.7 ± 0.1	Cr^{2+}	D_{2d}	Thermal conductivity ($T \geq 50 \text{ mK}$)		
4.9 ± 1	Cr^{2+}		Magnetothermal conductivity	This work	
23 ± 5	Cr^{3+}		Piezothermal conductivity		

Table 7.1 Zero-field ground-state splittings of GaAs:Cr

APPENDIX 1

A. The details of the samples used in the investigation are given in the table below:

SAMPLES	DOPANT (cm^{-3})			VALENCE STATES			MM DIMENSIONS
	Cr	Si	n_{el}	MAJ	MIN	AXIS	
GA735(e)	2×10^{17}	2×10^{17}	SI	Cr^{2+}	-	<110>	2.9x3.0x15
GA735(O64)	6×10^{16}	1.7×10^{17}	$\sim 10^{15}$	Cr^{1+}	Cr^{2+}	<001>	3.0x3.0x10
GA785	6×10^{16}	$>> 6 \times 10^{16}$	$\sim 10^{18}$	Cr^{1+}	-	<110>	4.0x4.2x20
GA781	NA	3×10^{16}	$p \sim 10^{14}$	Cr^{3+}	Cr^{2+}	<001>	3.0x3.0x10
GA781	NA	3×10^{16}	$p \sim 10^{14}$	Cr^{3+}	Cr^{2+}	<110>	3.0x3.0x10
TI#4	6×10^{15}	NA	SI	Cr^{1+*}	Cr^{2+}	<110>	2.7x5.0x24
TI#5	7×10^{16}	1.1×10^{16}	SI	Cr^{3+}	Cr^{2+}	<110>	4.1x5.3x21
GA803	-		.	-	-	<110>	3.1x3.4x16

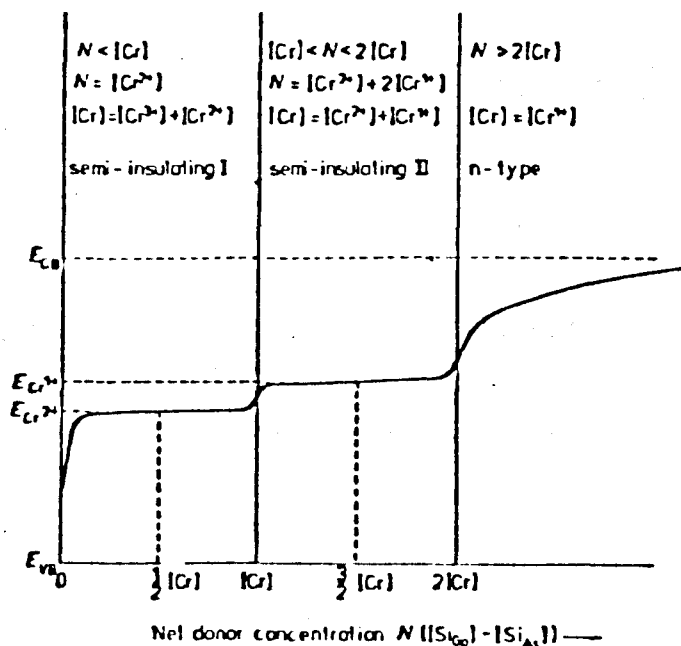
All the samples are cut from boat-grown ingots. The GA samples were kindly supplied by the Plessey Co. (Allen Clark Research Centre, Caswell) and the TI ones by Dr. Ishiguro. The GA samples were doubly doped with Cr/Si (GA735, GA785) or Cr/Zn (GA781). GA803 is not doped with Cr, and is the result of an attempt to get a SI ingot by doping with oxygen. The characteristics of the GA samples are deduced from mass spectrometry, localized vibrational mode absorption and Hall measurements.

SI = Semi-Insulating NA = Not available

B. The valence states (MAJ = majority, MIN = minority) are deduced from the model of Brozel et al (1978). The authors used Hall effect measurements, mass spectrometry, optical and electron microscopy, and localized vibrational mode (LVM) absorption measurements, to

* This assumes the same amount of Si as in TI#5.

study boat-grown GaAs doped with both silicon and chromium. They found that the net silicon donor concentrations ($[Si_{Ga}] - [Si_{As}]$) determined by LVM exceeded the carrier concentrations measured electrically. They attributed this to acceptor levels associated with chromium. The Fermi level in Cr-doped GaAs would then depend on the relative concentrations of Cr and Si (or any donor). This is schematically shown below.



Schematic diagram of expected Fermi level variation in chromium-doped gallium arsenide (constant chromium concentration $[Cr]$) with increasing donor concentration.

From Brozel et al (1978).

In the absence of donor impurities, Cr atoms located on a Ga site would be neutral with respect to the lattice; this state is usually denoted Cr^{3+} ($3d^3$) because 3 electrons from the d-core are used to form bonds (e.g. Krebs and Stauss 1977a). Capture of electrons leads successively to core states $3d^4$ (Cr^{2+}) and $3d^5$ (Cr^{1+}).

REFERENCES

- ADOLF, A., FORTIER, D., ALBANY, J.M. and SUZUKI, K., 1980
Phys. Rev. B 21, 5651
- ANDERSON, B.R. and CHALLIS, L.J., 1975
J. Phys. C 8, 1475
- AUGUSTUS, P.D. and STIRLAND, D.J., 1980
J. Microsc. 118, 111
- BANKOVSKIS, A., BATES, C.A., KING, P.J. and MONK, D.J., 1980
To be published in *J. Mag. Res.*
- BATES, C.A., 1978
Phys. Rep. 35, 187
- BATES, C.A., ABHVANI, A.S. and AUSTEN, S.P., 1980
Proc. Int. Conf. on Semi-Insulating III-V Compounds, Nottingham, Shiva Press
- BERMAN, R., 1976
in *'Thermal Conduction in Solids'*, Oxford University Press,
Chapter 8
- BERMAN, R., BROCK, J.C.F. and HUNTLEY, D.J., 1963
Phys. Lett. 3, 310
- BERMAN, R., FOSTER, E.L. and ZIMAN, J.M., 1955
Proc. Roy. Soc. London A231, 130
- BHATTACHARJEE, A.K. and RODRIGUEZ, S., 1972
Phys. Rev. B 6, 3836
- BIR, G.L., BUTIKOV, E.I. and PIKUS, G.E., 1963
J. Phys. Chem. Solids 24, 1467; 24, 1475
- BLUME, M. and ORBACH, R., 1962
Phys. Rev. 127, 1587
- BROECKX, J., CLAWS, P. and VENNIK, J., 1978
Sol. St. Commun. 25, 613
- BROWN, F.C., 1967
in *'The Physics of Solids'*, WA Benjamin, Chapter 5
- BROWN, M.A., 1971
Ph.D. Thesis, University of Nottingham
- BROZEL, M.R., BUTLER, J., NEWMAN, R.C., RITSON, A., STIRLAND, D.J.
and WHITEHEAD, C., 1978
J. Phys. C 11, 1857

- BURY, P., CHALLIS, L.J., KING, P.J., MONK, D.J., RAMDANE, A.,
RAMPTON, V.W. and WISCOMBE, P.C., 1980a
Proc. Int. Conf. on Semi-Insulating III-V Compounds, Nottingham
Shiva Press
- BURY, P., KING, P.J. and WISCOMBE, P.C., 1980b
To be published
- CALLAWAY, J. 1959
Phys. Rev. 113, 1046
- CARLSON, E.J. and Mott. G., 1963
Proc. IEEE 51, 1239
- CARLSON, R.O., SLACK, G.A. and SILVERMAN, S.J., 1965
J. Appl. Phys. 36, 505
- CASIMIR, H.B.G., 1938
Physica 5, 495
- CHALLIS, L.J., 1961
Cryogenics 2, 1
- CHALLIS, L.J., McCONACHIE, M.A. and WILLIAMS, D.J., 1969
Proc. Roy. Soc. A 310, 493
- CHALLIS, L.J., de GOËR, A.M., GUCKLESBERGER, K. and SLACK, G.A., 1972
Proc. Roy. Soc. London A 330, 29
- CHALLIS, L.J., de GOËR, A.M. and HASELER, S.C., 1977
Phys. Rev. Lett. 39, 558
- CHALLIS, L.J. and HALBO, L., 1972
Phys. Rev. Lett. 28, 816
- CHALLIS, L.J. and HASELER, S.C., 1978
J. Phys. C 11, 4681
- CHALLIS, L.J., HASELER, S.C. and RAMDANE, A., 1978
J. Phys. C 11, 4695
- CHALLIS, L.J. and RAMDANE, A., 1980
Proc. Int. Conf. on Phonon Scattering in Condensed Matter,
Brown University, Plenum Press
- CHALLIS, L.J. and WILLIAMS, D.L., 1978
J. Phys. C 11, 3787
- CHAUDHURI, N., WADHWA, R.S., TOKU PHOOLA and SREEDHAR, A.K., 1973
Phys. Rev. B 8, 4668
- CHERLOW, J.M., AGGARWAL, R.L. and LAX, B., 1973
Phys. Rev. B 7, 4547
- CLARK, I.A., 1975
Ph.D. Thesis, University of Nottingham
- CLERJAUD, B., HENNEL, A.M. and MARTINEZ, G., 1980
Sol. St. Commun. 33, 983

- CULLIS, A.G., AUGUSTUS, P.D. and STIRLAND, D.J., 1980
J. Appl. Phys. 51, 2556
- DEBYE, P., 1912
Ann. Phys. 39, 789
- DOBROV, W.I., 1964
Phys. Rev. 134, A734
- DREYFUS, B., 1972
Proc. Int. Conf. on Phonon Scattering in Solids, Paris,
Service de Documentation du CEN Saclay
- EAVES, L., ENGLERT, T., INSTONE, T., UIHLEIN, C., WILLIAMS, P.J.
and WRIGHT, H.C., 1980
Proc. Int. Conf. on Semi-Insulating III-V Compounds,
Nottingham, Shiva Press
- EAVES, L., ENGLERT, T. and UIHLEIN, C.,
To be published in 'Physics in High Magnetic Fields',
Springer Series in Solid State Sciences, Springer, Berlin,
New York, 1981
- EAVES, L. and WILLIAMS, P.J., 1979
J. Phys. C 12, L725
- FEHER, G., HENSEL, J.C. and GERE, E.A., 1960
Phys. Rev. Lett. 5, 309
- GANAPOL'SKII, E.M., 1975
Sov. Phys. Solid State 16, 1868
- GARLAND, C.W. and PARK, K.C., 1962
J. Appl. Phys. 33, 759
- GHAZI, A.A., 1978
Ph.D. Thesis, University of Nottingham
- de GOËR, A.M., 1969
J. de Physique 30, 389
- de GOËR, A.M. and CHALLIS, L.J., 1973
Sol. St. Commun. 13, 745
- GOSWAMI, N.K., NEWMAN, R.C. and WHITEHOUSE, J.E., 1980
To be published in Sol. St. Commun.
- GRIFFIN, A. and CARRUTHERS, P., 1963
Phys. Rev. 131 1976
- HAISTY, R.W. and CRONIN, G.R., 1964
Proc. 7th Int. Conf. on Physics of Semiconductors, Paris,
Dunod
- HALLER, E.E., JOÓŠ, B. and FALICOV, L.M., 1980
Phys. Rev. B 21, 4729

- LIN-CHUNG, P.J. and WALLIS, R.F., 1969
J. Phys. Chem. Solids, 30, 1453
- LUDWIG, G.W. and WOODBURY, H.H., 1961
Bull. Am. Phys. Soc. 6, 118
- MERLET, F., PAJOT, B., ARCAS, Ph. and JEAN-LOUIS, A.M., 1975
Phys. Rev. B 12, 3297
- MOORE, W.S. and Al-SHARBATI, T.M., 1972
J. Phys. D 6, 367
- NARAYANAMURTI, V., 1980
Proc. Int. Conf. on Phonon Scattering in Condensed Matter,
Brown University, Plenum Press
- NARAYANAMURTI, V., CHIN, M.A. and LOGAN, R.A., 1978
Appl. Phys. Lett. 33, 481
- NEUBRAND, H., 1978a *Phys. Stat. Sol.(b)* 86, 269
1978b *Phys. Stat. Sol.(b)* 90, 301
- ORBACH, R., 1960
Ph.D. Thesis, University of California
- POHL, R.O., 1962
Phys. Rev. Lett. 8, 481
- SALCE, B., 1978
Thèse de Doctorat d'Etat, University of Grenoble
- SALCE, B. and de GOËR, A.M., 1979
J. Phys. C 12, 2081
- SCHAWLOW, A.L., PIKSIS, A.H. and SUGANO, S., 1961
Phys. Rev. 122, 1469
- SCHMIDT, J. and SOLOMON, I., 1966
J. Appl. Phys. 37, 3719
- SCHWARTZ, J.W. and WALKER, C.T., 1967
Phys. Rev. 155, 959
- SHEINKMAN, M.K. and Ya. SHIK, A., 1976
Sov. Phys. Semicond. 10, 128
- SHIMIZU, T. and TANAKO, N., 1973
Phys. Lett. A 45, 5
- SOEPANGKAT, H.P. and FISCHER, P., 1973
Phys. Rev. B 8, 870
- STAUSS, G.H. and KREBS, J.J., 1977
Inst. of Phys. Conf. Ser. 33a, 84
- STAUSS, G.H., KREBS, J.J., LEE, S.H. and SWIGGARD, E.M.
To be published

- HAM, F.S., 1972
in 'Electron Paramagnetic Resonance', edited by S. Geschwind,
Plenum Press, p 1
- HASELER, S.C., 1976
Ph.D. Thesis, University of Nottingham
- HERRING, C., 1954
Phys. Rev. 95, 954
- HOLLAND, M.G., 1964a, Phys. Rev. 134, A471
1964b, Proc. 7th Int. Conf. on Physics of
Semiconductors, Paris, Dunod
- JAHN, H.A. and TELLER, E., 1937
Proc. Roy. Soc. London A 161, 220
- KAUFMANN, U. and SCHNEIDER, J., 1976 Sol. St. Commun 20, 143
1980 Appl. Phys. Lett. 36, 749
- KEYES, R.W., 1961
Phys. Rev. 122, 1171
- KILLORAN, N., CAVENETT, B.C. and HAGSTON, W.E., 1980
Proc. Int. Conf. on Semi-Insulating III-V Compounds,
Nottingham, Shiva Press; Sol. St. Commun. 35, 333
- KLEMENS, P.G., 1955
Proc. ~~Roy.~~ Soc. London A 68, 1113
Phys.
- KNOWLES, A.P., 1976
Ph.D. Thesis, University of Nottingham
- KREBS, J.J. and STAUSS, G.H., 1977a Phys. Rev. B 15, 17
1977b Phys. Rev. B 16, 971
1979a Phys. Rev. B 20, 795
1979b Second 'Lund' Conference
St^e Maxime (France)
- LANG, D.V. and LOGAN, R.A., 1977
Phys. Rev. Lett. 39, 635
- LANG, D.V., LOGAN, R.A. and JAROS, M., 1979
Phys. Rev. B 19, 1015
- LASSMAN, K. and ZEILE, H., 1980
Proc. Int. Conf. on Phonon Scattering in Condensed Matter,
Brown University, Plenum Press
- LEWINER, J. and MEIJER, P.H.E., 1970
Phys. Rev. B 1, 2950
- LIGHTOWLERS, E.C., HENRY, M.O. and PENCHINA, C.M., 1979
Inst. Phys. Conf. Ser. 43, 307
- LIN, A.L. and BUBE, R.H., 1976
J. Appl. Phys. 47, 1859

- STILLMAN, G.E., WOLFE, C.M. and DIMMOCK, J.O., 1977
in 'Semiconductors and Semimetals', Vol. 12,
Academic Press, Willardson, R.K. and Beer, A.C. Editors, p.169
- STIRLAND, D.J., 1977
Inst. of Phys. Conf. Ser. 33, 150
- SUZUKI, K., OKAZAKI, M. and HASEGAWA, H., 1964
J. Phys. Soc. Japan 19, 930
- SZAWELSKA, H.R. and ALLEN, J.W., 1979
J. Phys. C 12, 3359
- TANAKA, S. and Fan, H.Y., 1963
Phys. Rev. 132, 1516
- TANAKA, S., KOBAYASHI, M., HANAMURA, E. and UCHINOKURO, K., 1964
Phys. Rev. 134, A256
- TOKUMOTO, H. and ISHIGURO, T., 1976
Proc. Int. Conf. on Phonon Scattering in Solids, Nottingham,
Plenum Press
1977a Phys. Rev. B 15, 2099
1977b Proc. Int. Conf. on Internal
Friction and Ultrasonic
Attenuation in Solids, Tokyo
1979 J. Phys. Soc. Japan
46, 84
- VALLIN, J.T., SLACK, G.A., ROBERTS, S. and HUGHES, A.E., 1970
Phys. Rev. B 2, 4313
- VALLIN, J.T. and WATKINS, G.D., 1974
Phys. Rev. B 9, 2051
- VOILLOT, F., BARREAU, J., BROUSSEAU, M. and BRABANT, J.C., 1980
J. de Physique Lettres 41, L415
- VUILLERMOZ, P.L., LANGIER, A. and MAI, C., 1975
J. Appl. Phys. 46, 4623
- WAGNER, R.J. and WHITE, A.M., 1979
Sol. St. Commun. 32, 399
- WERTZ, J.E. and BOLTON, J.R., 1972
in 'Electron Spin Resonance - Elementary Theory and Practical
Applications', McGraw-Hill Book Company.
- WHITE, A.M., KREBS, J.J. and STAUSS, G.H., 1980
J. Appl. Phys. 51, 419
- WYBOURNE, M.N., JEFFERIES, D.J., CHALLIS, L.J. and GHAZI, A.A., 1979
Rev. Sci. Instrum. 50 (12), 1634
- ZADWORNÝ, F., 1965
Thèse de Doctorat d'État, University of Grenoble